

# Human thalamocortical connections and their involvement in language systems

Doctoral Thesis by:  
**Mengxing Liu**

Supervised by:  
**Dr. Pedro M. Paz-Alonso**  
**Dr. Garikoitz Lerma-Usabiaga**

2022

eman ta zabal zazu



Universidad  
del País Vasco

Euskal Herriko  
Unibertsitatea

Mengxing Liu  
All rights reserved.

BCBL Basque Center on Cognition, Brain and Language  
Paseo Mikeletegi, 69,  
Donostia-San Sebastian, Spain

This work was supported by grants from the European Union's Horizon 2020 research and innovation programme under the Marie Skłodowska-Curie (grant agreement No. 713673), and from "la Caixa" Foundation (No. 11660016).

# Human thalamocortical connections and their involvement in language systems

Doctoral Thesis by:  
**Mengxing Liu**

Supervised by:  
**Dr. Pedro M. Paz-Alonso**  
**Dr. Garikoitz Lerma-Usabiaga**

2022



Universidad  
del País Vasco

Euskal Herriko  
Unibertsitatea



BASQUE CENTER  
ON COGNITION, BRAIN  
AND LANGUAGE

# Acknowledgement

Thanks to Kepa, for recruiting me at first, and continuously teaching and training me. In the past five years, you keep replying that it is your job every time I say thank you to you. But I know you have done way more than your job asks you to do. If one day I managed to become a qualified researcher and start mentoring students, I hope I could be a mentor like you.

Thanks to Gari, for hosting me in a foreign country, and for all the training from you. I learned a lot from you.

Thanks to *la Caixa* Foundation, for the generous fellowship in exchange for only mentioning their names in my publications.

Thanks to the admin and lab groups in the BCBL, for all the help they have provided to make my life and research here easier.

# Content

<b>Acknowledgement</b>	<b>4</b>
<b>Content</b>	<b>5</b>
<b>List of abbreviations</b>	<b>6</b>
<b>1 Resumen en castellano</b>	<b>9</b>
<b>2 Abstract</b>	<b>14</b>
<b>3 Background and motivation</b>	<b>18</b>
<b>4 Thalamus</b>	<b>22</b>
4.1 General introduction of the structure	22
4.2 Thalamic atlases and nuclear divisions	23
4.3 Thalamic nuclei segmentation methods	26
4.4 First-order relay thalamic nuclei	29
4.4.1 Lateral geniculate nucleus	30
4.4.2 Medial geniculate nucleus	31
4.4.3 Ventral lateral nucleus	33
4.5 Higher-order relay thalamic nuclei	35
4.5.1 Anterior nuclear complex	35
4.5.2 Mediodorsal nucleus	37
4.5.3 Pulvinar	38
<b>5 Neurobiology of language</b>	<b>41</b>
5.1 History	41
5.2 Modern neuroanatomical models	45
5.2.1 Modality-general models	45
5.2.1.1 Price's model	45
5.2.1.2 MUC model	47
5.2.1.3 Lau's model	48
5.2.2 Reading models	49
5.2.3 Speech comprehension models	50
5.2.4 Production models	52
<b>6 Study 1: Structural connection of first-order thalamic nuclei</b>	<b>55</b>
6.1 Methods	56
6.1.1 Subjects	56
6.1.2 Data acquisition	57
6.1.3 Tractography pipeline	58
6.1.3.1 ROI definition	58
6.1.3.2 DWI data preprocessing	60
6.1.3.3 Tract identification and tractometry	60

6.1.4 Reproducibility measurement	62
6.2 Results	64
6.2.1 Computational reproducibility	66
6.2.2 Test-retest reproducibility	68
6.3 Discussion	69
<b>7 Study 2: Structural connectivity of higher-order thalamic nuclei: Anterior thalamic complex and mediodorsal nucleus</b>	<b>73</b>
7.1 Methods	75
7.1.1 Subjects and data acquisition	75
7.1.2 Tractography pipeline	75
7.1.2.1 ROI definition	76
7.1.2.2 DWI data preprocessing	77
7.1.2.3 Tract identification and tractometry	77
7.1.3 Reproducibility measurement	78
7.1.4 Post-hoc analysis	78
7.2 Results	79
7.2.1 Computational reproducibility	84
7.2.2 Test-retest reproducibility	85
7.2.3 Post-hoc analysis results	86
7.3 Discussion	87
<b>8 Study 3: task-based fMRI study of thalamic involvement in human language systems</b>	<b>93</b>
8.1 Methods	93
8.1.1 Participants	93
8.1.2 Materials and Experimental Procedure	94
8.1.3 MRI data acquisition	96
8.1.4 MRI data analysis	96
8.2 Results	99
8.2.1 Whole-brain contrasts	99
8.2.2 ROI results	100
8.2.3 Functional connectivity results	102
8.2.4 Structural connectivity	105
8.3 Discussion	105
<b>9 General Discussion</b>	<b>111</b>
<b>10 Bibliography</b>	<b>116</b>

## List of abbreviations

A1	primary auditory cortex
ACC	anterior cingulate cortex
AD	axial diffusivity
AN	anterior nuclear complex
ANOVA	analysis of variance
AR	acoustic radiation
BCBL	Basque Center on Cognition, Brain and Language
BOLD	blood-oxygen-level-dependent
CSD	constrained spherical deconvolution
dIPFC	dorsolateral prefrontal cortex
DT	dentatothalamic tract
DTI	diffusion tensor images/imaging
DWI	diffusion-weighted images/imaging
fMRI	functional magnetic resonance imaging
FODs	fiber orientation distributions
FoV	field of view
FWE	family wise error
FWHM	full-width half-maximum
GLM	general linear model
HCP	human connectome project
HRF	hemodynamic response function
IFG	inferior frontal gyrus
LGN	lateral geniculate nucleus
M1	primary motor cortex
MD	mediodorsal nucleus
MGN	medial geniculate nucleus
mPFC	medial prefrontal cortex
MR	motor radiation
MRI	magnetic resonance imaging
MUC	Memory-Unification-Control
OR	optic radiation
PFC	prefrontal cortex
pSTG	posterior superior temporal gyrus
ROI	region-of-interest

RTP2	reproducible-tract-profiles
SMA	supplementary motor area
SMG	supramarginal gyrus
T1	T1-weighted structural image
TE	time-to-echo
TR	time-to-repetition
V1	primary visual cortex
V2	secondary visual cortex
VLa	anterior ventral lateral nucleus
VLN	ventral lateral nucleus
VLp	posterior ventral lateral nucleus

# 1 Resumen en castellano

A lo largo de la evolución la expansión del neocórtex se ha relacionado con la aparición de funciones cognitivas de nivel superior, tales como el razonamiento, el pensamiento abstracto o el lenguaje en los seres humanos. La investigación en neurociencia cognitiva se ha centrado principalmente en la corteza cerebral. Sin embargo, el tálamo es una estructura subcortical que cuenta con extensas conexiones de sustancia blanca con la corteza cerebral, y cuya expansión durante la evolución es similar a la del neocórtex. Además, las conexiones talamocorticales están involucradas en la comunicación entre áreas corticales, por lo que, para comprender por completo las bases neurales de la cognición, es necesaria una mejor comprensión del papel que juega el tálamo en la función cortical. La presente tesis doctoral se centra en la estructura y función del tálamo: en el primer estudio se presenta un protocolo reproducible para reconstruir los tractos de materia blanca talámicos de primer orden a partir de datos de imágenes ponderadas por difusión; en el segundo estudio se investigan los tractos de sustancia blanca talámica de segundo orden y se propone un protocolo similar para reconstruir estos tractos; en el tercer estudio se investiga mediante resonancia magnética funcional (fRM) basada en tarea la participación de los núcleos talámicos de primer orden en los principales sistemas de lenguaje.

Los núcleos “primarios” o de “relevo de primer orden” del tálamo hacen llegar a la corteza cerebral la información relativa a la actividad del entorno o de los sistemas motores subcorticales. Debido al pequeño tamaño de estos núcleos y la alta especificidad de sus vías de entrada y salida, se requieren nuevos protocolos de neuroimagen para investigar las interacciones talamocorticales en la percepción, la cognición y el lenguaje humanos. El objetivo del primer estudio se definió para abordar esta cuestión y fue doble: I) desarrollar un protocolo de reconstrucción basado en resonancia magnética de difusión *in vivo* para extraer y medir los tractos de fibras axonales que se originan o terminan específicamente en núcleos de relevo de primer orden; y, II) probar la fiabilidad

de este protocolo de reconstrucción. Para ello, se investigaron en ambos hemisferios los haces de fibras talamocorticales/corticotalámicos que conectan cada uno de los núcleos de relevo de primer orden y sus principales áreas corticales diana, concretamente, el núcleo geniculado lateral (radiación óptica), el núcleo geniculado medial (radiación acústica) y el núcleo lateral ventral (radiación motora). Además, se examinó la principal vía de entrada subcortical al núcleo posterior lateral ventral, que se origina en el núcleo dentado del cerebelo. Nuestro protocolo consta de tres componentes: definición de regiones de interés; preprocesamiento de datos de difusión; y modelado de tractos de sustancia blanca y tractometría. Se utilizaron métodos computacionales y de test-retest para examinar si nuestro protocolo puede reconstruir de manera fiable estos tractos de interés. Los resultados mostraron que el protocolo tiene una reproducibilidad computacional casi perfecta y una reproducibilidad test-retest entre buena y excelente. Este nuevo protocolo puede ser de interés tanto para la investigación en neuroimagen como para estudios clínicos, y se ha puesto a disposición pública para la comunidad científica.

Por otro lado, a diferencia de los núcleos de relevo de primer orden, los núcleos de “relevo de segundo orden u orden superior” del tálamo están interconectados recíprocamente con la corteza cerebral a través de vías cortico-tálamo-corticales. Por ejemplo, el núcleo mediodorsal del tálamo está interconectado con múltiples subregiones de los lóbulos frontales. Además, también recibe proyecciones aferentes del lóbulo temporal y de la amígdala. Debido a las complejas conexiones estructurales, existen pocos estudios de tractografía capaces de reconstruir estos tractos de sustancia blanca talámicos de orden superior. Consecuentemente, el segundo estudio se centró en los tractos de materia blanca de los núcleos anterior y mediodorsal del tálamo, donde se desarrolló un protocolo de reconstrucción para obtener los tractos que se originan o terminan en estos núcleos. Además, se revisó la fiabilidad del protocolo de reconstrucción en una muestra de gran tamaño. Los núcleos anteriores cuentan con interconexiones con la corteza cingulada anterior y posterior y la

corteza retroesplenial, mientras que el núcleo mediodorsal está ampliamente conectado con prácticamente toda la corteza prefrontal, la parte más anterior del lóbulo temporal y la amígdala. Nuestro protocolo es capaz de reconstruir estos tractos de materia blanca de manera fiable, con únicamente una pequeña porción de los tractos mostrando una reproducibilidad relativamente menor. Se realizó un análisis post-hoc para explorar la asociación de estas características específicas de imagen y anatómicas con la reproducibilidad. Los resultados revelaron una fuerte correlación negativa entre el ruido en los datos de imágenes de difusión y la longitud del tracto con la reproducibilidad, y una correlación positiva entre el número de fibras reconstruidas con la reproducibilidad. Este protocolo está disponible públicamente tanto para investigación como para el uso clínico interesado en la reconstrucción de estos tractos de materia blanca talámicos de orden superior a partir de imágenes ponderadas por difusión *in vivo*. Además, los resultados de reproducibilidad abren nuevas posibilidades para futuros estudios, tales como examinar sistemáticamente los posibles factores que determinan la reproducibilidad de los tractos.

A pesar de que tradicionalmente se pensaba que los núcleos talámicos de primer orden únicamente transmiten información sensoriomotora desde la periferia y el cerebelo hasta las regiones corticales, trabajos recientes han demostrado que la actividad en los núcleos talámicos de primer orden puede ser modulada por las regiones corticales (Andolina et al., 2007; Cudeiro & Sillito, 2006; von Kriegstein et al., 2008). Hasta la fecha, la investigación de la neurobiología del lenguaje se ha centrado en las regiones corticales y ha descuidado las contribuciones de las estructuras subcorticales, como los núcleos talámicos de primer orden, por lo que, en el tercer estudio, se investiga la participación de los núcleos talámicos de primer orden en los procesos del lenguaje en un experimento de fRM basado en tareas. En este experimento, los participantes realizaron tres tareas de lenguaje basadas en diferentes sistemas sensoriomotores: lectura (vía visual), comprensión del habla (vía auditiva) y producción del habla (vía motora). Además, se realizaron otras tres tareas

perceptivas y motoras no-lingüísticas comparables con las tareas lingüísticas presentadas: ver imágenes codificadas (vía visual), escuchar audios con ruido (vía auditiva) y producir sonidos ininteligibles (vía motora). Se observó una contribución de los núcleos talámicos de primer orden dependiente de si la modalidad de la tarea era lingüística o no lingüística. Concretamente, los resultados revelaron una disociación de la actividad en los núcleos talámicos visual y auditivo entre las correspondientes modalidades, lingüística y no lingüística. Por ejemplo, el núcleo geniculado lateral izquierdo mostró una mayor activación al leer palabras reales que imágenes codificadas. Sin embargo, esta disociación entre tareas lingüísticas y no lingüísticas se encontró únicamente en el tálamo izquierdo. Por otro lado, también se encontró un fuerte co-activación entre los núcleos talámicos de primer orden y sus terminaciones corticales primarias en las correspondientes modalidades de cada tarea. Estos resultados muestran la especificidad en la implicación de los diferentes núcleos sensoriomotores talámicos humanos en los principales sistemas de lenguaje humano, donde estos núcleos parecen exhibir una preferencia funcional por estímulos lingüísticos frente a no lingüísticos. Este trabajo plantea la posibilidad de que los núcleos talámicos de primer orden reaccionen adaptativamente a la información cognitiva de alto nivel derivada de la información sensorial entrante. A pesar de que hasta la fecha se conozca muy poco acerca del papel de las estructuras subcorticales en las funciones cognitivas de alto nivel, el presente trabajo permite ampliar el enfoque tradicional de los mecanismos del lenguaje humano desde la corteza cerebral a una perspectiva más amplia, en la que se consideran las contribuciones del tálamo en el procesamiento del lenguaje.

En conjunto, esta tesis doctoral investiga las conexiones estructurales entre el tálamo y la corteza cerebral, y propone dos protocolos de reconstrucción disponibles públicamente para la obtención de tractos de materia blanca talámicos de primer orden y orden superior de manera fiable. También, este trabajo examina algunos factores potencialmente relacionados con la

reproducibilidad de la reconstrucción de la tractografía y se proporciona evidencia de que algunos tractos pueden conllevar menor reproducibilidad al tener específicas características anatómicas o de imagen. Finalmente, nuestros datos de fRM basado en tarea permiten identificar la participación de los núcleos talámicos de primer orden en el procesamiento del lenguaje, y destaca la importancia de considerar el papel de estructuras subcorticales como el tálamo al investigar las bases neurobiológicas del lenguaje humano.

## 2 Abstract

During evolution, the expansion of the neocortex has been linked with the emergence of higher level cognitive functions such as reasoning, abstract thinking, and language in human beings. Current research in the field of cognitive neuroscience is mainly focused on the cerebral cortex. Whereas the thalamus is a structure that has extensive white-matter connections with the cerebral cortex, its expansion during evolution is parallel to the expansion of the neocortex. The thalamocortical connections are involved in communication between cortical areas. Thus, to fully understand the neural basis of cognition, a better understanding of the role of the thalamus in cortical function is necessary. The present doctoral dissertation is focused on the structure and function of the thalamus: the first study proposes a reproducible protocol to reconstruct the first-order thalamic white-matter tracts from diffusion-weighted imaging (DWI) data; the second study investigates the higher-order thalamic white-matter tracts and a similar protocol is proposed to reconstruction those tracts; the third study uses task-based functional magnetic resonance imaging (fMRI) to examine the involvement of first-order thalamic nuclei in the main language systems.

The “primary” or “first-order” relay nuclei of the thalamus feed the cerebral cortex with information about ongoing activity in the environment or the subcortical motor systems. Due to the small size of these nuclei and the high specificity of their input and output pathways, new imaging protocols are required to investigate thalamocortical interactions in human perception, cognition and language. The goal of the first study was twofold: I) to develop a reconstruction protocol based on *in vivo* diffusion MRI to extract and measure axonal fiber tracts that originate or terminate specifically in individual first-order relay nuclei; and, II) to test the reliability of this reconstruction protocol. In the left and right hemispheres, we investigated the thalamocortical/corticothalamic axon bundles linking each of the first-order relay nuclei and their main cortical target areas, namely, the lateral geniculate nucleus (optic radiation), the medial geniculate nucleus (acoustic radiation) and the ventral lateral nucleus (motor radiation). In addition, we examined the main subcortical input pathway to the ventral lateral posterior nucleus, which originates in the dentate nucleus of the cerebellum. Our protocol comprised three components: defining regions-of-interest, preprocessing diffusion data, and modeling

white-matter tracts and tractometry. We then used computation and test-retest methods to check whether our protocol could reliably reconstruct these tracts of interest and their profiles. Our results demonstrated that the protocol had nearly perfect computational reproducibility and good-to-excellent test-retest reproducibility. This new protocol may be of interest for both neuroimaging and clinical research, and it has been made publicly available to the scientific community.

In contrast to the first-order relay nuclei, the “second-order” or “higher-order” relay nuclei of the thalamus are reciprocally interconnected with the cerebral cortex *via* cortico-thalamo-cortical pathways. For example, the mediodorsal thalamus is interconnected with practically the entire prefrontal cortex (PFC). In addition, it also receives afferents from the anterior temporal lobe and amygdala. The anterior nuclei have interconnections with the cingulate cortex and the retrosplenial cortex. Due to the complex structural connections, there are little tractography studies being able to reconstruct those higher-order thalamic white-matter tracts. In the second study, we focused on the white-matter tracts of the anterior and mediodorsal nuclei of the thalamus and developed a reconstruction protocol to obtain the tracts originating from or terminating at these nuclei. We also tested the reliability of the reconstruction protocol on a relatively large dataset. This protocol has proved to be able to reconstruct those white-matter tracts reliably, with only tracts with specific imaging or anatomical characteristics showing relatively lower reproducibility. A post-hoc analysis was conducted to explore the association of specific imaging and anatomical characteristics with reproducibility. The results revealed a strong negative correlation between both diffusion imaging data noise and tract length with reproducibility, and a positive correlation between streamline count and reproducibility. This protocol is publicly available for both research and clinical use. The reproducibility results also opened new avenues for future studies; for example, for systematically examining the possible factors that could have a stronger impact on tract reproducibility.

The first-order thalamic nuclei are traditionally believed to relay sensorimotor information from the periphery and cerebellum to cortical regions. Recent work has shown that the engagement of the first-order thalamic nuclei can be modulated by the cortical regions (Andolina et al., 2007; Cudeiro & Sillito, 2006; von Kriegstein et al., 2008). Neurobiology of language research has been

focused on the cortical regions (aside from a few exceptions) and has ignored the contributions of subcortical structures such as the first-order thalamic nuclei. In the third study, we investigated the involvement of the first-order thalamic nuclei in language processes in a task-based functional MRI experiment. In this experiment, the participants performed language tasks that rely on different sensorimotor systems: reading (visual pathway), speech comprehension (auditory pathway) and speech production (motor pathway). These three linguistic tasks rely on different sensorimotor systems recruiting first-order thalamic nuclei during perceptual and motor information processing. In addition, we also included three non-linguistic tasks that were parallel to the linguist tasks: seeing scrambled images (visual pathway); listening to noise audios (auditory pathway) and producing unintellectual sounds (motor pathway). We found modality-specific engagement of the first-order thalamic nuclei in both linguistic and non-linguistic tasks. More importantly, the results revealed a modulation in the engagement of both the visual and auditory thalamic nuclei as a function of the linguistic versus non-linguistic nature of the stimuli. For example, the left lateral geniculate nucleus (LGN) showed stronger activation for reading real words than for seeing scrambled images. This modulation was not observed in the right thalamus. We also found strong functional coupling between the first-order thalamic nuclei and their primary cortical regions for tasks associated with their corresponding modalities. These results suggest a segregation in the implication of different human thalamic sensorimotor nuclei in the main human language systems, and that these nuclei exhibit a functional preference for linguistic versus non-linguistic stimuli. This work raised the possibility that the first-order thalamic nuclei react adaptively to the high level cognitive information of the sensory input. So far very little is known about the role of subcortical structures in high-level cognitive functions. The current study began to extend the traditional view of human language mechanisms from cerebral cortex to a broader scope and started to acknowledge the possible contributions of the thalamus in language processing.

Altogether, the current thesis investigated the structural connections between the thalamus and the cerebral cortex, and proposed two reconstruction protocols that are available to the scientific community to obtain reliable first-order and higher-order thalamic white-matter tracts. We also

examined some possible factors that are linked with tractography reconstruction reproducibility and provided evidence that some tracts can be less reproducible when having specific imaging or anatomical characteristics. Finally, we showed the involvement of the first-order thalamic nuclei in language processing in a task-based functional MRI experiment, and argued the necessity of considering the role of subcortical structures, like the thalamus, when investigating the neural basis of human language function.

### 3 Background and motivation

Current views of cortical function and experimental approaches to understanding the mechanisms of high-level cognitive functions, such as human language, are heavily dominated by what can be described as a corticocentric view. In this view, the cerebral cortex is believed to have the most important role in high-level cognition and behavior, whereas the subcortical structures are seen to have a subservient role, or no role in these functions (Parvizi, 2009). This notion is prevalent enough to raise a concern. In a survey in 2008 about corticocentric trends in the neuroscience field, it was found that 72% of studies in current neuroscience research in which subcortical structures could have been the focus of the study, ended up being ignored. Also, 50% of studies in which subcortical findings were reported chose not to discuss the findings about subcortical structures (Parvizi, 2009). Lacking knowledge about the nature of the connectivity between cortical and subcortical structures might be the main cause of the corticocentric view.

As an example, the thalamus has long been referred to as a passive relay, a necessary link in the flow of information from the periphery to the cerebral cortex. The main responsibility of the thalamus is to transmit perceptual information (visual, auditory, somatosensory) and information in other forms (motor instructions from the cerebellum). But this only accounts for a small part of the thalamus (Sherman, 2007). The largest nucleus of the thalamus, the pulvinar, has extensive connections with the visual cortex and also with the extrastriate cortex. It was proved to receive afferent information from the layers V and VI of these visual areas topographically and project back to the superficial layers of these areas (Guillery & Sherman, 2002). These cortico-thalamo-cortical pathways are not only used to relay peripheral information to the cerebral cortex, but rather play a key component in cortico-cortical communications. The pulvinar is not the only structure in the thalamus that receives afferent information from the cerebral cortex. The LGN of the thalamus is the relay of visual information from the retina to the visual cortex, but also receives modulatory axons from layer VI of the primary visual cortex (Sherman & Guillery, 2009). The exact function of the modulatory axons from layer VI of the primary visual cortex to the LGN is still not clear, but it is a useful example of why the thalamus should not be treated as a mere relay.

The interconnections between the thalamus and the cerebral cortex are key to understanding thalamic function. An early method to obtain thalamocortical connections was to study the retrograde degeneration of thalamic cells when cortical structures were damaged by local lesions (for a brief introduction, see Sherman & Guillery, 2009). For example, if a retrograde degeneration of the LGN of the thalamus was observed along with a limited lesion in the visual cortex, earlier investigators could speculate that this structure is interconnected with the visual cortex. This method has now been superseded by more modern methods that rely on axonally transported tracers. Restricted cortical injections of transported tracers in specific layers could show which thalamic cells send axons to a given area (e.g., Parent et al., 1999). Nevertheless, it has limited application on human beings as it is an invasive method.

Recent advances in non-invasive structural imaging have opened new approaches for investigating *in vivo* white matter structures in human beings. Among them, DWI allows for indirect estimation of the axon group orientations by measuring the motion of water protons (Bammer, 2003; Mukherjee et al., 2008). This procedure of reconstructing white matter tracts from DWI data is conventionally called *tractography*. Tractography has proven successful in quantitatively measuring the structural connectivity between different brain structures (Aydogan et al., 2018). It has been used to investigate thalamocortical white matter fibers (Johansen-Berg et al., 2005; Klein et al., 2010; Traynor et al., 2010). More details in this regard will be reviewed in chapter 4. In the first two studies of this thesis, we will use tractography to reconstruct specific thalamocortical white-matter tracts, and propose precise and reproducible protocols that can be used by the scientific community for future studies concerning thalamocortical pathways. The first study will focus on the first-order thalamic tracts that serve to relay peripheral and cerebellar input to the cerebral cortex. The second study will focus on the high-order thalamic tracts that connect the anterior and mediodorsal thalamus with cortical structures. In the two protocols, we will adopt a probabilistic atlas to segment the human thalamus to obtain precise and reliable individual thalamic nuclei, which allows tracking white-matter fibers from DWI data in a more precise and accurate fashion. The two proposed protocols will be validated on a large dataset to prove different reproducibility aspects. In the end, I will wrap the two

protocols into containers that are easy to use and guarantee reproducibility for other researchers who are interested in thalamic structure connectivities.

In the third study, I will examine the involvement of the thalamus in some main human language systems. As will be introduced in chapter 5, the regionalization of language functions in the human brain has started since the work of Broca and Wernicke in the 19th century. After then, many influential neurobiological models were proposed to address the underpinnings of human language functions, either in a general approach or focused on specific language systems (such as reading models, speech comprehension and production models). Most of these models have focused on cortical structures across the cerebral cortex, while ignoring the contributions of the thalamus in human language function. Given the extensive connections between the thalamus and the cerebral cortex, it is worth investigating the involvement of the thalamus in human language systems. The three main human language systems, reading, speech comprehension and speech production, rely on three sensorimotor information processes: visual, auditory and motor information, respectively. The thalamus is the critical hub to relay this sensorimotor information from the periphery and cerebellum to primary sensorimotor cortices. More specifically, the three first-order thalamic nuclei are responsible for this labor: LGN relays visual information, medial geniculate nucleus (MGN) and ventral lateral nucleus (VLN) relay auditory and motor information respectively. These three nuclei also receive feedback axons from the primary sensorimotor cortices, which provide the neuroanatomical basis for them playing roles beyond being mere relays. Thus, in Study 3, I will examine the involvement of three first-order thalamic nuclei during specific language tasks using task-based functional MRI.

In the following chapters, I will first review the structure and function of the thalamus, the white-matter fiber connections of the thalamus with cortical and subcortical structures in chapter 4. Then, in chapter 5, I will provide an overview of the history of the neurobiology of language and some influential neurobiological models of language. Following that, I will present the empirical part of the present doctoral dissertation, which contains three studies. Study 1 (chapter 6) and Study 2 (chapter 7) investigate first-order and higher-order thalamic tracts with the aim of developing reproducible protocols to reconstruct them with DWI data. Study 3 (chapter 8) will be focused on the

thalamic involvement in different human language systems, including reading, speech comprehension and production. Finally, chapter 9 will provide a general discussion of the overall work conducted in the present doctoral dissertation.

# 4 Thalamus

## 4.1 General introduction of the structure

The thalamus refers to a small gray matter structure on each side of the midline, lying on the dorsal diencephalon (Figure 4.1A). Its medial surface makes up the lateral wall of the third ventricle. This oval structure measures about 3 cm in length and makes up 80% of the diencephalon in humans. Although the thalamus mainly consists of gray matter, a Y-shaped white matter structure named internal medullary lamina travels through it from posterior to anterior. It branches at the anterior section, separating the gray matter mass into three parts: the anterior, the medial and the lateral (Figure 4.1B). The customary understanding of thalamus function believes that it serves as a relay from periphery to cortex. Virtually all information reaching the cortex (with the exception of the olfactory information) must pass through the thalamus (Sherman, 2005). Nowadays, the understanding of the thalamus and its functional role has developed and recent findings over the last 15-20 years have shown that the relay function is not the only role played by the thalamus in brain functioning. The thalamus continuously plays a critical role in further cortical information processing, by acting as a hub that transfers information between cortical structures *via* multiple cortico-thalamo-cortical white-matter routes. The thalamus is not a homogeneous structure; it has a very complex internal organization. It consists of several structurally and functionally distinct cell groups, or nuclei, which are usually named according to their topographic location.

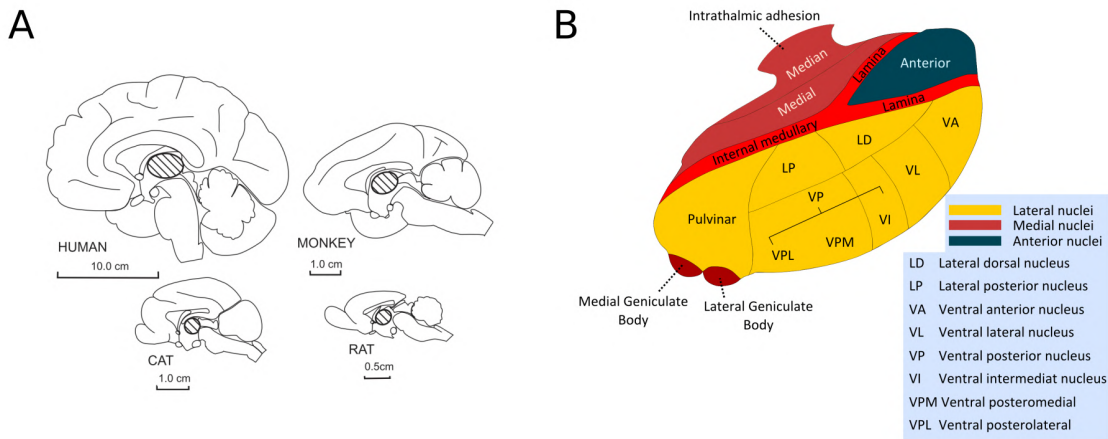


**Figure 4.1. A)** Midsagittal view of the thalamus from a human, a monkey, a cat, and a rat to show the position and relative size of the thalamus (diagonal stripes). Figure adapted from Sherman & Guillery 2006. **B)** The internal medullary lamina separates the thalamus into three parts: anterior, medial and lateral. Figure adapted from Wikipedia (<https://en.wikipedia.org/wiki/Thalamus>).

## 4.2 Thalamic atlases and nuclear divisions

The complexity of the internal organization of the thalamus has made it difficult to reach a consistent and derivable scheme about how to categorize and label its nuclei. Figure 4.2 shows some different parcellation schemes in the history of thalamus research. The differences on how to parcellate the main divisions of the thalamus are obvious, regardless of different naming of individual structures. These parcellation differences are mainly due to the existence of great individual variations of thalamic topography, age/disease-related changes, and also differences of perspective among researchers (Mai & Majtanik, 2019). Among these three factors, the largest variation in parcellation schemes might come from the differences in perspective among researchers. Figure 4.3 shows how different specialists delineate and name the thalamic nuclei on the exact same thalamus section. Although it is clear that the thalamic nuclei should be distinguished by anatomically significant features and named intelligibly, appreciable differences with respect to segmentation and terms being used for the thalamic nuclei can be noticed among those maps. Researchers with different training backgrounds, trained in groups with a given history or tradition in the way of segment and classify thalamic nuclei, experience with animal or human brain, and perspective towards thalamic function could possibly lead to diverging parcellation schemes.

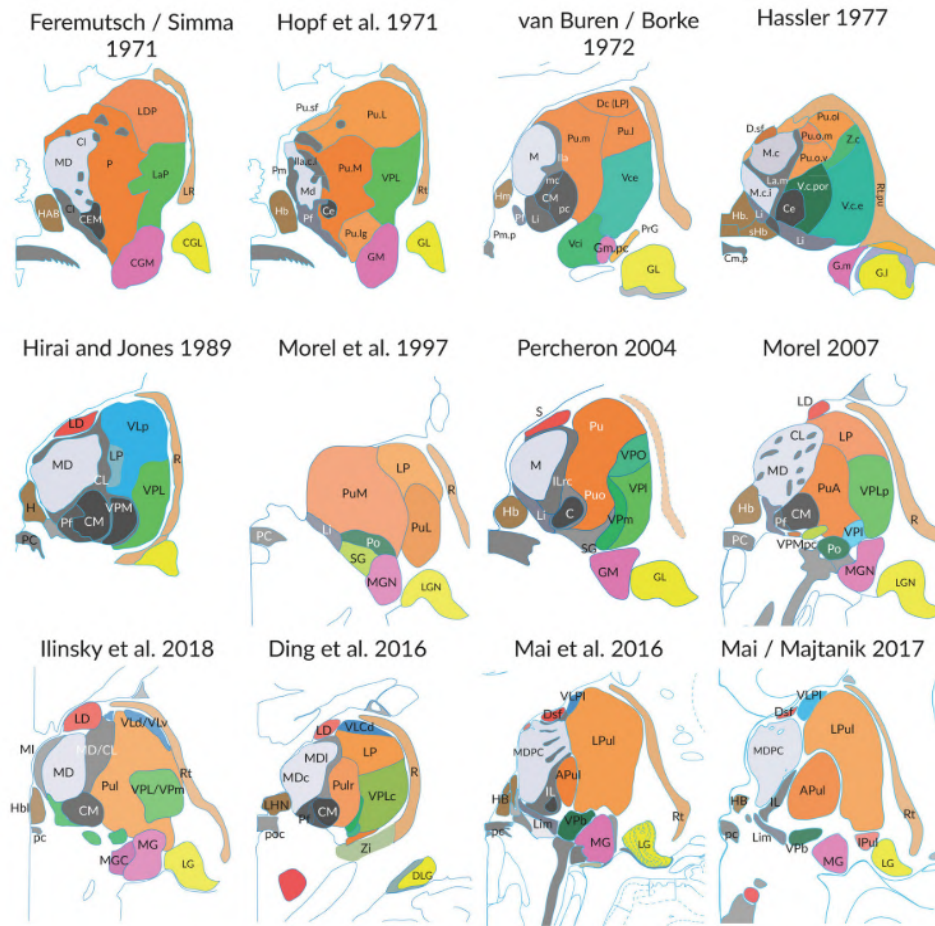


**Figure 4.2.** The profile of 12 coronal sections through the thalamus of different brains cut at the level of the posterior commissure. Figure adapted from Mai & Majtanik 2019.

Sometimes also the same researcher or research group has adopted different parcellation and terminology throughout their academic life. For instance, in Mai & Forutan’s chapter *Thalamus* from the book “*The Human Nervous System*” (Mai & Forutan, 2012), they classify the nuclei into six groups: superior region, medial region, lateral region, intralaminar formation, periventricular formation and posterior formation. In total, they reported 28 anatomically and functionally distinct structures. While in 2019 (Mai & Majtanik, 2019), after quantitatively comparing several atlases, Mai and Majtanik described 9 thalamic nuclear groups that have different structure than it in Mai & Forutan (2012). For example, in Mai & Forutan (2012), the anterior nuclei (anteroventral nucleus, anteromedial nucleus, anterodorsal nucleus, dorsal superficial nucleus) are defined as the superior group, while the same nuclei are grouped into the anterodorsal group in Mai & Majtanik (2019).

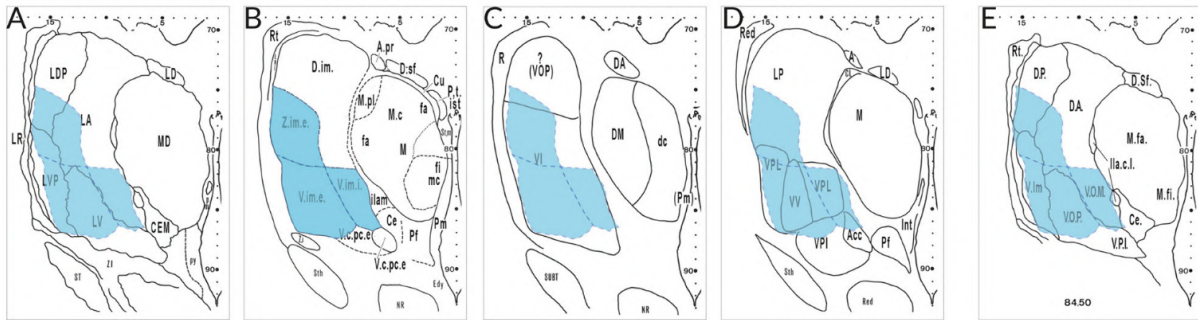


**Figure 4.3.** Different parcellation scheme and terminology on the same thalamus section by different specialists (from A-E). The ventrointermedius region outlined by the second specialist (B) was superimposed over all the five delineation diagrams (blue color) to illustrate the difference of parcellation and terminology among specialists.

In this thesis, I will adopt a probabilistic atlas that combines *ex vivo* MRI images and histological data to describe human thalamic nuclei (Iglesias et al., 2018), in which nuclear groups and thalamic nuclei were delineated based on the characterization of the human and mammalian thalamus by (Jones, 2012). This atlas was proposed by our research group in collaboration with researchers from other institutes. It consists of seven thalamic groups: *anterior, lateral, ventral, intralaminar, medial, posterior, and others* that consist of 26 well-defined thalamic nuclei (see Table 4.1 and Figure 4.4). This atlas was built using manual delineation of 26 thalamic nuclei on the histological images of 12 whole thalami from six human brain samples, combined with manual delineation of the whole thalamus and surrounding structures in *in vivo* MRI T1 images from 39 subjects. The advantage of this atlas is that it is built upon 3D reconstructed histological data, and there is an automated segmentation tool accompanying it. The tool, part of the Freesurfer neuroimaging analysis package, segments the thalamic nuclei from *in vivo* MRI images using Bayesian inference and reliably obtains thalamic nuclei in individual-subject space.

Table 4.1 A list of all the nuclei in the atlas proposed by Iglesias et al. (2018).

Group	Color	Abbrev.	Nucleus	Definition	
Anterior	Dark Green	AV	Anteroventral	Well defined nucleus, starting very rostrally. Continued by the LD. Small/medium sized neurons. We include the anterior medial and anterior dorsal nuclei into the AV.	
Lateral	Light Green	LD	Laterodorsal	Made up of small cells, pale and homogeneously distributed.	
	Blue	LP	Lateral posterior	Group of loosely arranged small and medium neurons. It continues the ventral lateral nucleus an its posterior part (VLp) caudally, as far as the PuA.	
Ventral	Brown	VA	Ventral anterior	Located at the anterior pole of the thalamus, and formed by medium size neurons crossed by bundles of fibers.	
	Orange	VAmc	Ventral anterior magnocellular	Formed by big and dark neurons, loosely arranged.	
	Light Green	VLa	Ventral lateral anterior	Formed by small neurons in clusters, in the dorsolateral part of the nucleus.	
	Yellow	VLp	Ventral lateral posterior	Made up of large neurons, loose appearance.	
	Pink	VPL	Ventral posterolateral	Formed by small and medium sized neurons from the ventral part of VLp to the Pul and PuL. The medial portion (ventral posteromedial nucleus) is included in our definition of VPL.	
	Light Green	VM	Ventromedial	The neurons are similar to VA neurons, but without bundles of crossing fibers. It lies ventral to VA.	
Intralaminar	Brown	CeM	Central medial	Formed by a compact group of dark neurons, located close to MV-Re and Pv.	
	Light Green	CL	Central lateral	Made up of big neurons, arranged in clusters. It lies dorsal to the MD, lateral to MDI, and underneath AV and LD.	
	Purple	Pc	Paracentral	Lateral to MDI. Medial to VLp. Small and connected islands, loose.	
	Yellow	CM	Centromedian	Formed by small, condensed neurons. It is surrounded by fibers of the internal medullary lamina.	
	Blue	Pf	Parafascicular	Formed by small and compact neurons. It lies ventral and medial to the CM.	
Medial	Purple	Pt	Paratenial	Rostrocaudally oriented group of small neurons along the stria medullaris.	
	Blue	MV-re	Reuniens (medial ventral)	Rostrally situated, it consists of a mix of large and small neurons. Fused with the other side through the adhesion interthalamica. Anteroventral to CM and medial to VA.	
	Brown	MDm	Mediodorsal medial magnocellular	Made up of big and darkly stained neurons, sometimes in irregular groups at the ventral part.	
	Light Green	MDI	Mediodorsal lateral parvocellular	Smaller neurons which form varied forms of groupings. Bordered by the Pc, CL and Pf ventrally.	
	Posterior	Dark Blue	LGN	Lateral geniculate	Formed by magnocellular layers ventrally, and parvocellular dorsally.
		Light Green	MGN	Medial Geniculate	Located medial and posterior to the LGN. It is made up of three parts: magnocellular, dorsomedial, and ventromedial.
Pink		L-SG	Limitans (suprageniculate)	Made up of medium and large, deeply stained neurons, which form islands with an irregular profile. It lies on top of the pretectal complex.	
Light Blue		PuA	Pulvinar anterior	Group of neurons located ventromedially to the LP.	
Cyan		PuM	Pulvinar medial	Formed by small and pale neurons of uniform appearance and distribution. It lies at the posterior end of the thalamus.	
Light Blue		PuL	Pulvinar lateral	Big in size, it occupies most of the lateral part of the caudal thalamus. It is crossed by many fibers.	
Light Blue		PuI	Pulvinar inferior	Located ventrally and laterally to the PuM, and formed by small and medium neurons.	
Others	Red	R	Reticular	Groups of medium or large neurons, which wrap the thalamic nuclei. Traversed by numerous bundles of fibers along its extent, and separated from the VA, VLa, VLp, VPL, PuL by the external medullary lamina.	

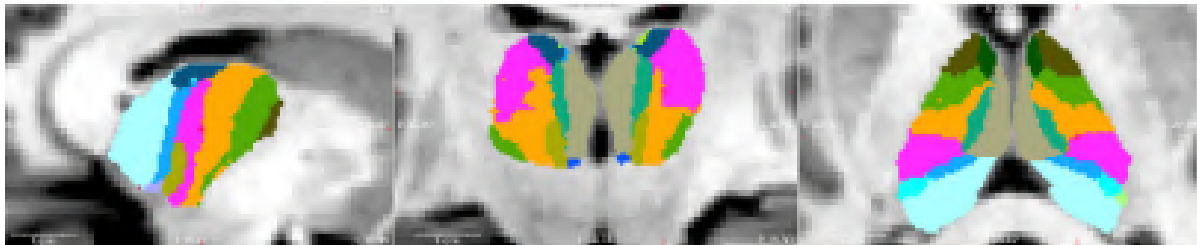


**Figure 4.4.** The atlas of the thalamus and its companion segmentation tool used in the empirical studies of the present doctoral dissertation, superimposed on sagittal (left), coronal (middle), and axial (right) slices of a brain MRI scan. The color map is described in Table 4.1.

### 4.3 Thalamic nuclei segmentation methods

Recent advances in neuroimaging technologies and methods offer a window to study the human brain *in vivo*, which indeed is changing our understanding of the thalamus. With MRI, we are able to investigate thalamic nuclei from different approaches, for example, structural MRI, functional MRI and diffusion MRI. Accurate segmentation of individual thalamic nuclei in structural MRI is a prerequisite for most MRI-based studies to quantitatively investigate structure and function. It also

allows higher specificity and more precision for surgical planning and placement of deep brain stimulation implants. With the advance of neuroimaging technologies and data analysis algorithms, many automated segmentation approaches have been proposed to delineate these thalamic nuclei.

One popular approach to define boundaries between thalamic nuclei is based on diffusion imaging techniques. Diffusion imaging measures the apparent diffusion properties of water. In brain white-matter fibers, the principal diffusion direction of water corresponds to the direction of the fibers. Thus, it is possible to identify brain white-matter fiber bundles by measuring the principal diffusion direction in each voxel using diffusion imaging methods. Given the fact that the thalamus is virtually connected with the entire cerebral cortex, and distinct thalamic nuclei have different structural connectivity patterns, it is possible to separate these nuclei based on their structural connectivity with different cerebral cortex regions. The first studies using this approach were published by Tim Behrens and colleagues (Behrens et al., 2003; Johansen-Berg et al., 2005). They used probabilistic tractography to segment the thalamic nuclei according to the white-matter connections between thalamic nuclei and predefined cerebral regions based on known neuroanatomy (Figure 4.5A). First, the cerebral cortex is segmented into well defined cortical zones, and then tractography between each thalamic voxel and those cortical zones is performed. By quantitatively measuring the structural connectivity between different thalamic voxels and cerebral regions, combining with existing knowledge of the white-matter fibers connecting different thalamic nuclei and specific cerebral regions, it is possible to classify thalamic voxels into different nuclei or nuclear groups. In general, this approach lacks precision and specificity. For example, the segmentation method proposed by Behrens et al. (2003) and Johansen-Berg et al. (2005) separates the thalamus into only seven regions. Each of them covers more than one structurally and anatomically different thalamic nuclei (e.g. the red thalamic region in Figure 4.5A includes LGN, parts of inferior pulvinar and intralaminar nuclei). Another disadvantage of this approach is that it can not detect those thalamic voxels that are not directly connected with the cerebral cortex, such as the ones connected to subcortical regions and the cerebellum. There are other thalamic segmentation algorithms that adopt

similar approaches using diffusion tractography (e.g., Lambert et al., 2017 in Figure 4.5B; Abivardi & Bach, 2017; Kasenburg et al., 2016; Traynor et al., 2010).

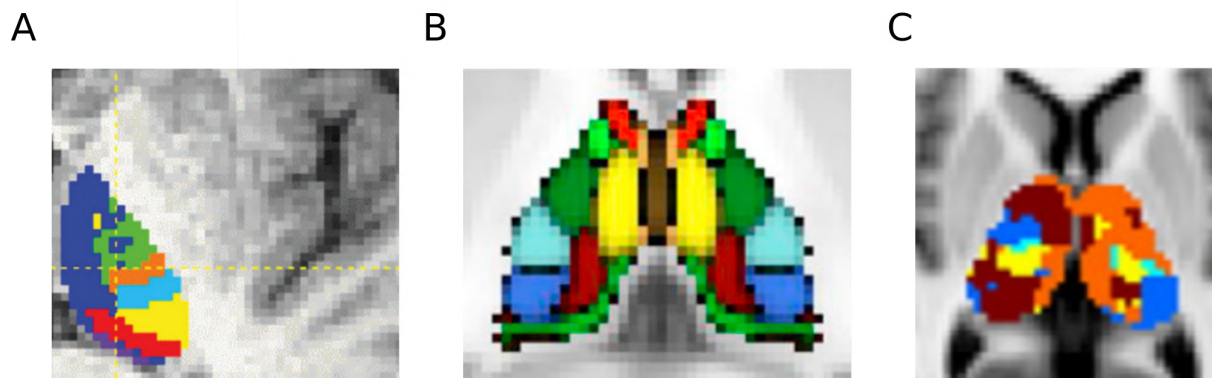


**Figure 4.5.** **A)** Thalamic segmentation based on diffusion tractography from Behrens et al. (2003) and Johansen-Berg et al. (2005). Figure adapted from Behrens et al. (2003). **B)** Similar approach to segment thalamic nuclei using diffusion tractography in Lambert et al. (2017). Figure adapted from Lambert et al. (2017). **C)** Thalamic segmentation proposed in Hale et al. (2015) based on function connectivity between thalamus and cerebral cortex. Figure adapted from Hale et al. (2015).

Another way to segment the thalamus based on diffusion-related methods is to use local diffusion information (Duan et al., 2007; Mang et al., 2012; Wiegell et al., 2003). This approach does not require manual segmentation of the cerebral cortex, or extensive white-matter fiber tracking. This segmentation method first calculates the local diffusion information for each voxel in the thalamus from diffusion imaging data, then classifies voxels that have similar diffusion information to specific thalamic groups. This approach in general requires less computation time than the one mentioned above, but it has the disadvantage of not being able to detect small thalamic nuclei either due to the diffusion image resolution or partial volume effects.

It is also possible to segment the thalamus based on resting-state functional MRI (Hale et al., 2015; B. Ji et al., 2016). Similar to the idea of diffusion-based segmentation, resting-state-based segmentation methods measure the connectivity between thalamic regions and pre-defined cerebral regions. This method measures functional connectivity based on the temporal coincidence of blood-oxygen-level-dependent (BOLD) signals, instead of structural connectivity. This approach suffers from the same disadvantage, it lacks precision and specificity. For example, Hale et al. (2015) segmented the thalamus into only five coarse subregions based on resting-state functional connectivity, since they separated the whole cerebral cortex into five regions (Figure 4.5C).

As mentioned in section 4.2, the atlas used in this thesis has a companion automated segmentation tool that can be applied to *in vivo* MRI structural images (Iglesias et al., 2018), and it will be used to obtain individual thalamic nuclei. The segmentation tool uses Bayesian inference to directly apply the probabilistic atlas derived from *ex vivo* MRI and histological data on *in vivo* MRI structural images (further details can be found in Iglesias et al., 2018). It allows dividing the thalamus into 26 nuclei (as shown in Table 4.1 and Figure 4.4 ) in individual space. The yielded volumes of the nuclei are proved to have reasonable agreement with another histological atlas of the thalamus (Krauth et al., 2010). This tool also demonstrated excellent test-retest reliability and robustness against changes in MRI contrast. Moreover, it is implemented in FreeSurfer, a popular neuroimaging software for processing, analyzing, and visualizing human brain MR images, facilitating access for the broader neuroimaging community.

## 4.4 First-order relay thalamic nuclei

Essentially the majority of information we perceive from the world or ourselves reaches the cerebral cortex *via* the *thalamus*. Thalamus in this way serves as a relay, which receives information from the eye, ear or cerebellum and passes it to the cerebral cortex (Sherman, 2005). Beyond that, there are reports suggesting that thalamus also receives information from the cerebral cortex and modifies it, then passes it to either the same or another cortical region (Guillery, 1995).

Conventionally, the thalamic nuclei can be divided into two types by the afferent source: first-order relay nuclei receive afferents from primary afferents pathways, and higher-order relay nuclei receives no or few afferents from periphery but instead receives afferents from cortex. First-order relay nuclei also receive afferents from the cerebral cortex, though minorly (Sherman, 2007, 2012). Anatomical evidence shows that different thalamic nuclei are involved in this labor dissociation. For example, the MGN receives acoustic information from the auditory nerve and relays them to the auditory cortex *via* the acoustic radiation (Brugge, 2013; Guillery & Sherman, 2002; Ramcharan et al., 2005), while the mediodorsal nucleus (MD) is believed to receive inputs from the PFC instead of the periphery (Anastasiades et al., 2021; Mitchell, 2015; Pergola et al., 2018). Roughly, the first-order relay nuclei include the LGN, the MGN and VLN. The higher-order relay

nuclei typically include the anterior nuclear complex (AN), MD, and pulvinar. In the current section, I will discuss the above-mentioned four first-order relay thalamic nuclei. The higher-order relay nuclei will be discussed after.

#### 4.4.1 Lateral geniculate nucleus

The LGN is a small, egg-shaped nucleus located in the ventral and posterior part of the thalamus. It receives visual information directly from retinal ganglion cells and relays information to the visual cortex through the optic radiation (OR). The LGN activation can be detected using functional MRI (fMRI) techniques with a variety of visual stimuli, for example, flickering checkerboard stimuli (Chen, Kato, Zhu, Strupp, et al., 1998; Kastner et al., 2004), moving dots (Büchel et al., 1997), faces (Prochnow et al., 2013), or visual objects (Zafar et al., 2015). It has also been found functional engagement of the LGN during visual imagery (Chen, Kato, Zhu, Ogawa, et al., 1998) and visual attention modulation tasks (O'Connor et al., 2002), which extended its simple relay role in visual processing to a relatively higher level.

The OR fibers arise from the LGN, pass through the sublenticular and retrolenticular portions of the internal capsule, and end in the visual cortex bordering the calcarine sulcus on the medial surface of the occipital lobe. These fibers follow a curved course around the temporal horn and atrium, where they separate from the ventricular surface (De Benedictis et al., 2014). The OR fibers can be divided into 3 portions after its origin: the anterior bundle, the central bundle, and the posterior bundle (Párraga et al., 2012). The important role that the OR plays in visual processing has attracted researchers' interest in reconstructing OR using non-invasive diffusion techniques. Over the last decades several studies have reported successful reconstruction of the OR with diffusion data with a variety of approaches (Figure 4.6; Bassi et al., 2008; Behrens et al., 2003; Benjamin et al., 2014; Sherbondy et al., 2008). The reconstruction methods adopted vary in several ways, such as seeding strategy, fractional anisotropy threshold, streamline length and angle restriction.

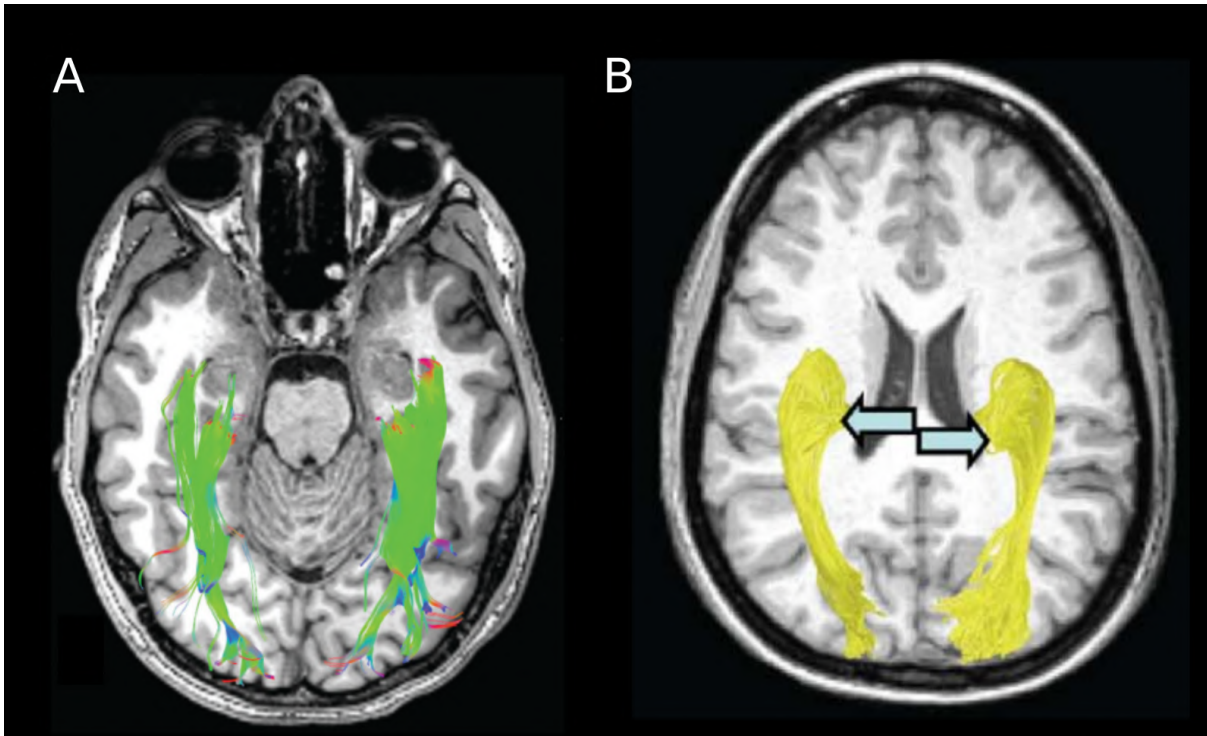


**Figure 4.6.** The OR reconstructed in **A)** Benjamin et al. (2007); **B)** Sherbondy et al. (2008).

#### 4.4.2 Medial geniculate nucleus

The MGN, also known as medial geniculate body, is an oval mass located medially and posteriorly on the ventral lateral surface of the thalamus (Figure 4.1B). It is the synaptic station for acoustic information flowing from the inferior colliculus to the auditory cortex (Winer et al., 2005). Although the MGN can be further subdivided into three nuclei, due to the relatively small volume of human MGN and typically limited spatial resolution of MRI images, the current work will not differentiate the MGN subregions regarding the structure and function, but will take the MGN as a whole.

The acoustic radiation (AR) fibers constitute the major input of the MGN to the ipsilateral primary auditory cortex (A1, BA 41, and partly 42 or Heschl's gyrus) which lies in the temporal operculum. The AR maintains a topographical representation on the cortex, similar to the somatosensory and motor projections, but also presents a tonotopic organization (see Cherches, 2016). Functionally, the AR is basically the main sensory pathway relaying acoustic information from the MGN to the A1 (Berman et al., 2013), and being implicated in multiple high-level behaviors such as speech processing (Ojemann, 1991). A recent study showed that the task-dependent modulation of the

left MGN was increased when processing speech with noise background in contrast to the clear speech processing (Mihai et al., 2021). There is an hypothesis that some phonological deficits are caused by abnormal AR or MGN structure. For example, histological alterations were found in MGN after postmortem examination of readers with dyslexia (Galaburda et al., 1994). Additionally, one functional MRI study found that the MGN activation pattern is different when the task required attending to phonemes compared with other speech features in readers with dyslexia, and the activation level is correlated with the scores of the dyslexia diagnosis (Diaz et al., 2012). Diffusion evidence also showed that the connectivity strength of AR is reduced in readers with dyslexia compared to normal readers (Tschantscher et al., 2019).

There are several studies trying to track the course of the AR based on *in vivo* diffusion MRI data (Behrens et al., 2007; Berman et al., 2013; Javad et al., 2014; Maffei et al., 2018, 2019; Profant et al., 2014). The AR, as a non-dominant fiber group, crosses with other fibers, which results in multiple-orientation signals in voxels at the crossing section. Thus, the AR is more difficult to identify with a single direction per voxel tractography model. Behrens et al. (2007) defined the MGN as a cuboid medial to the LGN and started tracking from there to the A1 using a probabilistic algorithm. In Behrens et al's (2007) study they failed to reconstruct the AR with single fiber tractography, but succeeded when they used multi-fiber tractography. In a more recent study, Maffei et al. (2019) explored how the diffusion MRI acquisition parameters and tracking parameters can affect the reconstruction of AR. They found that higher b-values ( $\geq 5,000$  s/mm<sup>2</sup>) and more gradient directions ( $\geq 128$ ) increase the accuracy of the reconstruction for both probabilistic and deterministic tracking algorithms, but with low b-values ( $\leq 3000$  s/mm<sup>2</sup>) only the probabilistic algorithm can successfully reconstruct the AR (Figure 4.7).

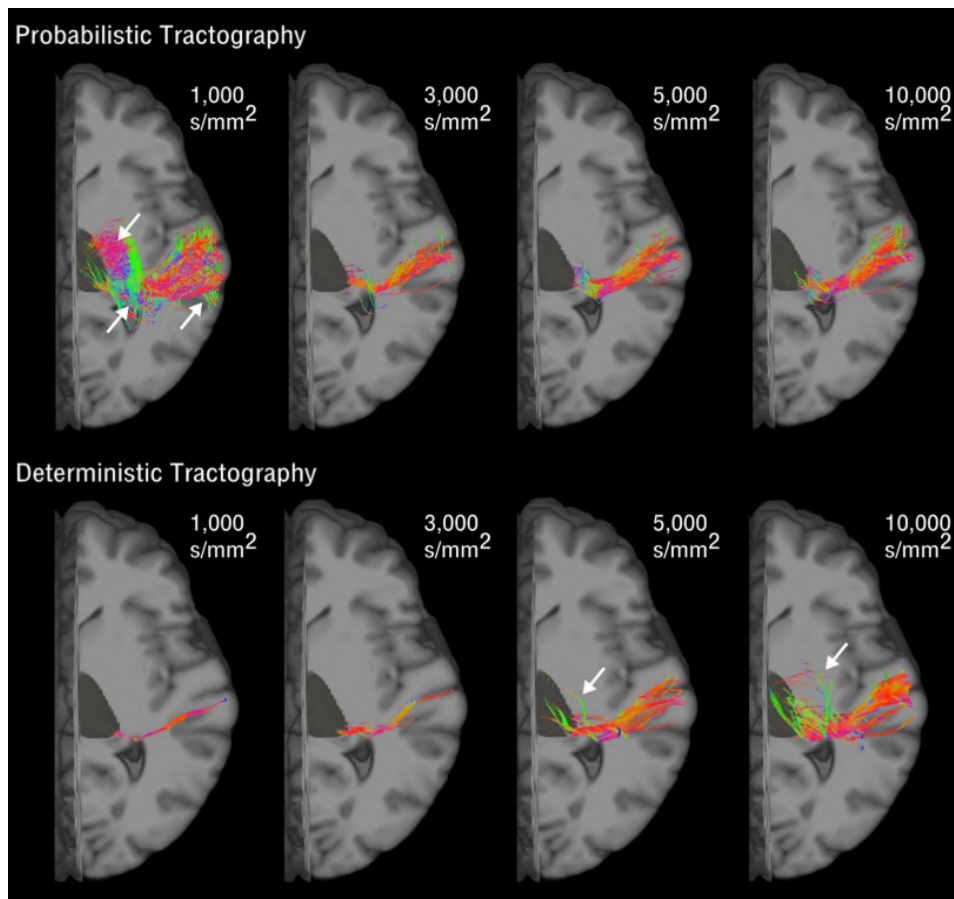


**Figure 4.7.** The effect of DWI acquisition parameters and tracking algorithms on the AR reconstruction. These images from one representative subject showed variant reconstruction of the AR when applying both probabilistic and deterministic algorithms to DWI data with different diffusion b-value shells. The white arrows indicate the false positives of the reconstruction. Figure adapted from Maffei et al. (2019).

#### 4.4.3 Ventral lateral nucleus

The VLN, lying in the ventral lateral part of the thalamus, is an integrative hub for motor control. The major inputs to VLN are from deep nuclei of the cerebellum, pallidum and the substantia nigra. In turn, it projects to the motor areas of the cerebral cortex. On top of that it also receives feedback information from the motor areas. Topographically the VLN can be divided into two subnuclei: the anterior VLN (VL<sub>a</sub>) and the posterior VLN (VL<sub>p</sub>), two anatomically, histochemically and functionally different subregions. The involvement of the VLN in motor functions has been demonstrated using simple motor-related tasks, such as finger tapping (Lutz et al., 2000; Mallol et al., 2007). Evidence also found that activation of the VLN in a more complex motor task decreased after intensive learning (Lehéricy et al., 2005). Success of speech production needs motor execution, thus

requires the involvement of the VLN. Tourville & Guenther (2011) included VLN as one important node in their speech production neuroanatomy model. Patients with VLN lesions have been found to exhibit difficulties in naming objects and in short-term verbal memory (see review Petrovici, 1980).

The main fiber group connecting VLp with cerebellum is known as the dentatothalamic tract (DT). The DT originates from the dentate nucleus in the cerebellum, projects *via* the superior cerebellar peduncle (i.e., brachium conjunctivum) to terminate in the contralateral VLp after decussating to the contralateral red nucleus (Coenen et al., 2014; Kwon et al., 2011). The DT is the main cerebellar efferent tract and it is mainly involved in movement control and multiple motor behaviors such as speech production (Ojemann, 1975). Lesions to the DT can produce abnormal movement, including ataxia, tremor, and dystonia (Kwon et al., 2011). Some effective surgical interventions for patients with essential tremor often target the VLp and adjacent white-matter tracts (Dallapiazza et al., 2019). The VLN projects to the primary motor cortex (M1) *via* the motor radiation (MR, Ilinsky & Kultas-Ilinsky, 2002). The VLN also projects to the preSMA (BA 6), which is an area of the motor cortex that traditionally has been assigned as responsible for updating motor plans and learning new motor sequences (Hamani et al., 2006). Functionally, this VLN-M1 primary pathway is thought to be implicated in transmitting cerebellar inputs to the M1.

The fact that the DT travels through deep and small nuclei makes it difficult to be identified with DWI techniques. There are only a handful of studies that successfully reconstructed the DT from DWI data in healthy populations (Figure 4.8A; Kwon et al., 2011; Meola et al., 2016) or patients (Figure 4.8B; Coenen et al., 2011, 2014; Nowacki et al., 2019). In Nowacki et al.'s (2019) study, they tested four different tracking protocols to identify the DT, which led to divergent results. All the four procedures were based on deterministic algorithms, but no probabilistic algorithms were tested. Some studies also reconstruct the DT and MR as one single tract (Q. Ji et al., 2019; Vo et al., 2015). Hyam et al. (2012) investigated the white-matter fiber bundles between VLN and motor cortex and successfully reconstructed the MR. But this study only used part of the VLN (referred as *ventralis intermedius* and *ventralis oralis* in their study) as seed when applying the tractography.

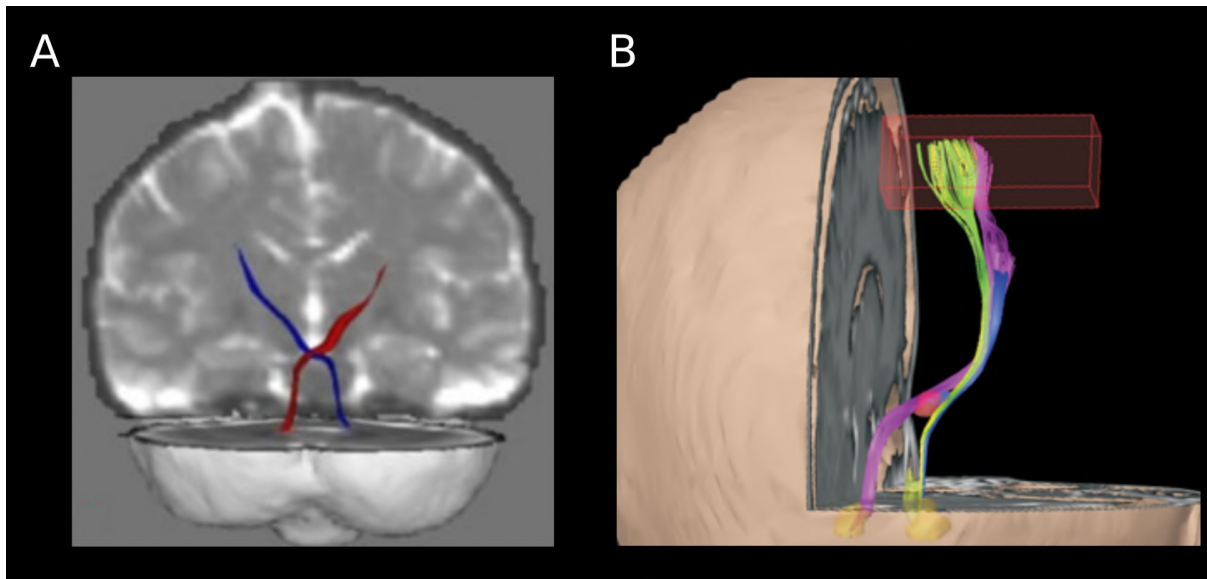


**Figure 4.8.** DT reconstructed in **A)** Kwon et al., 2011 and **B)** Nowacki et al., 2019 (four colors indicate the four different methodologies of tracking the DT).

## 4.5 Higher-order relay thalamic nuclei

In contrast to the first-order relay nuclei, which receive afferent inputs from peripheral sensory centers (retina, auditory and somatosensory relays, cerebellum, etc.) and relay information to the cerebral cortex; the higher-order relay nuclei receive few or no afferents from periphery, but instead receive their afferents from the cerebral cortex. The major thalamocortical fibers from the first-order relay nuclei project to the primary cortical areas, such as visual cortex, auditory cortex, somatosensory and motor cortex, whereas the thalamocortical fibers from the higher order nuclei send information to areas that are involved in more complex functions and are traditionally called association cortical areas (Guillery, 1995). Unlike a clear classification of first-order nuclei, the higher-order nuclei are far from being fully defined. Although large inconsistencies remain, the AN, MD and pulvinar are the ones consistently categorized as higher-order relay nuclei.

### 4.5.1 Anterior nuclear complex

The AN is located in the rostral and dorsal part of the thalamus and separated from other dorsal thalamic nuclei by the Y-shaped internal medullary lamina. The AN typically consists of three nuclei: anterior medial, anterior dorsal and anterior ventral nuclei. In the probabilistic atlas proposed by Iglesias et al. (2018), the thalamic nuclei AV actually represents the whole AN. In the

current thesis we will use this thalamic nuclei but with the name of AN to describe the whole anterior nuclear complex. The AN is a critical node in the Papez circuit, which begins in the hippocampus and continues through fornix, reaching to the mammillary body (Parmeggiani et al., 1971). The mammillary body connects to AN with the mamillothalamic tract. The AN in turn projects through the cingulum bundle to cingulate cortex, retrosplenial cortex, which connects to hippocampus, thus completing the circuit (Shah et al., 2012). More specifically, the AN receives afferent inputs from the mammillary body and relays it to anterior and posterior cingulate, and retrosplenial cortex.

The AN has been found involved in memory-related processes. For example, Aggleton & Brown (1999) proposed that the AN contribute to the information retrieval from memory during item absence through the connection with the hippocampus, and that the direct hippocampal-AN connection and the indirect hippocampal-mamillo-AN connection are involved in allocentric spatial memory. A fMRI study also presented a significant involvement of AN in recall tasks but not in encoding tasks (Pergola et al., 2013).

There are some studies that use diffusion data to reconstruct the Papez circuit, which includes the white-matter fibers connection of the AN with other structures involved in this circuit (Concha et al., 2005; Granziera et al., 2011; Wei et al., 2017). However, those studies fail to distinguish the white-matter bundles connecting the AN with other structures separately. For example, the cingulum bundle consists of the white-matter fibers of AN to anterior cingulate, posterior cingulate, and retrosplenial cortex, while in the above-mentioned studies, the cingulum bundle is taken as a whole (Figure 4.9).

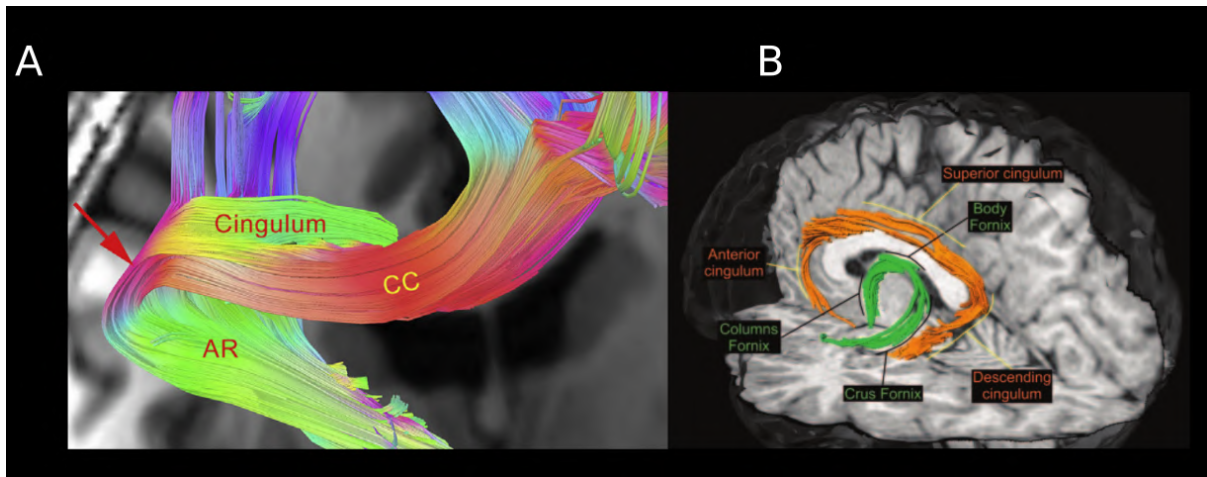


**Figure 4.9.** The cingulum bundle reconstructed from diffusion data in **A)** Wei et al., 2017; **B)** Concha et al., 2005.

#### 4.5.2 Mediodorsal nucleus

The MD is an ovoid structure extending from the level of the intrathalamic adhesion until the level of the habenular commissure. It is relatively easy to distinguish from other structures on most cross-sectional levels since its medial surface borders the third ventricle and the rest is surrounded by the internal medullary lamina with its embedded nuclei. The MD is typically divided into two cytoarchitecturally distinct parts: the medial one-third to one-half is magnocellular in Nissl preparations and the lateral half to two-thirds, which has smaller cells and present parvocellular properties (Jones, 1985). In the present doctoral dissertation, we treat the MD as whole due to the MRI spatial resolution.

The MD is robustly connected with the frontal lobe, more specifically the PFC. Indeed the connection of MD and PFC has been playing an important role in the research history of PFC function: the classic definition of PFC was the cortical projection zone of the MD (Mai & Forutan, 2012). The MD not only projects to PFC but also receives afferents from other structures, such as amygdala (Aggleton & Mishkin, 1984), and the temporal pole (Gower, 1989). The MD has been proposed to be involved in higher cognitive functions *via* its extensive connections with frontal lobe and subcortical structures (Mitchell, 2015; Ouhaz et al., 2018). For example, fMRI research with humans has revealed that the MD-PFC network is activated during successful encoding and retrieval (Pergola et al., 2013). Also, evidence from lesion studies indicates that the damage of MD could

disrupt executive functions, attention control, prospective memory, arousal, motivation, language functions (see reviews, Mitchell, 2015; Pergola et al., 2018).

A number of studies have used diffusion MRI to reconstruct the projections of MD (Figure 4.10; Eckert et al., 2012; Giraldo-Chica et al., 2018; Jakab et al., 2012; Klein et al., 2010; Lambert et al., 2017; Le Reste et al., 2016; Li et al., 2022). Jakab et al. (2012) adopted a probabilistic algorithm to track the white-matter fibers from the lateral and medial MD to the rest of the brain. The probabilistic tractography showed that the lateral MD is the source of fibers projecting to the superior and middle frontal gyri, while the fibers originated from medial MD mainly terminate in the frontal orbital cortex and various temporal loci.

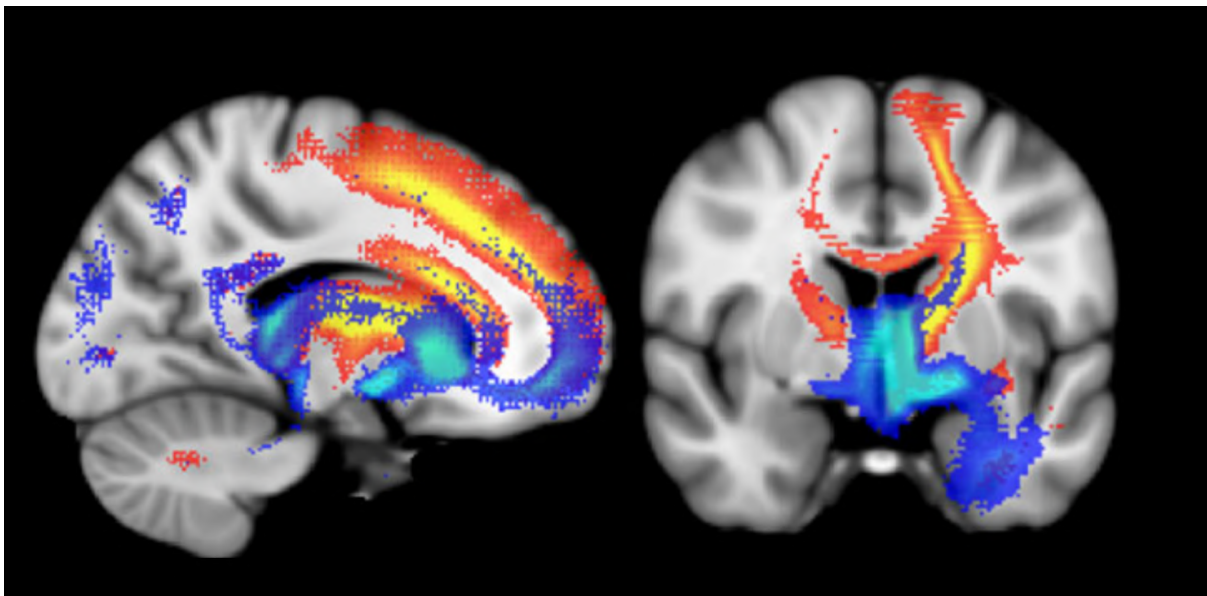


**Figure 4.10.** The tractography of MD with the rest of the brain from Jakab et al. (2012). Warm color voxels indicate the trajectory of white-matter fibers originated from lateral MD and cold color voxels for the medial MD. Figure adapted from Jakab et al. (2012).

### 4.5.3 Pulvinar

The pulvinar lies in the posterior part of the thalamus and it is the largest thalamic nuclear complex, reaching about 30% of its volume in humans (Mai & Forutan, 2012). The pulvinar is typically subdivided into four subnuclei based on neuroanatomical properties (Jones, 1985): anterior, inferior, lateral and medial. This pulvinar subdivision was adopted by the probabilistic atlas used in the current work (Iglesias et al., 2018). Aside from its size, the pulvinar is widely connected with all

the cerebral lobes, which makes it one of the most complex higher-order thalamic structures (Mai & Forutan, 2012).

Specific functions associated with each cortico-pulvino-cortical pathway have been explored in neuroimaging research, but still they are far from being clear (Fiebelkorn & Kastner, 2019). Research have linked the human pulvinar to multiple cognitive functions, such as emotion recognition (Ward et al., 2007), visual attention (Fischer & Whitney, 2012), visual motion (Villeneuve et al., 2005), and fear recognition (McFadyen et al., 2019). Also, there is discussion about the notion that the pulvinar behaves as a ‘connectional hub’ integrating convergent information and then transmitting processed signals to cortical and subcortical structures (Bridge et al., 2016). Yet, little is known regarding whether the pulvinar relay function is to help communication between cortical areas without changing the information being relayed, or the pulvinar also manipulates and processes that information (Sherman & Guillery, 2009).

To date, there are few tractography studies investigating the connections of human pulvinar, mainly due to its complex white-matter connectivity with extensive cerebral cortex. Leh et al. (2008) used diffusion tensor imaging tractography and reconstructed pulvinar tracts (Figure 4.11A). The reconstructed tracts were found to project to the frontal eye fields, prefrontal areas, visual cortex, and parietal association areas. Another tractography study focused on the optic nerve that connects the optic chiasm with pulvinar (Maleki et al., 2012), in which they used the optic chiasm and pulvinar as inclusion ROIs and LGN and primary visual cortex (V1) as exclusion masks (Figure 4.11B). The investigation of the structural connectivity of the pulvinar and its functional role in language-related processes are beyond the scope of the present doctoral work, due in part to its complexity and the limited time. However, this is one of the first research lines we are planning to pursue after the doctoral dissertation.

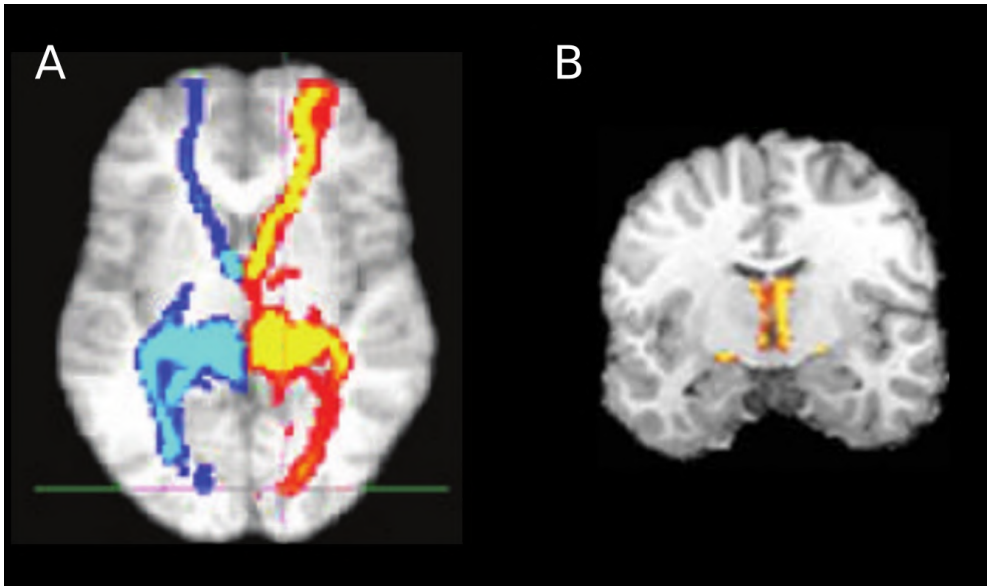


**Figure 4.11.** **A)** Reconstructed tracts that connect the pulvinar with cortical and subcortical structures in Leh et al., (2008). **B)** Optic nerve from optic chiasm to the pulvinar reconstructed in Maleki et al. (2012).

## 5 Neurobiology of language

When we study human language, we are approaching what some might call the “human essence”, the distinctive qualities of mind that are, so far as we know, unique to man.

-Noam Chomsky, *Language and Mind*

As human beings, we live in a world of language. We hear and speak to our friends, relatives, and co-workers. We read novels, newspapers, and textbooks. The ability to process and produce language, more likely than any other abilities, distinguishes humans from other animals. According to some people in Africa, a newborn child is described as a *kintu* (thing), not a *mntu* (person) yet. Only by the acquisition of language does the child become a *mntu* (Fromkin et al., 2003). To understand our humans and human history, we need to understand language. The study of neurobiology of language is one of the many approaches aimed at understanding how we implement language and, more specifically, to describe and explain the relationship between language, an efficient symbolic communication tool, and the brain, a highly complex system.

In this chapter, first I will provide an overview of the history of neurobiology of language. Then I will introduce some modern neuroanatomical models put forward to explain the main language mechanisms. Last, I will present models that are specific to different language modalities.

### 5.1 History

It is well recognized that the first scientific research that brought brain and language together was conducted by the French physician Pierre Paul Broca in 1861. Broca’s patient Louis Victor LeBorgne had severe difficulty speaking. The only word that LeBorgne could say was “tan”. Only after the autopsy of this patient Broca discovered that a portion of the left posterior inferior frontal gyrus (IFG) was damaged (Figure 5.1; for English translation, see Berker et al., 1986). Several months later, Broca was consulted by a second patient named LeLong, who suffered a similar speech production difficulty. After autopsy, Broca found a lesion approximately in the same location as the lesion in LeBorgne’s brain. After being subsequently presented with other cases of speech production difficulty with lesions in the inferior frontal lobe of the left hemisphere, Broca believed he found the

brain structure is responsible for speech production. His detailed documentation built the connection between speech production and the left inferior frontal lobe. This area ended up being called Broca's area.



**Figure 5.1.** The brain of LeBorgne. A lesion is clearly visible in the inferior frontal lobe. Figure adapted from [Small & Hickok \(2016\)](#).

The era of brain localization of language started after Broca's discovery. Another brain area that is often brought up with Broca's area is Wernicke's area. In his famous doctoral dissertation, Carl Wernicke, a German neurologist and psychiatrist, described two patients who cannot comprehend well spoken language (Geschwind, 1974). The autopsy revealed lesions in the left posterior section of the superior temporal gyrus (pSTG). This was the first study linking a specific brain structure with speech comprehension. Although Wernicke's area was brought up with the functional definition of the area where speech comprehension occurs, the widely accepted definition nowadays is based on anatomy: the Wernicke's area often means the left pSTG and supramarginal gyrus (SMG, Binder, 2015).

After the pioneer work of Broca and Wernicke, in 1885, a German physician named Ludwig Lichtheim proposed a language model that integrated language function and brain anatomy (Figure 5.2A) on top of Wernicke's aphasia model (Lichtheim, 1885). He assumed that there is an inborn faculty for language function, the critical elements of which are lying in the left hemisphere. This model is composed of centers and pathways that connect separate centers. He posited that Wernicke's area is involved in language perception, Broca's area is for language production, and the pathway

connecting two regions is assumed to be involved in semantic processing. Both Wernicke and Lichtheim proposed that a damage to the pathway that connects the Wernicke's area and Broca's area could lead to a speech disorder that has problems with spontaneous speech, naming and repetition but with good speech comprehension. Lichtheim preferred to name it as *commissural aphasia* to make a difference between two types of aphasia: one due to damage to Broca's area or Wernicke's area, and the other one due to impaired commissural pathways between the two critical structures.

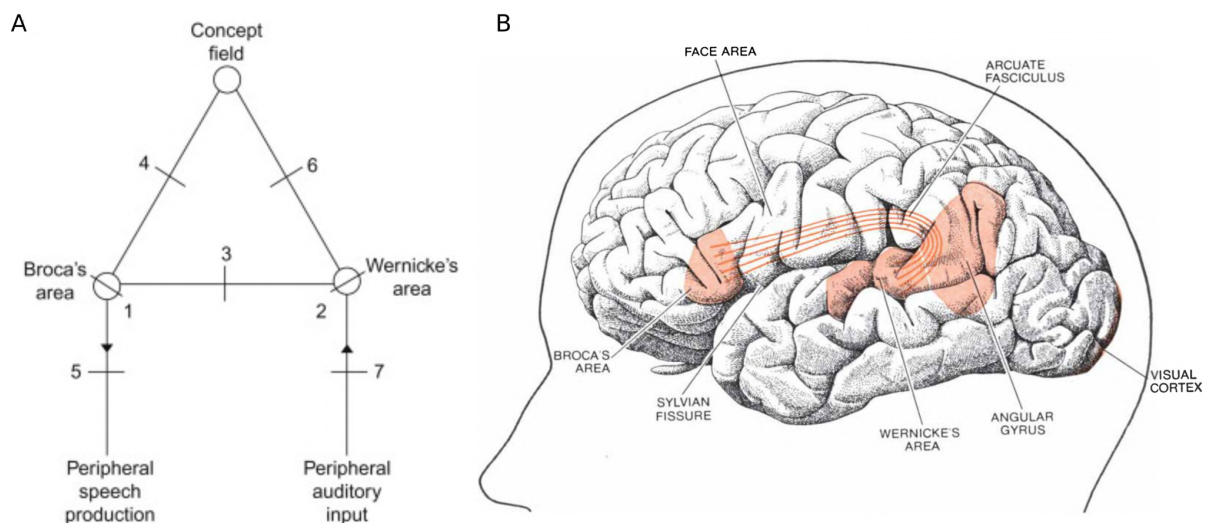


**Figure 5.2.** **A)** Lichtheim's model integrating language function and brain anatomy. Figure adapted from Small & Hickok (2016). **B)** Geschwind's model that reconceptualized from Lichtheim's model. Figure adapted from [Geschwind \(1972\)](#). In this figure, the label of angular gyrus mistakenly covers the posterior of STG and MTG.

Decades later, behavioral neurologist Norman Geschwind presented a connectionist view of the neural mechanisms of human language function on top of the Lichtheim model (Geschwind, 1970, 1972). He adopted most of the assumptions of the Lichtheim model, but suggested that semantic processing has a separate structure as well, most likely involving the inferior parietal lobe (Figure 5.2B). Due to its use of the work from Broca, Wernicke, Lichtheim and Geschwind, this model is often referred to as the Broca-Wernicke-Lichtheim-Geschwind model, and it is also known as the Classic model.

The Classic model has had extensive influence over the research of neurobiology of language in the last few decades and even nowadays. A short online survey conducted within the Neurobiology of Language Society showed that 47% of respondents believed that the Classic model is outdated, yet

it was still considered as a heuristic model (Tremblay & Dick, 2016). The terms Broca's area and Wernicke's area are still widely in use, although there is no consensus definition on them (Figure 5.3).

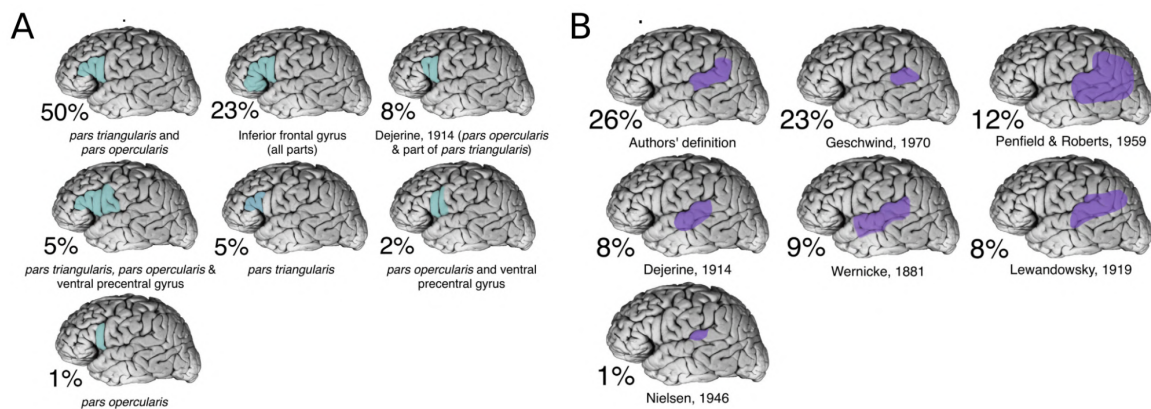


**Figure 5.3.** Anatomical definitions of **A) Broca's area** and **B) Wernicke's area**, and the percentage of respondents to the survey endorsing each definition in Tremblay et al., 2016. Figure adapted from Tremblay & Dick (2016).

When we look back and revisit the Classic model with current knowledge of brain structure and function, we would agree that there are intrinsic flaws in this model due to the neuroanatomy techniques and limited samples at that time. First, the spatial accuracy of the Classic model is quite limited for testing specific hypotheses about the relationships between brain and language. For example, the author's definition on Wernicke's area covers pSTG, part of SMG and AG. Second, the model only focuses on specific "language centers", i.e. Broca's and Wernicke's areas. This is because the model was mainly derived from lesion studies. Now we know that the language functions involve virtually the whole brain, and that the white-matter bundles connecting the cerebral cortex also play critical roles in language function. Third, it lacks linguistic specifications. The model only tried to explain the aphasia restricted to word-level language phenomena, but precluded systematic explanations of any higher level language functions, for example, syntactic or sentence processing.

In the approximately last 30 years, with the advancement of non-invasive brain imaging methods (MRI, PET, MEG, EEG) along with growing linguistic and psycholinguistic knowledge, new data beyond lesion studies were generated focusing on different aspects of language processing, from acoustic phonetics to natural language processing. And the new data resulted in new models, which are relatively more sophisticated both anatomically and cognitively and that integrate the large evidence obtained in terms of function and structure in the last decades. In the following section, I

review and discuss some modern neuroanatomical models that are related to the empirical work conducted in the present doctoral dissertation.

## 5.2 Modern neuroanatomical models

The Classic model of brain and language was based on deficit-lesion relationships. With the new techniques available to study the human brain non-invasively, new neuroanatomical models were proposed from a considerable amount of neuroimaging evidence. These models explain the neuroanatomic mechanisms of language from large-scale data, but basing their proposals on specific levels or language modalities, for example, the model based on lexical level processing (Price, 2000), or models focused on specific language modality (for example, model from Indefrey & Levelt 2004 for language production). The current thesis involves language processing in three modalities: reading, speech comprehension and speech production. Thus for the following part, I will first generally review models that are modality-general, regardless of the architecture level of language process, then I will introduce models that are exclusively derived from empirical data that involve specific language modalities, i.e, models based reading, speech comprehension and speech production.

### 5.2.1 Modality-general models

#### 5.2.1.1 Price's model

One of the modern successors of the Classic model is Kathy Price's model proposed in 2000, one decade after the invention of the functional MRI technique (Figure 5.4, Price 2000). Integrating evidence from neuropsychology and neuroimaging data, with cognitive theories, Price proposed a model of language processing that involves reading, speech comprehension and production.

According to this model, the acoustic computation of speech words involves the superior temporal cortex, and the visual form analysis of written words takes place in the posterior inferior temporal and mid-fusiform gyri. Semantic representation requires a network that includes the angular gyrus and the anterior inferior temporal cortex. As for the speech production component, articulatory planning involves integration of anterior insula and frontal operculum input, and motor control of speech

outputs is computed by the bilateral sensorimotor cortices. This model emphasized semantic processing on top of the Classic model, suggesting specifically the involvement of the angular gyrus and the inferior temporal cortex in semantic processing. But this model mainly takes empirical evidence of word-level language processing, it only reflects the semantic processing at lexical level, without going further to explain the semantic composition happening in higher linguistic computation.

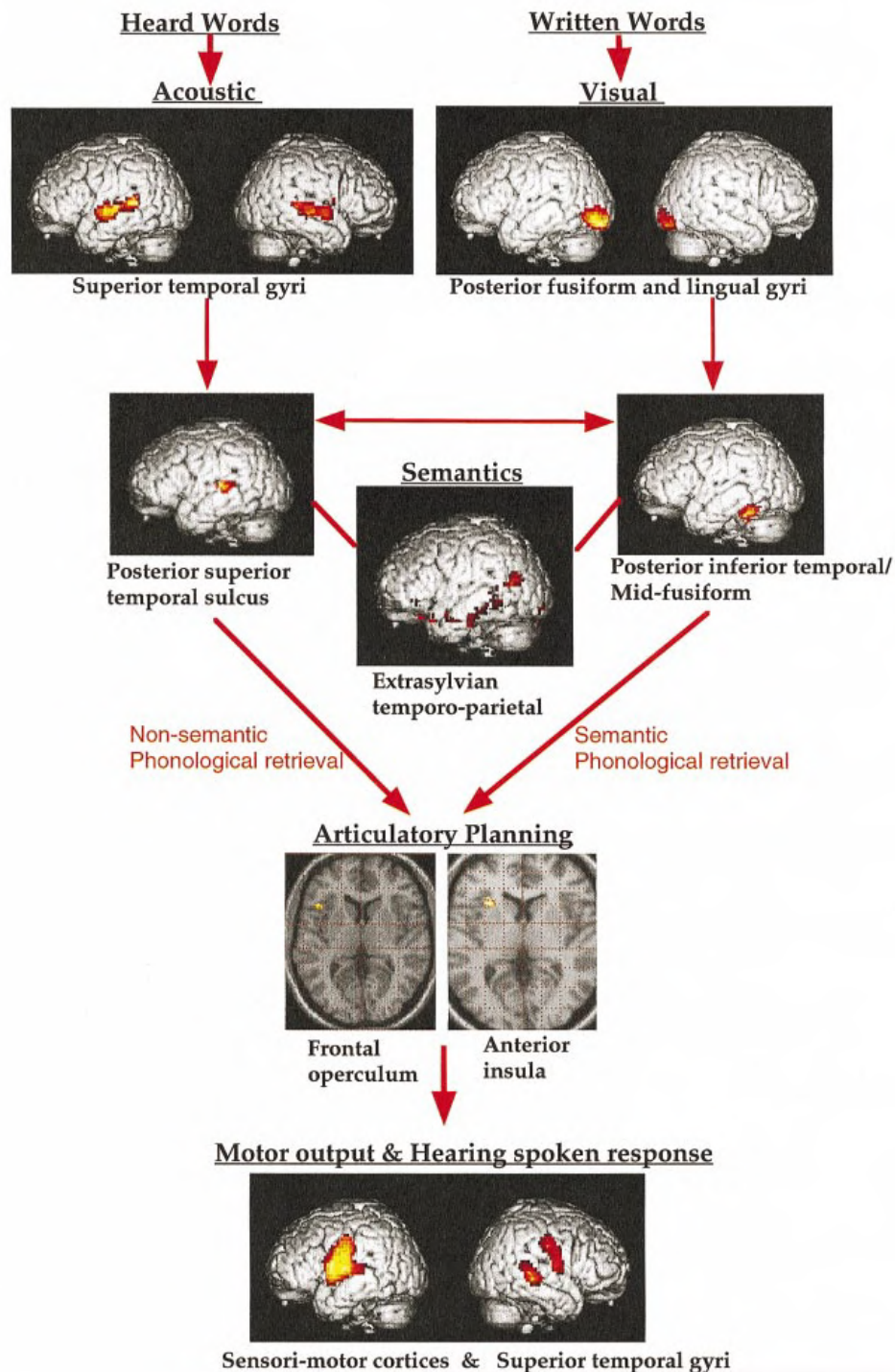


**Figure 5.4.** Neurological and cognitive model of language proposed in Price 2000. Figure adapted from Price 2000.

### 5.2.1.2 MUC model

Both the Classic model and Price's model constrain their framework at word-level language processing and preclude any language components beyond word processing. Hagoort (2005, 2013) proposed a Memory-Unification-Control (MUC) model that takes into account what goes on beyond production and comprehension of single words. The MUC model divides language processing into three components: Memory, Unification, and Control (Figure 5.5A). The Memory component represents the linguistic information that gets encoded and consolidated memory during language acquisition, such as phonology and phoneme knowledge, semantic memory and syntactic properties of words. This component projects to the left temporal cortex according to the MUC model. The Unification in this context is the operation of unifying lexical information into overall representations that span multi-word utterances, which is critical in higher level language processing. The Unification takes place in the left inferior frontal cortex, with a spatial gradient (Figure 5.5B). Depending on the type of information, semantic information is unified in *pars orbitalis*; syntactic unification recruits *pars triangularis*; phonology unification involves the *pars opercularis*. The Control component refers to attentional control and action planning during a conversational setting, which, for example, allows a bilingualism to switch to the correct language during conversation. The model suggests that the Control component involves the anterior cingulate cortex (ACC) and the dorsolateral prefrontal cortex (dlPFC). The MUC model is a substantial augmentation of the Classic model with three major additions: first, the connectivity of the critical language regions is more expanded and not restricted to the arcuate fasciculus, which is proposed by the Classic model. Second, the components in that model are not separated in terms of production and comprehension as in the Classic model, but instead are divided into memory, unification and control. Third, the network proposed is more extended than it in the Classic model, which was mainly based on evidence from single word processing. Although the network is not exclusively for language processing, it is necessary to be recruited for the sake of successful language processing.

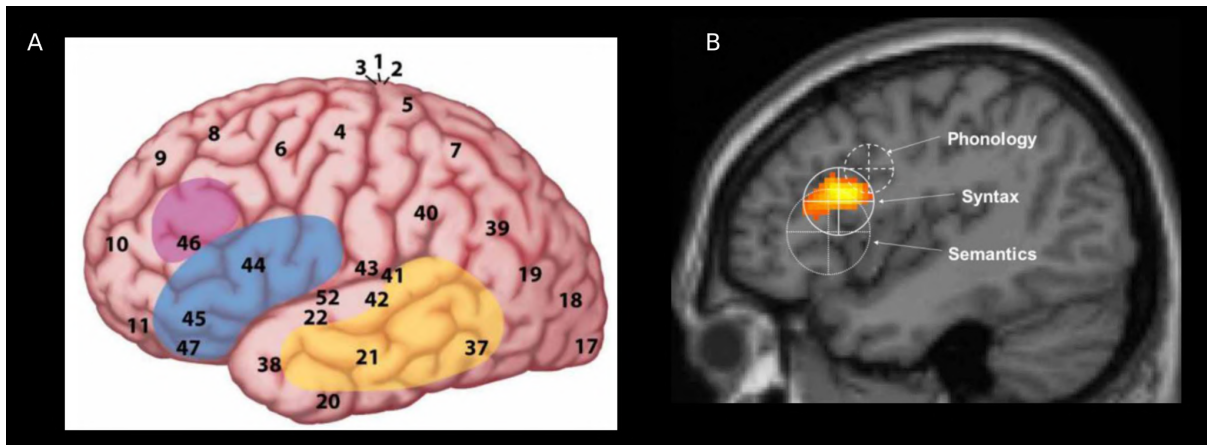


**Figure 5.5.** **A)** The MUC model proposed by Hagoort (2005, 2013). Memory (yellow) in the left temporal cortex, Unification (blue) in left IFG, and Control (pink) in the dlPFC. The ACC (part of the Control component) is not shown. Figure adapted from Hagoort (2013). **B)** The unification gradient in the left inferior frontal cortex.

### 5.2.1.3 Lau's model

Similar to the MUC model, Lau and colleagues proposed a semantic processing in context or sentence processing model that divides semantic processing into four components: lexical storage and access, lexical retrieval, lexical selection and combinatorial semantics (Figure 5.6). Both the semantic information storage and combinatorial semantics components are shared between the MUC model and Lau's model, while the neuroanatomical labor divisions are slightly different. In Lau's model, lexical information is stored in posterior MTG. The anterior temporal cortex and angular gyrus are involved in combining incoming lexical information with existing semantic and syntactic representation. In the MUC model the semantic memory storage was predicted to recruit the whole temporal cortex, and the combinatorial semantic operations were predicted to take place in IFG. In contrast, the IFG is involved in different functions in Lau's model: the anterior IFG (aIFG) is recruited in lexical representation retrieval and control, and the posterior IFG (pIFG) mediates lexical selection from multiple active candidates.

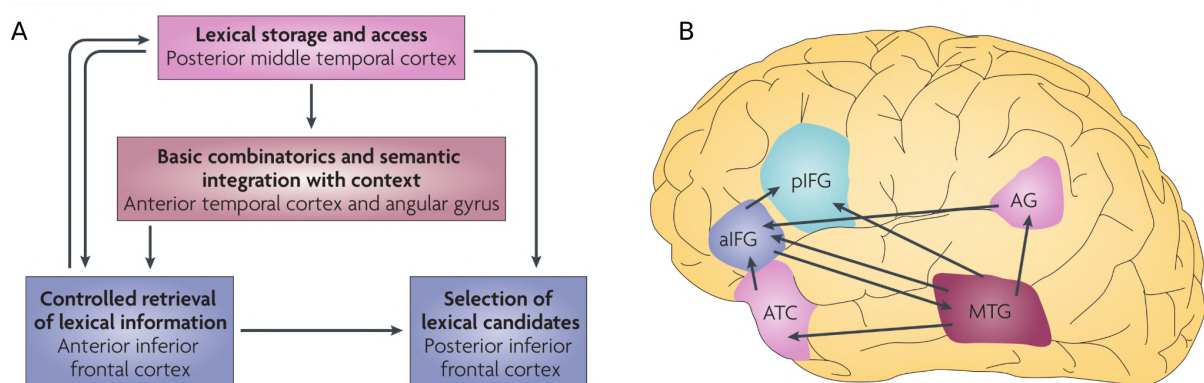


**Figure 5.6.** A) Schematic model for semantic processing of words in context proposed by [Lau et al. 2008](#). B) The corresponding functional neuroanatomic framework. Figure adapted from Lau et al. 2008.

### 5.2.2 Reading models

A reading dual pathway model was proposed by Pugh and colleagues (Pugh et al., 2000, 2001) based mainly on neuroimaging evidence of single word reading from reading-impaired and normal populations (Figure 5.7). In this model, the reading networks comprise anterior and posterior circuits. The anterior circuits are located in the IFG and are associated with phonological recoding during reading. The posterior reading circuits include both dorsal (angular gyrus, SMG and pSTG) and ventral (occipito-temporal junction) components. The dorsal circuits are critical in mapping the visual input of printed words to phonology and the ventral circuits are involved in visual orthographic information processing.

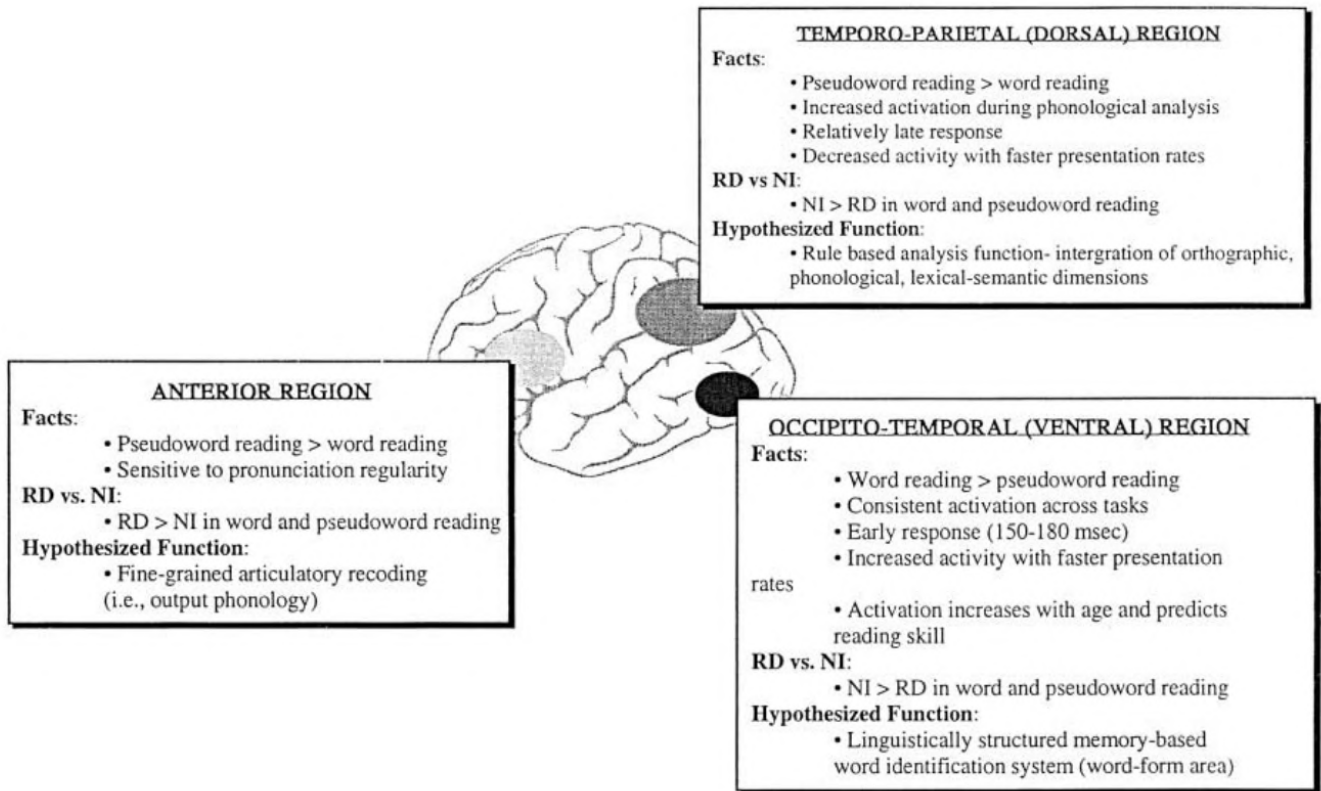


**Figure 5.7.** Three critical components in the dual pathway model proposed by Pugh and colleagues. Figure adapted from Pugh et al. (2001).

### 5.2.3 Speech comprehension models

There are two popular neuroanatomical models explaining speech comprehension. Both of them could be simply referred to as dual stream models, proposed by Hickok and Poeppel (2000, 2007), and by Friederici (2002, 2011, 2012).

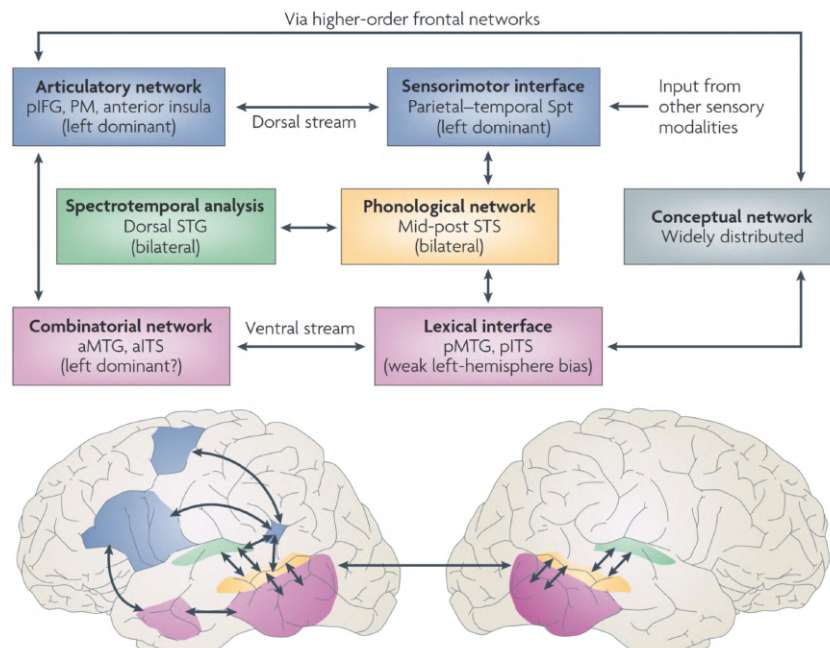


**Figure 5.8.** The dual stream model proposed by Hickok and Poeppel. Figure adapted from Hickok & Poeppel 2007.

According to the Hickok and Poeppel dual stream model, the speech comprehension starts from the bilateral auditory cortex, which involves spectrotemporal analysis (Figure 5.8). The phonological processing involves the bilateral mid-post STS. Afterwards, two streams emerge and carry the phonological information to the frontal lobe through different pathways. The dorsal pathway goes through the Sylvian fissure at the parieto-temporal boundary and reaches the IFG and premotor cortex. This pathway mainly maps phonological information onto articulatory representations in the frontal cortex, which is critical for speech development and production. The ventral pathway goes through the posterior MTG and ITS after leaving the mid-post STS, and reaches the anterior MTG and ITS. This pathway is responsible for accessing semantic representation from the phonological information (posterior MTG and ITS) and combinatorial semantics (anterior MTG and ITS). In general the dorsal pathway is left hemisphere-dominant while the ventral pathway is bilateral.

Friderici's dual stream model shares neuroanatomical regions with Hickok and Poeppel's model (Figure 5.9). This model is derived mainly from speech sentence processing and proposes that both the dorsal pathway and the ventral pathway serve more functions than the ones originally proposed by Hickok and Poeppel. For example, the dorsal pathway not only subserves mapping from auditory to motor, but can also be involved in syntactic processing in sentence comprehension. Taking

into account white-matter fibers involved in the speech comprehension network, two dorsal pathways are proposed in this model: one connecting the pSTG/STS to the premotor cortex (auditory-motor mapping), the other pathway reaching to the posterior IFG (BA44) from pSTG/STS *via* the arcuate fasciculus (syntactic processing). Similarly, the ventral stream can be also subdivided into two pathways: one pathway connects the temporal cortex with BA45 and BA47, which is supporting auditory-semantic mapping; the other pathway connects the anterior STG to frontal operculum and seen as supporting the combinations of adjacent elements in a sequence, which is important in sentence comprehension.

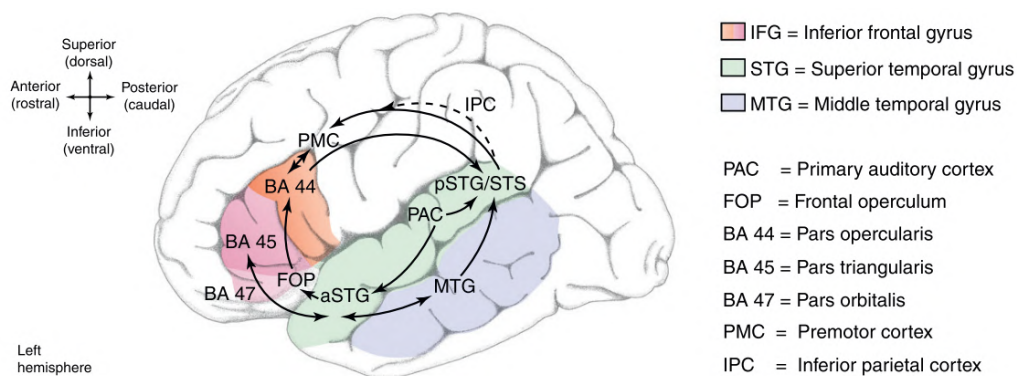


**Figure 5.9.** The dual stream model proposed by Friderici. Figure adapted from Friderici 2012.

## 5.2.4 Production models

Indefrey and Levelt proposed a word production model based on the time course of critical component processes and the involvement of brain regions in word production (Indefrey, 2011; Indefrey & Levelt, 2004). The word production networks consist of the left posterior IFG, the left precentral gyrus, the supplementary motor area (SMA), the left mid and posterior parts of the STG and MTG (Figure 5.10). The thalamus and cerebellum are also included in this model, being involved in phonetic encoding and articulation processes.

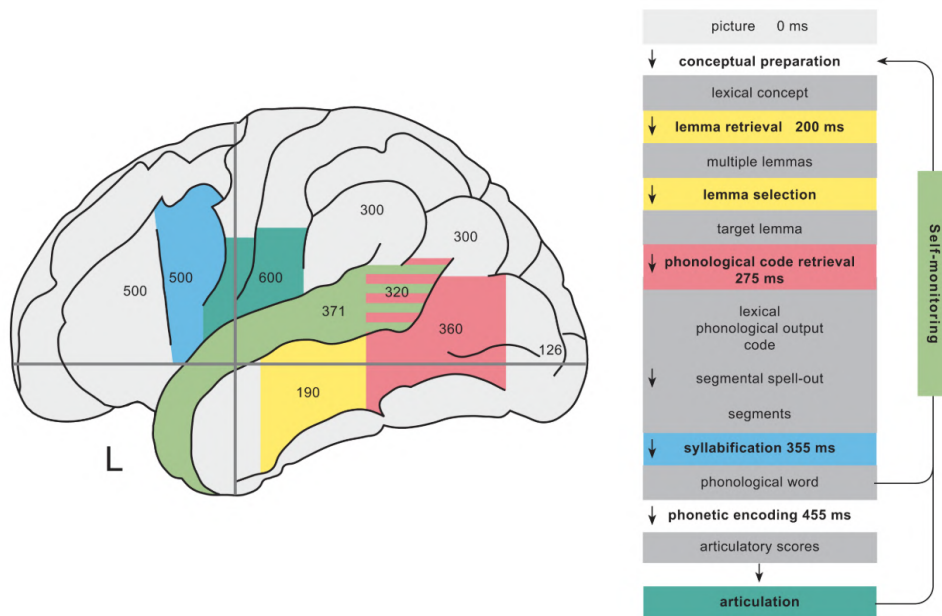


**Figure 5.10.** Neuroanatomical model of word production proposed by Indefrey and Levelt. The numbers within regions indicate median peak activation time estimates in milliseconds. Figure adapted from Indefrey (2011).

Tourville and Guenther developed the DIVA model of speech production (Figure 5.11; Tourville & Guenther, 2011). This model is built on a computational model under the same name, and unified neuroanatomical evidence that involves speech acquisition and production. This model comprises multiple components that contribute the successes of speech production and assign them to corresponding brain regions (see anatomical labels in Figure 5.11). In the DIVA model the thalamus also plays a critical role with its projections to the motor cortex serving as gates on the outflow of motor commands, and being involved in representing the feedforward motor programs.

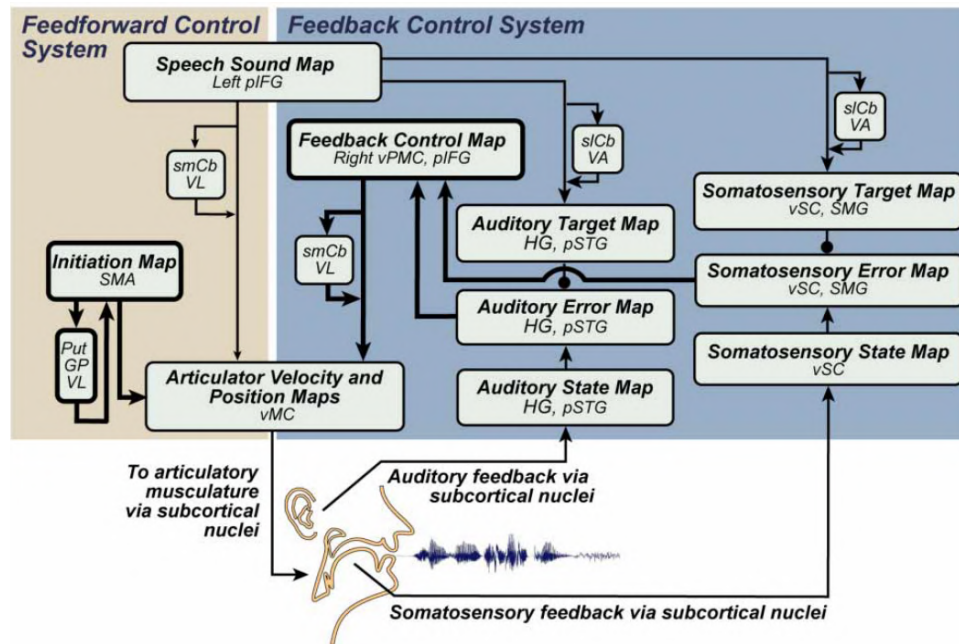


**Figure 5.11.** The DIVA model of speech acquisition and production. In the box there are the cognitive components of the model and the corresponding anatomical regions. Figure adapted from [Tourville & Guenther \(2011\)](#).

In sum, since Broca and Wernicke’s pioneering work linking human language functions and specific brain regions, the knowledge about the neurobiological underpinning of language has been tremendously expanded. Many neurobiological models have been proposed since then to account for the representations of language functions in different brain regions. The influential models reviewed above made connections between critical components of language processing and brain structures. However, most of these models are focused on cortical structures, neglecting to some extent the role of thalamus in language (only the DIVA model on speech production included the thalamus in the speech articulation phase) despite its widespread connections with the cerebral cortex. One of the main goals of the present doctoral work is to investigate the role that thalamus is playing in some of the main language systems.

## 6 Study 1: Structural connection of first-order thalamic nuclei

The present study was aimed at developing and testing a reproducible protocol for obtaining four first-order relay thalamic input and output white-matter tracts. The novelty of this protocol capitalizes on 4 aspects: (1) it is focused on well-known white-matter tracts constituted by myelinated axons that originate and/or target the first-order relay nuclei of the thalamus, testing them within the same study, and using similar methods and reconstruction procedures across them; 2) different from most previous studies, here we specifically investigated in a large dataset the reliability of the protocol in terms of both computational and test-retest reproducibility; 3) the present protocol uses state-of-the-art MRI protocols (multiband, multi-shell) and tractography methods with the aim of developing an advanced protocol that can be applied to current ongoing studies and future research; and, 4) the protocol is designed to be reproducible, easy to use and automatized, which unfortunately has not been the norm in the past. Also, it builds on previous well-validated tools including the first probabilistic atlas of the thalamus based on combining high-resolution ex vivo MRI and histology (Iglesias et al., 2018) and the reproducible-tract-profiles (RTP2) containerized tool which is based on state-of-the-art techniques implemented on top of Vistasoft's code, which have been tested and used in many publications over the last 15 years (<https://www.github.com/vistalab/vistasoft>; Lerma-Usabiaga et al., 2022). The ultimate goal of this work was to provide a reliable protocol for obtaining and estimating first-order relay thalamic pathways for basic research and clinical studies.

To this end, we first defined multiple parameters to optimally reconstruct the above-mentioned four thalamic pathways in left and right hemispheres. Second, we tested the computational and test-retest reproducibility of our protocol by examining a range of white-matter proxies related to the microstructural and macrostructural properties of these tracts. To examine the reliability of the protocol we obtained tracts from DWI of 113 normal adults. The protocol consisted of three components: Defining the regions-of-interest (ROI); preprocessing DWI data; modeling white-matter tracts and tractometry. Reproducibility was tested using two approaches: 1) Computational reproducibility, tested by identifying each tract using the same parameters 10 independent times for all 113 subjects, and 2) Test-retest reproducibility, tested by re-scanning a subset of 24 participants using the same MRI protocol twice within an average interval of 15 days. Our hypothesis was that we would obtain a high degree of reproducibility for the microstructural and macrostructural properties of these tracts. However, we expected some variability in specific tracts, such as the DT which crosses hemispheres and it is relatively long, and hypothesized that this variability would be higher for test-retest than for computational reproducibility.

## 6.1 Methods

### 6.1.1 Subjects

A total of 113 healthy volunteers (mean age = 24.5 years, SD = 4.33 years; 65 females) participated in the study. Twenty-four of the volunteers (mean age = 24.7 years, SD = 4.06 years; 13 females) returned for a second session in which they were scanned using exactly the same MRI protocol (mean interval = 15 days, SD = 21.82 days, range: 7-104

days). All participants were right-handed and had normal or corrected-to-normal vision. No participant had a history of major medical, neurological, or psychiatric disorders. The study protocol was approved by the Ethics Committee of the Basque Center on Cognition, Brain and Language (BCBL) and was carried out in accordance with the Code of Ethics of the World Medical Association (Declaration of Helsinki) for experiments involving human participants. Prior to their inclusion in the study, all participants provided informed written consent. Participants received monetary compensation for their participation.

### 6.1.2 Data acquisition

Whole-brain MRI data acquisition was conducted on a 3-T Siemens Prisma Fit whole-body MRI scanner (Siemens Medical Solutions) using a 64-channel whole-head coil. The MRI acquisition included one T1-weighted structural image (T1w) and DWI sequences. High-resolution MPRAGE T1-weighted structural images were collected with the following parameters: time-to-repetition (TR) = 2530 ms, time-to-echo (TE) = 2.36 ms, flip angle = 7°, field of view (FoV) = 256 mm, voxel size = 1 mm isotropic, 176 slices. In total 100 diffusion-weighted images were acquired with the anterior to posterior phase-encoding direction and 50 isotropically distributed diffusion-encoding gradient directions. The 100 diffusion weighted images included 50 images with b-value of 1000 s/mm<sup>2</sup> and 50 images with b-value of 2000 s/mm<sup>2</sup>. Twelve images with no diffusion weighting (b-value of 0 s/mm<sup>2</sup>) were obtained for motion correction and geometrical distortion correction, which comprised five images with the same phase-encoding direction as the DWI images and seven images with the reversed phase-encoding direction (posterior to anterior). Both DWIs and b0 images shared the following parameters: TR = 3600 ms, TE = 73 ms, FA = 78°, voxel size = 2 isotropic, 72 slices with no gap and a multiband acceleration factor of 3.

### 6.1.3 Tractography pipeline

Tract reconstruction was conducted using a custom containerized workflow called RTP2 (Reproducible Tract Profiles 2) pipeline (Lerma-Usabiaga et al., 2019, 2020), which guarantees data provenance and reproducibility. The RTP2 divides this process into three main parts: (1) ROI definition, (2) DWI preprocessing, and (3) tract identification and tractometry. In step 3, we used the preprocessed diffusion data from step 2 to model streamlines based on the ROIs created in step 1. Details are given below. The code and parameters are available through GitHub ([github.com/MengxingLiu/Thatract-paper](https://github.com/MengxingLiu/Thatract-paper)) and Docker Hub (<https://hub.docker.com/u/garikoitz>).

#### 6.1.3.1 ROI definition

The first step of the RTP2-pipeline (called RTP2-anatROIs) involves processing the subject's anatomical T1w image to obtain the ROIs to be used in tractography. The input for this step is the subject's T1w file and ROIs defined in MNI space; the output is a segmented T1w image and the ROIs of interest in individual subject T1w space.

The ROIs used for the identification of each fiber group (see Table 6.1) were obtained as follows. First, Freesurfer (<http://surfer.nmr.mgh.harvard.edu/>) was used to perform cortical/subcortical segmentation and parcellation. Next, the thalamic nuclei were obtained by running the thalamic segmentation module implemented in Freesurfer on a probabilistic atlas built with histological and high-resolution ex vivo MRI data (Iglesias et al., 2018). For this study, we only considered first-order relay nuclei as ROIs: the LGN, MGN, VLN, and VLp. The VLN was created by combining VLa and VLp. All tracts described in this paper travel from these thalamic nuclei to other locations in the brain. We next describe how we obtained the ROIs.

To parcellate the visual cortex we ran the Neuropythy (Benson & Winawer, 2018; <https://github.com/noahbenson/neuropythy>) tool on the Freesurfer results. A combination of the resulting V1 and secondary (V2) visual ROIs was used for our visual cortex ROI when defining the OR. The OR projections to V1 are well established (see Rokem et al., 2017 for a review on OR tractography), whereas OR projections to V2 are relatively less studied. There is tracer evidence from non-human primates suggesting that LGN projects beyond V1 (Garey & Powell, 1971; Maciewicz, 1975; Manger & Rosa, 2005), specifically to V2 (Bullier & Kennedy, 1983; Kennedy & Bullier, 1985). In-vivo tractography evidence from humans reconstructing the OR and measuring the terminating points suggested that a considerable number of streamlines also terminated in V2 (Alvarez et al., 2015; Arrigo et al., 2016). Thus, both V1 and V2 are included in the current protocol to reconstruct the OR. The remaining ROIs were obtained from atlases defined in MNI space. To convert them to individual subject space, we first performed a non-linear registration of a 1mm<sup>3</sup> MNI template using Advanced Normalization Tools (ANTs, <http://stnava.github.io/ANTs/>). A1 and M1 were converted from the human connectome project (HCP) atlas (Glasser et al., 2016). The cerebellar dentate nucleus ROIs were obtained and transformed from the cerebellar parcellation proposed by Diedrichsen et al. (2011).

To make sure the ROIs extended to the interface of gray and white matter, all ROIs were dilated by one cubic voxel. Also, we used inclusion or exclusion ROIs to improve neuroanatomical accuracy when obtaining both the OR and DT. For the OR, the inclusion ROI was a waypoint, first drawn in MNI space (coronal plane of  $y = -80$  that transpasses the posterior limb of the internal capsule) and then transformed to native space, to select fibers passing through the internal capsule. In contrast, for the DT, two ROIs, the ipsilateral cerebellar cortex and the contralateral thalamus, were used with “NO” logic, that is,

excluding fibers that passed through them. These were generated from one of the default parcellations of Freesurfer (i.e., *aparc+aseg.mgz*).

#### 6.1.3.2 DWI data preprocessing

The second step in the RTP2-pipeline (called RTP2-preproc) consisted in preprocessing the diffusion data and registering it in anatomical space. This step was mainly based on MRtrix's (Tournier et al., 2019) recommendations and used MRtrix tools, the ANTs tool described above and FSL (Jenkinson et al., 2012). The data was preprocessed using several MRtrix functions in the following steps: first, data denoising based on random matrix theory, which exploits data redundancy in the patch-level principal component analysis domain (Veraart et al., 2016) using *dwidenoise*; second, Gibbs Ringing correction (Kellner et al., 2016) using *mrdegibbs*; third, susceptibility induced distortions and motion correction with the FSL's *topup* and *eddy* tools (Smith et al., 2004) called by *dwifslpreproc*; fourth, B1 field inhomogeneity correction with *dwibiascorrect* and Rician background noise removal with *mrcalc*; fifth, a rigid transformation matrix to align the DWI images to the corresponding T1w image using ANTs.

To make sure the DWI data from test and retest sessions were in the same space, DWI data from both sessions were aligned to the same T1w collected in the initial test session. Therefore, both test and retest sessions used the same ROIs; only DWI preprocessing and the streamline tracking were session-specific.

#### 6.1.3.3 Tract identification and tractometry

In the third and final main step, the container RTP2-pipeline was used to obtain the final white-matter tracts. This container used the ROIs and preprocessed DWI data to systematically identify the tracts of interest bilaterally: OR, AR, MR and DT. We initially ran

this step with 4 random subjects. An expert anatomist (FC) defined the optimal parameter combinations used to identify each tract of interest.

We first modeled the diffusion information to obtain a map of possible directions with weights, called fiber orientation distributions (FODs), for every voxel, using MRtrix3's multi-tissue constrained spherical deconvolution (CSD; Jeurissen et al., 2014). This tool can discern crossing fibers and provide more than one direction in each voxel. Next, streamline tractography was performed on the estimated FODs using a probabilistic algorithm (iFOD2; Tournier et al., 2010) with the following parameters: step size 1mm, maximum fiber length 200mm, minimum fiber length 20mm, FODs amplitude threshold 0.05, angle threshold 45 degrees. The ROIs used in the streamline tractography are described in Table 6.1 (please note that the DT is a cross-hemispheric tract; in the present study we defined the hemisphere of this tract based on the thalamic hemisphere for the convenience of the description). The streamlines were seeded from ROI#1 and terminated in ROI#2 for all tracts except the OR, which combined streamlines from both directions to limit the impact of volume differences between seed and target. Matlab utilities developed in Vistasoft (<https://github.com/vistalab/vistasoft>) were used to remove the outlier streamlines from each tract generated in MRtrix and to obtain the main tract metrics.

We generated along-tract profiles using the tract metrics obtained from Vistasoft. Although CSD was used to model the fibers because it discerns crossing fibers, classical diffusion tensor (DTI) modeling was used to obtain the typical diffusion summary statistics, such as fractional anisotropy (FA), axial diffusivity (AD) and radial diffusivity (RD). To generate tract profiles, we obtained the central location of all the streamlines in the tract and sampled this as 100 same-length segments. We then summarized the diffusion properties of each segment by taking a weighted average of the diffusion properties corresponding to a disc

centered in the segment. Finally, an along-tract profile was generated for each tract using Vistasoft.

Table 6.1. Parameters used to identify each tract of interest.

tract name	ROI#1	ROI#2	ROI#3	ROI #4
Left OR	Left LGN	Left V1V2	OR_roi3_L*	-
Right OR	Right LGN	Right V1V2	OR_roi3_R*	-
Left AR	Left MGN	Left A1	-	-
Right AR	Right MGN	Right A1	-	-
Left MR	Left VLN	Left M1	-	-
Right MR	Right VLN	Right M1	-	-
Left DT	Left VLP	Right Dentate	Right Thalamus**	Left Cerebellum Cortex**
Right DT	Right VLP	Left Dentate	Left Thalamus**	Right Cerebellum Cortex**

Abbreviations: VLP = posterior ventral lateral nucleus; V1V2 = primary and secondary visual cortex. \*waypoint ROI, only streamlines that pass through this ROI were kept; \*\*excluding ROI, streamlines that pass through this ROI were excluded.

#### 6.1.4 Reproducibility measurement

Reproducibility was measured in two different ways (Figure 6.1). First, to test *computational reproducibility*, we repeated the tractography reconstruction using the RTP2-pipeline 10 times. Our aim was to measure how consistently our pipeline generated the tracts of interest. Second, to check for *test-retest reproducibility*, we used a subset of 24 participants, who returned for a second acquisition session within a mean temporal interval of 15 days. We examined how consistently our pipeline generated their tracts at these two different time points.

To evaluate these two types of reproducibility at the microstructural scale, we performed pairwise correlations on tract profiles for all possible pairs from the 10 repeated computations to measure computational reproducibility, and across test and retest to measure test-retest reproducibility. For simplicity, we only show the correlations for FA values.

At the macrostructural level, we quantitatively analyzed tract volume overlap, streamline density and distance to check the reproducibility of tract shapes. These analyses included: (1) Dice similarity index to check for volume-based overlap of all tract pairs; (2) density correlation for the voxel-level streamline density of all tract pairs; and, (3) bundle adjacency, the average distance between streamlines from two tracts. The measurements used to examine computational reproducibility and rest-retest reproducibility were computed using the package `scilpy` (see details in Schilling et al. 2021 and <https://github.com/scilus/scilpy>). These analyses were conducted across all possible pairs of computational reproducibility and rest-retest reproducibility, as well as for each tract.

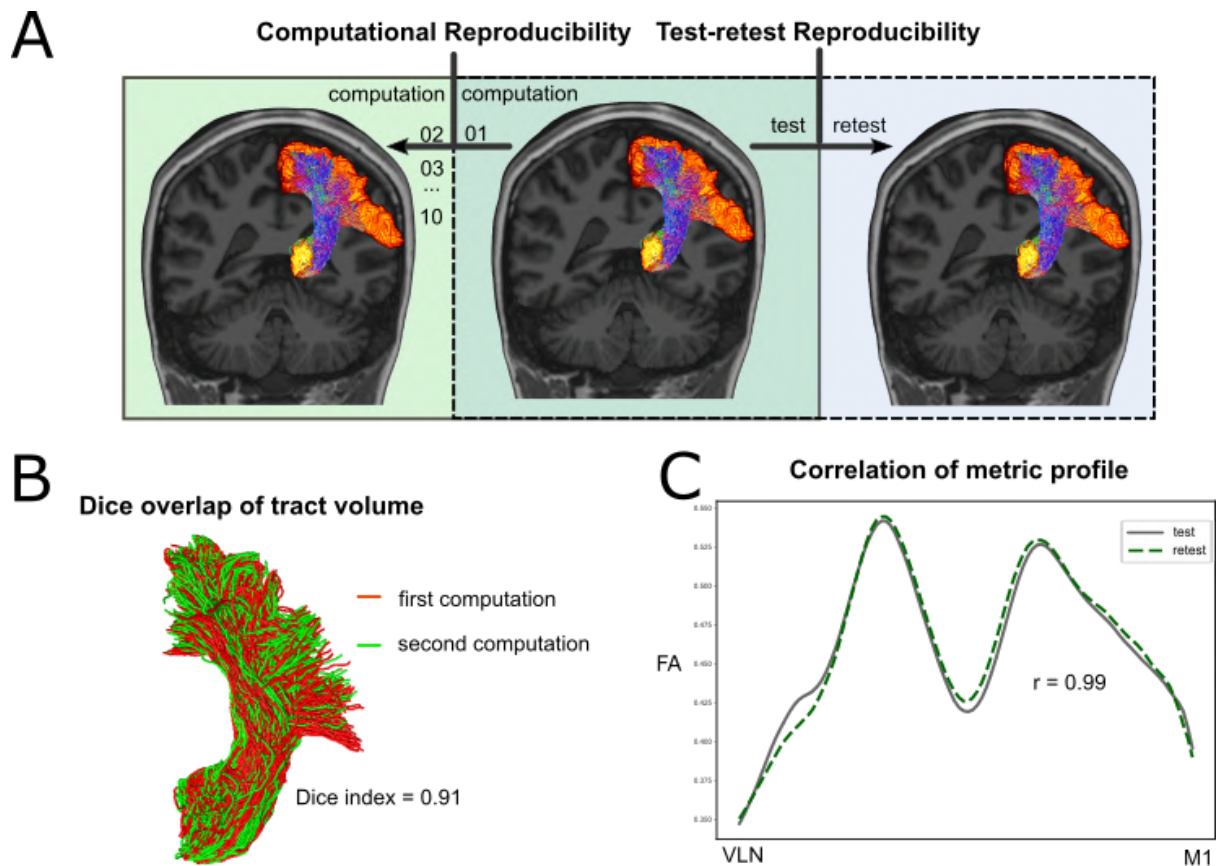


**Figure 6.1.** The reproducibility measurement scheme. **A)** *Computational reproducibility* (reproducibility across computations); *test-retest reproducibility* (reproducibility across test and retest sessions). **B)** The Dice overlap of MR reconstructed at the first second computations, from subject S038. **C)** Correlation of the FA profile of MR from subject S038’s test and retest sessions.

## 6.2 Results

In the present study, we obtained and measured fibers bundles connecting three first-order sensory (LGN, MGN) and motor (VLN) thalamic nuclei with their main corresponding cortical target areas. In addition, we reconstructed the subcortical input pathway to VLp from the dentate nucleus of the cerebellum. These four tracts were identified as homologous tract pairs in the left and the right hemisphere. Figures 6.2 and 6.3 show these tracts in a representative subject. To examine the reproducibility of our protocol, we followed a double analytical approach testing: (1) *computational reproducibility* by repeating the computation on the same diffusion data 10 times and quantifying changes from computation to computation for the same tract; and, (2) *test-retest reproducibility*, by obtaining DWI data

from the same subjects and using the same MRI protocols across two different sessions to quantify test-retest changes in the same tracts.

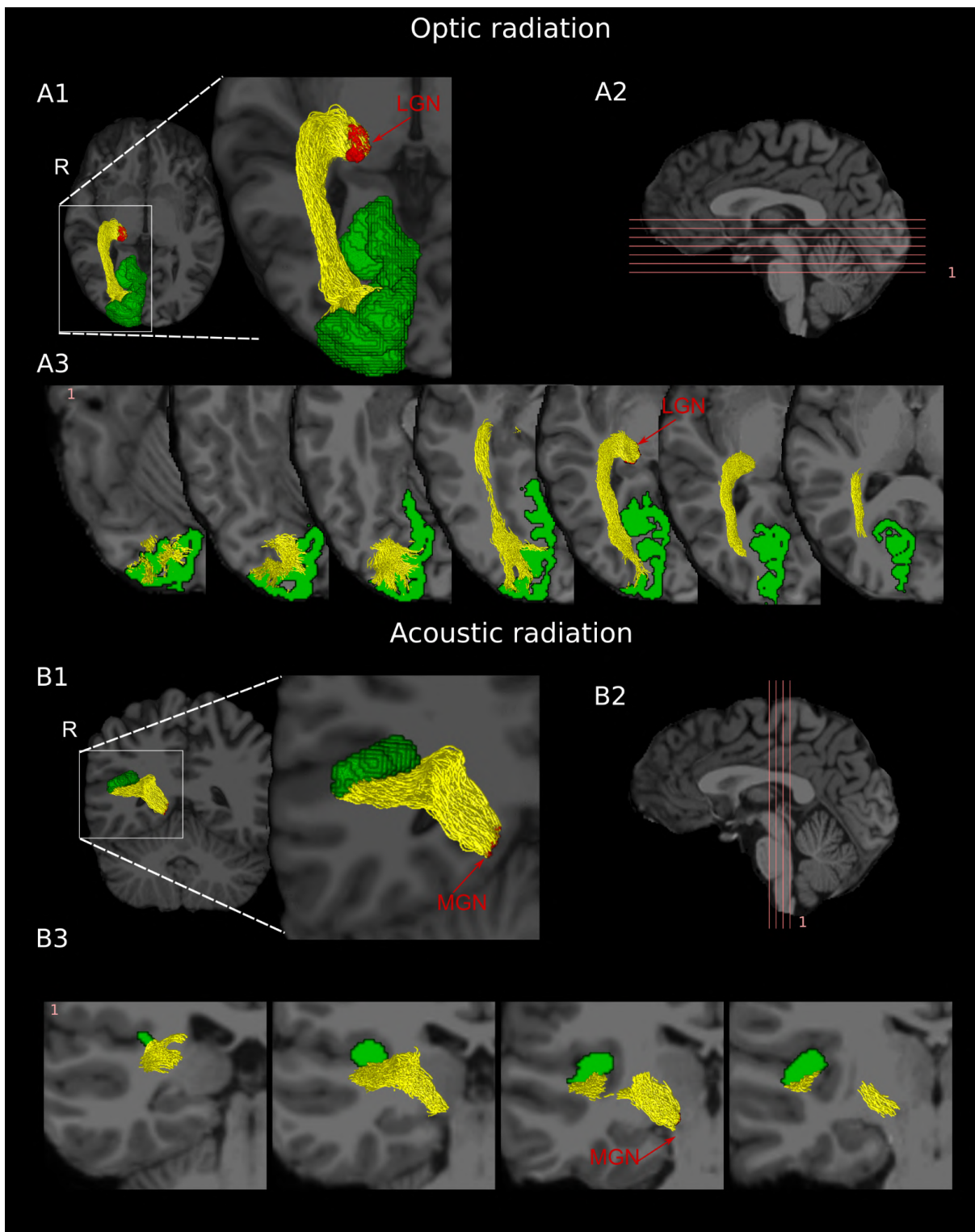


**Figure 6.2.** The OR (A) and AR (B) reconstructed in a representative subject. A1 and B1 show the 3D representations of the OR and AR in yellow. A2 and B2 show the positions from which the slices in A3 and B3 are respectively drawn. A3 and B3 depict axial and coronal views of the core subcomponents of OR and AR, respectively. Green color indicates the cortical ROIs V1/V2 and A1.

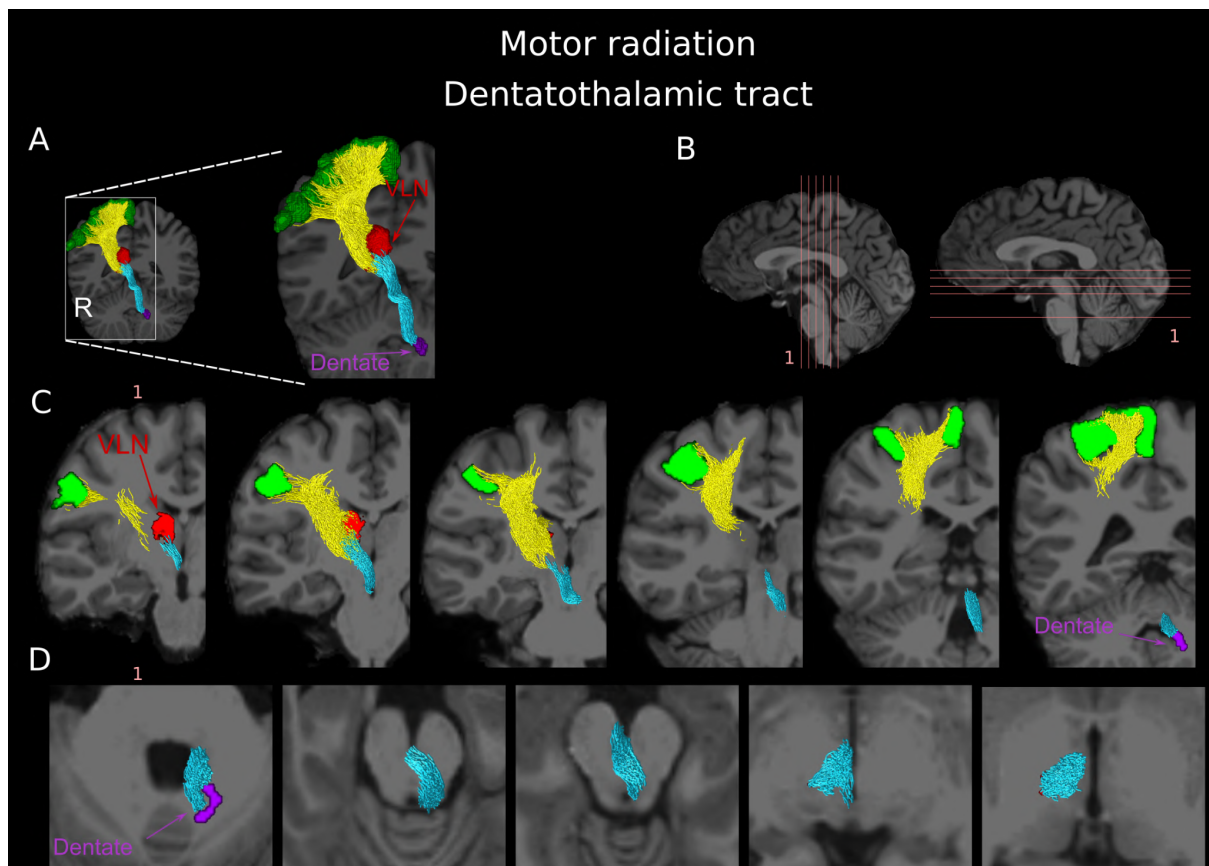


**Figure 6.3.** The MR and DT reconstructed in a representative subject. A shows the 3D representations of the MR and DT. B shows the positions from which the slices in C and D are drawn. C and D depict coronal views of the core subcomponents of MR and DT. Green color indicates the cortical ROI M1. Yellow streamlines are MR and blue streamlines represent the DT. D shows the axial view of the core subcomponents of the DT.

### 6.2.1 Computational reproducibility

For the four pairs of white-matter fibers with the established protocol, the repeated computations on same diffusion data resulted in mostly identical tract profiles and high agreement of streamlines. The mean correlations of FA profile were above 0.99 for all the tracts examined (see Table 6.2; Figure 6.4B). At individual level, for all the possible pairs of computation, most correlation coefficients were higher than 0.97 for each fiber, except for left AR and right DT, which have a long tail towards 0.82. Bearing this in mind, with 10 repeated

computations, there will be at least 9 relatively low coefficients if only one computation resulted in a different tract than all the others.

Agreement indices also showed that the identified white-matter fibers have consistent shapes and density across repeated computations (Table 6.2). Figure 6.4C shows agreement indices for each individual pair of computations. These three agreement indices revealed the same pattern as the one observed in the correlation coefficient of FA profile, with more variability in left AR. And the same pattern was also found for the right homologous AR. It is noteworthy that some of this variability in agreement indices derives from the same single subject (e.g., outlying clusters for bundle adjacency and Dice coefficient in right AR, and for Dice coefficient and density correlation in left OR).

**Table 6.2.** Reproducibility indices and their standard deviations (in parentheses) for all measures and fiber bundles.

	computational				test-retest			
	FA profile correlation	bundle adjacency	dice index	density correlation	FA profile correlation	bundle adjacency	dice index	density correlation
L OR	0.9996(0.0016)	0.09(0.01)	0.92(0.01)	0.998(0.001)	0.9956(0)	0.11(0.01)	0.90(0.01)	0.990(0.005)
R OR	0.9996(0.0005)	0.09(0.01)	0.92(0.01)	0.998(0.001)	0.9944(0)	0.11(0.01)	0.90(0.01)	0.989(0.005)
L AR	0.9976(0.0074)	0.18(0.09)	0.85(0.05)	0.990(0.008)	0.9265(0.12)	0.39(0.27)	0.76(0.09)	0.907(0.082)
R AR	0.9989(0.0013)	0.11(0.09)	0.90(0.04)	0.997(0.002)	0.9473(0.07)	0.34(0.41)	0.80(0.12)	0.940(0.047)
L MR	0.9985(0.0012)	0.09(0.01)	0.91(0.01)	0.993(0.001)	0.9787(0.02)	0.13(0.05)	0.89(0.01)	0.971(0.010)
R MR	0.9982(0.0017)	0.09(0.01)	0.91(0.01)	0.993(0.001)	0.9713(0.03)	0.12(0.03)	0.89(0.01)	0.971(0.014)
L DT	0.9988(0.0038)	0.07(0.03)	0.93(0.02)	0.994(0.004)	0.9638(0.03)	0.21(0.11)	0.82(0.08)	0.853(0.097)
R DT	0.9986(0.0032)	0.06(0.01)	0.94(0.01)	0.994(0.004)	0.9458(0.06)	0.22(0.14)	0.82(0.09)	0.782(0.182)

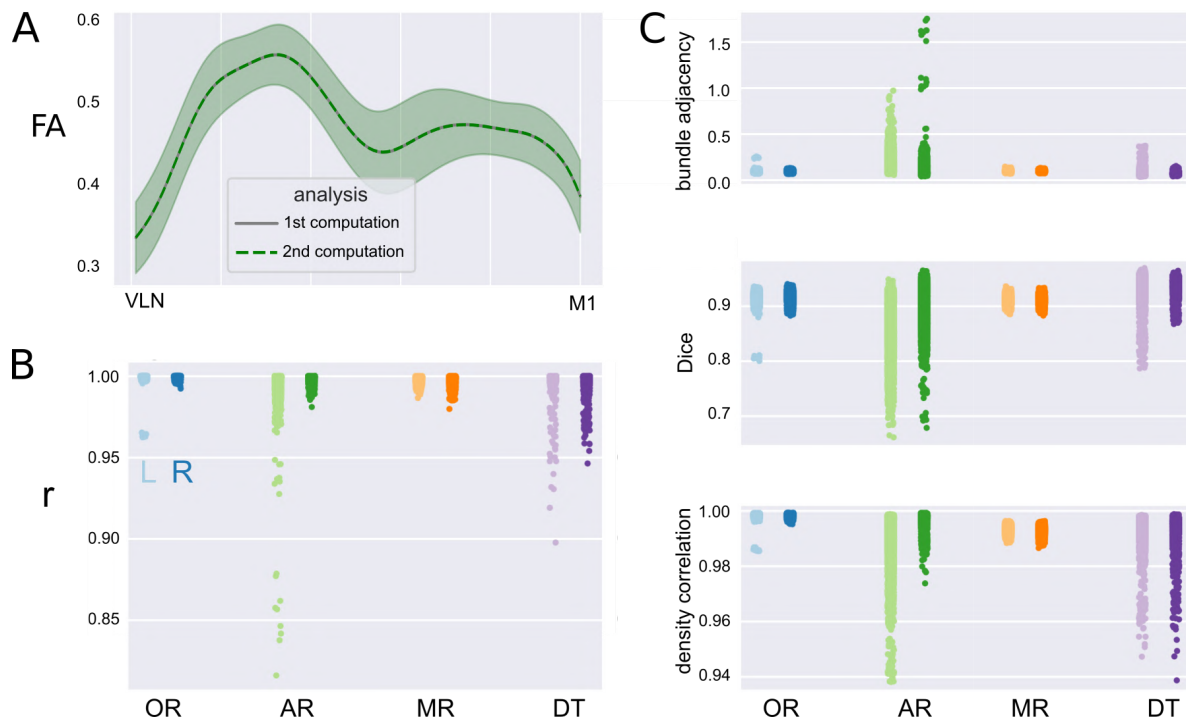


**Figure 6.4.** Evaluation of computational reproducibility for the OR, AR, MR and DT. **A)** Examples of group average FA profiles for left MR from the first (gray continuous line) and second (green dashed line) computations. The light green shaded area indicates the standard deviation. **B)** Strip plots showing the distribution of correlation coefficients between all possible pairs computed for each tract and each subject (lighter color columns represent the left hemisphere, darker color columns represent the right hemisphere). Each dot represents the correlation coefficient for a specific computation pair for one participant. **C)** Agreement indices distribution: bundle adjacency (top), Dice coefficient (middle), and density correlation (below) for all possible computation pairs for each tract and each subject (light color columns represent the left hemisphere, darker color columns represent the right hemisphere).

### 6.2.2 Test-retest reproducibility

To examine test-retest reproducibility, 24 participants came back for a retest session where we used exactly the same MRI protocol. The mean of FA profile correlations was above 0.9 across the ten tracts of interest, although as expected the values were numerically lower than those observed in the computational reproducibility analyses. As in the computational reproducibility analysis, the left AR also showed higher variability in the test-retest reproducibility analysis, with lower values within the mean correlation coefficients (0.93, Table 6.2 and Figure 6.5A & 6.5B). Nevertheless, it is important to highlight that all of these values reflect a high degree of reproducibility.

Test-retest reproducibility was also confirmed by the agreement indices. The group averages for bundle adjacency were all under 0.4 for the ten tracts, indicating that the streamlines identified in the test were very close to the streamlines identified in the retest (see Table 6.2 and Figure 6.5C). High reproducibility was also reflected by the Dice index and streamline density correlation. Among the ten tracts, the AR and DT tended to show more variability bilaterally.

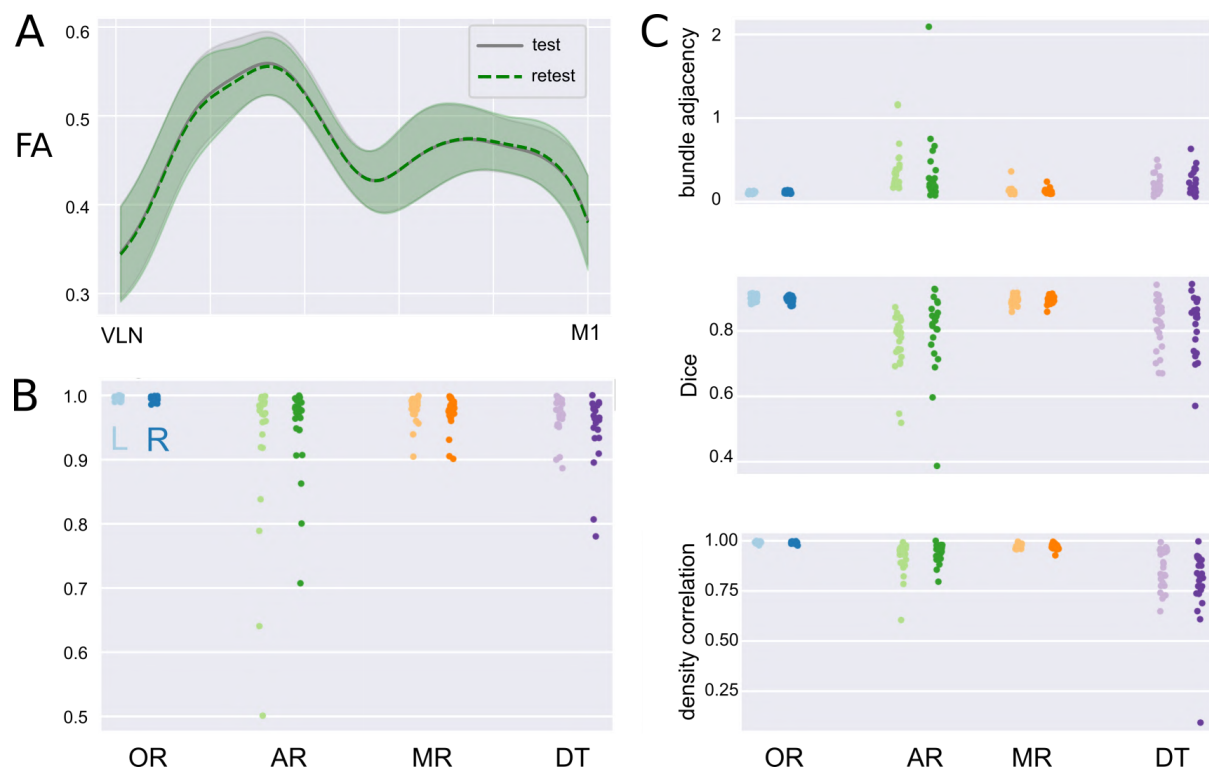


**Figure 6.5.** Evaluation of test-retest reproducibility for the OR, AR, MR and DT. **A)** Examples of group average FA profiles for left MR from test (gray continuous line) and retest (green dashed line). The light green shaded area indicates the standard deviation. **B)** Strip plots showing the distribution of the correlation coefficients between test and retest for each tract and each subject (lighter color columns represent the left hemisphere, darker color columns represent the right hemisphere). **C)** Agreement indices distribution: bundle adjacency (top), Dice coefficient (middle), and density correlation (below) for test and retest for each tract and each subject (lighter color columns represent the left hemisphere, darker color columns represent the right hemisphere).

### 6.3 Discussion

We present a reproducible protocol for tractography reconstruction of first-order human thalamocortical tracts, which play a critical role in sensory and motor information relay between the thalamus and cortex. We tested the reproducibility of our protocol for

obtaining these tracts of interest by examining their microstructural tractometric properties and volume-based macrostructural similarity across repeated computations and test-retest sessions. Results showed nearly perfect computational reproducibility across ten repetitions and high-to-excellent test-retest reproducibility.

In terms of computational reproducibility, it is worth highlighting that across ten separate and independent computations using the same raw data and protocol, reproducibility was nearly perfect; for example, providing an average FA profile correlation of 0.99 (individual-subject values ranging from 0.82 to 0.99) and an average Dice similarity value of 0.91 (individual Dice index values ranged from 0.66 to 0.97) across all the bundles examined. We expected computational reproducibility would be high, but it was important to demonstrate that the protocol is reliable and appropriate for obtaining the tractography measures of interest. Concerns about this type of reproducibility, which we refer to as computational reproducibility, have grown in recent years (e.g., Theaud et al., 2020). One goal of our protocol is to offer neuroscientists and medical practitioners efficient and reproducible processing guidelines to reconstruct first-order thalamocortical tracts. Hence, we packed our solution in software containers that can be run using Singularity or Docker technologies. In both cases, exactly the same set of algorithms, associated libraries and operating systems can be run in a computationally reproducible manner. This allows researchers to run previously as well as recently acquired data using exactly the same software and configuration options many times.

Test-retest reliability, which ensures stability across time, is one of the most widely used measures for a protocol or tool. Since test-retest reproducibility entails inputting different data, we expected to obtain lower numerical tractometric and volume-based similarity values than those observed in our computational reproducibility calculations. At the microstructural level, our data showed an average 0.97 (individual-subject values ranged

from 0.50 to 0.99) test-retest reproducibility for FA profile correlations after an average of 2 weeks. These correlation coefficient values for tract profiles are high and consistent with the values obtained in a previous study aimed at validating test-retest reliability in classic fiber bundles (Kruper et al., 2021).

At the macrostructural level, the Dice index is commonly used to assess the overlap of bundles reconstructed at two time points (Besseling et al., 2012; Boukadi et al., 2019; Cousineau et al., 2017). In the present study, Dice index values averaged 0.85 (individual-subject values ranged from 0.39 to 0.94) for all white-matter bundles examined. Based on the Dice index values reported in previous studies focused on white-matter bundles (e.g., minimum group-level Dice index of 0.70 in Besseling et al. 2012 and Cousineau et al. 2017; 0.71 in Boukadi et al. 2019), the range of the Dice index reported here (i.e., 0.76-0.90 across tracts at group level) indicates that all the white-matter bundles we investigated had high test-retest reliability.

It is important to understand the nature of the variability observed in these two types of reproducibility measurements. Our results showed that computational reproducibility is nearly perfect, but there is some variance across repeating computations. The main source of this variance is random seed generation. Basically, there are steps in our reconstruction pipeline that involve non-deterministic processes, which will be different across computations. A fully reproducible pipeline can be achieved by fixing the random seed initialization, but we decided not to proceed in this way. We used a probabilistic algorithm to generate the streamlines, whose advantage has been discussed by many researchers (see for instance (Bonilha et al., 2015; Grisot et al., 2021; Khalsa et al., 2014)). Indeed, fixing random seed initialization would work against the probabilistic nature of the algorithm and the philosophy of probabilistic tractography. In addition, fixing the random seed is not compatible with using multi-threaded steps that allow for faster computation. Multi-threading

introduces randomness in terms of the order of step execution, which will generally affect the reproducibility of results. It is relevant to note that previous studies that focused on probabilistic tractography have not examined computational reproducibility. Together with random seed generation, there could possibly be other factors contributing to some extent to the computational reproducibility variance. Instead of assuming no or slight changes among computations, researchers should be aware that computational variance exists depending on the parameters chosen to conduct the tractography. It is important that future research further investigates, in a systematic manner, factors that might be associated with computational variance in probabilistic tractography beyond random seed generation.

The test-retest reproducibility reported here showed some variability especially for specific bundles. We observed overall more variability in test-retest reproducibility for the AR and DT tracts. This can be in part explained by specific characteristics of these tracts, for instance: i) the small seed used for reconstruction (i.e., MGN/A1, dentate nucleus); ii) long streamlines (i.e., DT); and iii) anatomical complexity (i.e., DT). Previous studies have related lower reproducibility to smaller seed size (Bonilha et al., 2015; Buchanan et al., 2014; Zhang et al., 2019) and longer streamlines (Bonilha et al., 2015; Mori & Van Zijl, 2002; Tsai, 2018). Fiber tracking from small seeds may be influenced by systematic errors and noise, leading to spurious findings. Moreover, smaller seeds are likely to generate less fibers and therefore decrease the likelihood of successful tracking. Similarly, streamlines with longer paths lead to more interruptions in fiber tracking, which can also lead to larger variation. Also, the anatomically complex DT connects small and deep nuclei, making it more vulnerable to partial volume effects between different tissues (Mori & Van Zijl, 2002). Small ROIs, long fibers, and anatomical complexity affect computational reproducibility in the same manner as to the test-retest reproducibility. Nevertheless, our protocol was able to reconstruct the four pairs of tracts in all 113 subjects. This is an important achievement considering the

complexity of the tracts, and the fact that we used a fairly standard modern scanner and acquisition MRI sequences.

The present work has some limitations that could be addressed in future work. First, here we limited our study to first-order relay thalamic nuclei input and output pathways tracts. These pathways are of great basic and clinical interest, as they are pivotal elements of the forebrain networks supporting complex functions such as language and skilled movement. Future studies should implement protocols suitable for the study of the structural connectivity between higher-order relay nuclei of the thalamus and cerebral cortex. Second, the data used to measure the reproducibility were collected using a specific acquisition MRI sequence. Follow-up studies should examine to what extent data reproducibility at the computational and test-retest levels is maintained for a range of DWI MRI protocols. Important variations may include: single-shell versus multi-shell DWI, multiband versus monoband protocols, the number of directions included, the types of MRI scanners, etcetera. Third, the reproducibility profiles of the present protocol focused on first-order relay human thalamic white-matter tracts in healthy adults. It is not clear how generalizable these results would be if the same protocol were applied to clinical or special populations. Testing different population groups would help determine whether this protocol successfully generalizes to, for instance, clinical samples and developmental samples, who undergo rapid neuroplasticity changes. Testing different DWI MRI protocols and populations was beyond the scope of the present work. The containerized implementation of the protocol facilitates the testing of other relevant aspects in future studies. We will provide support to researchers interested in using this protocol (<https://github.com/garikoitz/RTP-pipeline/wiki/Parameter-recommendations>).

## 7 Study 2: Structural connectivity of higher-order thalamic nuclei: Anterior thalamic complex and mediodorsal nucleus

The second study follows the same structure as the first study, but aimed to develop and test a reproducible protocol to obtain white-matter tracts of two higher-order thalamic nuclei: the AN and MD. These nuclei are more functionally and anatomically complex, unlike the first-order thalamic nuclei, the AN and MD have structural connections with multiple cortical structures. The cingulum bundle connects the AN with cingulate cortex and retrosplenial cortex. As for the MD, it projects to virtually the whole PFC. The above mentioned white-matter bundles are the interest of the current work. First, we defined multiple parameters to optimally reconstruct the thalamocortical fiber tracts of interest related to AN and MD. Second, we examined different white-matter proxies related to the microstructural and macrostructural properties of these tracts and tested their computational and test-retest reproducibility following our protocol. The ultimate goal of this work was to provide a reliable protocol to obtain the AN and MD related white-matter thalamocortical fibers for research and clinical practice.

The same DWI data in Study 1 were used in Study 2 to examine the reliability of the protocol. The protocol consisted of three components: ROIs definition, DWI data preprocessing and white-matter tract modeling and tractometry. The reproducibility was tested using two approaches: 1) Computational reproducibility, by repeatedly identifying in 113 subjects each tract 10 different independent times using the same parameters, and 2) Test-retest reproducibility, by re-scanning and re-analyzing a subset of 24 participants of the dataset with the same MRI protocol within an average interval of 15 days. Based on previous experience, our hypothesis was that the tracts will have a high degree of reproducibility, for both the microstructural and macrostructural properties of these tracts. Also, we expect some

inter-tract variability, some tracts are more reliable than others. Additionally, we expect higher variability for test-retest reproducibility relative to computational reproducibility.

## 7.1 Methods

### 7.1.1 Subjects and data acquisition

The protocol was tested on the diffusion dataset of Study 1, which consists of 113 healthy volunteers. Twenty-four of the volunteers returned for a second session in which they were scanned using the exact same MRI protocol. The MRI acquisition included one T1-weighted structural image (T1w) and DWI sequences. The DWI acquisition included 100 anterior to posterior phase-encoding volumes, in which there are 50 with b-value of 1000  $\text{s/mm}^2$  and 50 with a b-value of 2000  $\text{s/mm}^2$ , resulting in 50 isotropically distributed diffusion-encoding gradient directions for both the  $b=1000$  and  $b=2000$  shells. Twelve  $b_0$  images were acquired for motion correction and geometrical distortion correction, which consist of 5  $b_0$  volumes with the same anterior-posterior phase-encoding direction and 7  $b_0$  volumes with reversed phase-encoding direction (posterior-anterior). More details can be found in sections 7.1.1 and 7.1.2.

### 7.1.2 Tractography pipeline

The tract reconstruction was conducted using the same tool as in Study 1, which is using RTP2-pipeline (Lerma-Usabiaga et al., 2019, 2020), guaranteeing data provenance and reproducibility. The RTP2-pipeline divides the process into three main parts: (1) ROI definition, (2) DWI preprocessing and (3) tract identification and tractometry. In step 3 we use the preprocessed diffusion data from step 2 to model streamlines based on the ROIs created in step 1. Details are described next. The code and parameters are available through GitHub ([github.com/MengxingLiu/Thatract2-paper](https://github.com/MengxingLiu/Thatract2-paper)) and Docker Hub

(<https://hub.docker.com/u/garikoitz>). In total, 42 pairs of homogeneous white-matter tracts were reconstructed bilaterally, 3 were AN-related and 39 were MD-related fiber groups. In AN-related fiber groups, we examined the fiber connections between bilateral AN and 1) ACC; 2) posterior cingulate cortex and 3) retrosplenial cortex. In MD-related fiber groups, we examined fiber connections between MD and 39 subdivisions of the PFC.

#### 7.1.2.1 ROI definition

The AN and MD were defined from the same thalamic segmentation implemented in freesurfer as in Study 1 (Iglesias et al., 2018). In this probabilistic atlas the AN is labeled as AV, while in the present study we would keep using AN to describe the anterior nuclei group. The MD was defined by combining the medial MD and lateral MD in this atlas.

The other cortical and subcortical ROIs were obtained using different strategies. The cortical ROIs (except the cingulate ROIs) were obtained from HCP atlas, by transforming the atlas from MNI space to individual space using a non-linear transformation in ANTs (<http://stnava.github.io/ANTs>). The cingulate ROIs were obtained from the default parcellations of freesurfer: the anterior cingulate ROI was obtained by extracting the anterior cingulate gyrus and sulcus from `aparc.a2009s+aseg.mgz` volume. The posterior cingulate ROI was obtained by combining the dorsal and ventral part of the posterior cingulate gyrus in `aparc.a2009s+aseg.mgz` volume. Several inclusion or exclusion ROIs were used for different fiber groups to either include or prevent streamlines. `CGC_roi1_L` and `CGC_roi1_R` were obtained by converting hand-drawn plane ROIs in MNI space to individual space. The left and right cerebral white matter ROIs were obtained from the freesurfer `aparc.a2009s+aseg.mgz` parcellation. Fimbria was defined by the amygdala segmentation mentioned above. To make sure the ROIs extend to the interface of gray and white matter, all the ROIs in ROI#1 and ROI#2 were dilated by one cubic voxel. The inclusion and exclusion ROIs were also dilated in different degrees to achieve a better inclusion or exclusion effect.

The full parameter table can be found in the Github repository ([https://github.com/MengxingLiu/THATRACT2\\_paper](https://github.com/MengxingLiu/THATRACT2_paper)).

#### 7.1.2.2 DWI data preprocessing

The same preprocessed DWI data used in Study 1 was used here. The details of the DWI preprocessing can be found in 6.1.3.2.

#### 7.1.2.3 Tract identification and tractometry

In the third and last main step, the container RTP2-pipeline was used to obtain the final white-matter tracts. This container took the ROIs and the preprocessed DWI data to systematically identify the tracts of interest bilaterally. We initially ran this step with 4 random subjects and iterated multiple parameters. The optimal parameter combinations to identify each tract of interest were defined based on an expert anatomist's validation.

We first modeled the diffusion information at the voxel level to obtain a map of preferred directions with FODs. For this modeling we used MRtrix3's CSD algorithm (Jeurissen et al., 2014), as it can discern crossing fibers and provide more than one direction in each voxel. Next, streamline tractography was performed from the estimated FODs using MRtrix's iFOD2 algorithm (Tournier et al., 2010). The parameters to generate the streamlines, such as step size, length threshold, FODs amplitude threshold, and angle threshold are described in the GitHub repository ([https://github.com/MengxingLiu/THATRACT2\\_paper](https://github.com/MengxingLiu/THATRACT2_paper)). Streamline generation was conducted bidirectionally (i.e., combining the streamlines obtained when seeding from ROI#1 to the target ROI#2, and in the opposite direction). Matlab utilities developed in vistasoft (<https://github.com/vistalab/vistasoft>) were used to remove the outlier streamlines from each tract generated from MRtrix and to obtain the main tract metrics.

We generated tract profiles using the tract metrics obtained using *vistasoft*. Even if CSD was used to model the fibers because of its ability to discern crossing fibers, the classical DTI modeling was used to obtain the typical diffusion summary statistics, such as FA, AD and RD. To generate the tract profiles, we obtained the central location of all the streamlines in the tract and we sampled it into 100 same-length segments. The diffusion properties were summarized at each segment by taking a weighted average of the diffusion properties corresponding to a disc centered in the segment. Finally, an along-tract profile was generated for each tract.

### 7.1.3 Reproducibility measurement

Along the same line, two types of reproducibility were measured: *computational reproducibility* and *test-retest reproducibility*. In computational reproducibility, we repeated the tractography reconstruction in RTP2-pipeline 10 times. Our aim was to measure how consistently our pipeline generated tracts of interest. Second, to check for *test-retest* reproducibility, we used a subset of 24 participants that came for a second repeated acquisition session within a mean temporal interval of 15 days. We examined how consistently our pipeline generated tracts at two different time points. The reproducibility was measured at two levels: microstructural and macrostructural levels. More details can be found in 6.1.4.

### 7.1.4 Post-hoc analysis

After acquiring measurements of both computational reproducibility and test-retest reproducibility, the results revealed that reproducibility varies across the 86 tracts of interest. Thus, a post-hoc analysis was conducted to explore the possible factors that could be related to the reproducibility variance that existed across tracts. The possible factors included in this post-hoc analysis were: 1) DWI noise; 2) streamline length; 3) streamline quantity.

For each tract and each subject, we extracted the DWI noise by first creating a mask of the tract and corresponding seed and target; then we applied this mask to the noise image generated in the DWI preprocessing step to extract the average noise within this mask. The streamline length was calculated by averaging the length of each streamline in one specific tract. Both the streamline length and amount were calculated for each tract and each subject. The tracts used in this post-hoc analysis were generated by the first computation.

Tract-wise correlation analysis was conducted between the three possible factors and the four reproducibility indices for computational and test-retest reproducibility separately. In order to do the correlation analyses, three reproducibility indices, FA profile correlation, density correlation and Dice index were transformed to a normal distribution. Fisher-Z transform was adopted for the two correlation indices, to transform the Pearson correlation coefficient to a Z score. The Dice index has a restricted range of [0,1] and is often close to the value of 1. A logit transform was applied to the Dice index, where  $\text{logit}(\text{Dice}) = \ln(\text{Dice}/(1-\text{Dice}))$ . This monotone transformation maps the Dice range of [0,1] to  $[-\infty, +\infty]$ , and  $\text{logit}(0.5) = 0$ . This distribution is close to a normal distribution for a large sample size (Zou et al., 2004). For each tract, the group level average of the possible factors and reproducibility indices (after transformation if applied) were calculated across subjects. Then, paired-sample correlation analyses were conducted for each pair of factor and reproducibility index values at tract level.

## 7.2 Results

In the present study, we reconstructed 42 pairs of fiber bundles connecting two higher thalamic nuclei with their main corresponding cortical areas (3 AN-related and 39 MD-related fiber bundles) from DWI data. To examine the reproducibility of our protocol, we followed a double analytical approach testing: (1) computational reproducibility by repeating the computation on the same diffusion data 10 times and quantifying changes from computation to computation for the same

tract; and, (2) test-retest reproducibility, by obtaining DWI data from the same subjects and using the same MRI protocols across two different sessions to quantify test-retest changes in the same tracts. The results are presented with the tracts of interest divided into 5 groups: (1) AN related tracts (Figure 7.1); (2) tracts of MD with dorsolateral prefrontal regions (dlPFC, Figure 7.2); (3) tracts of MD with medial prefrontal regions (mPFC, Figure 7.3); (4) tracts of MD with orbital and frontal polar regions (Figure 7.4); (5) tracts of MD with inferior gyrus regions (IFG, Figure 7.5).

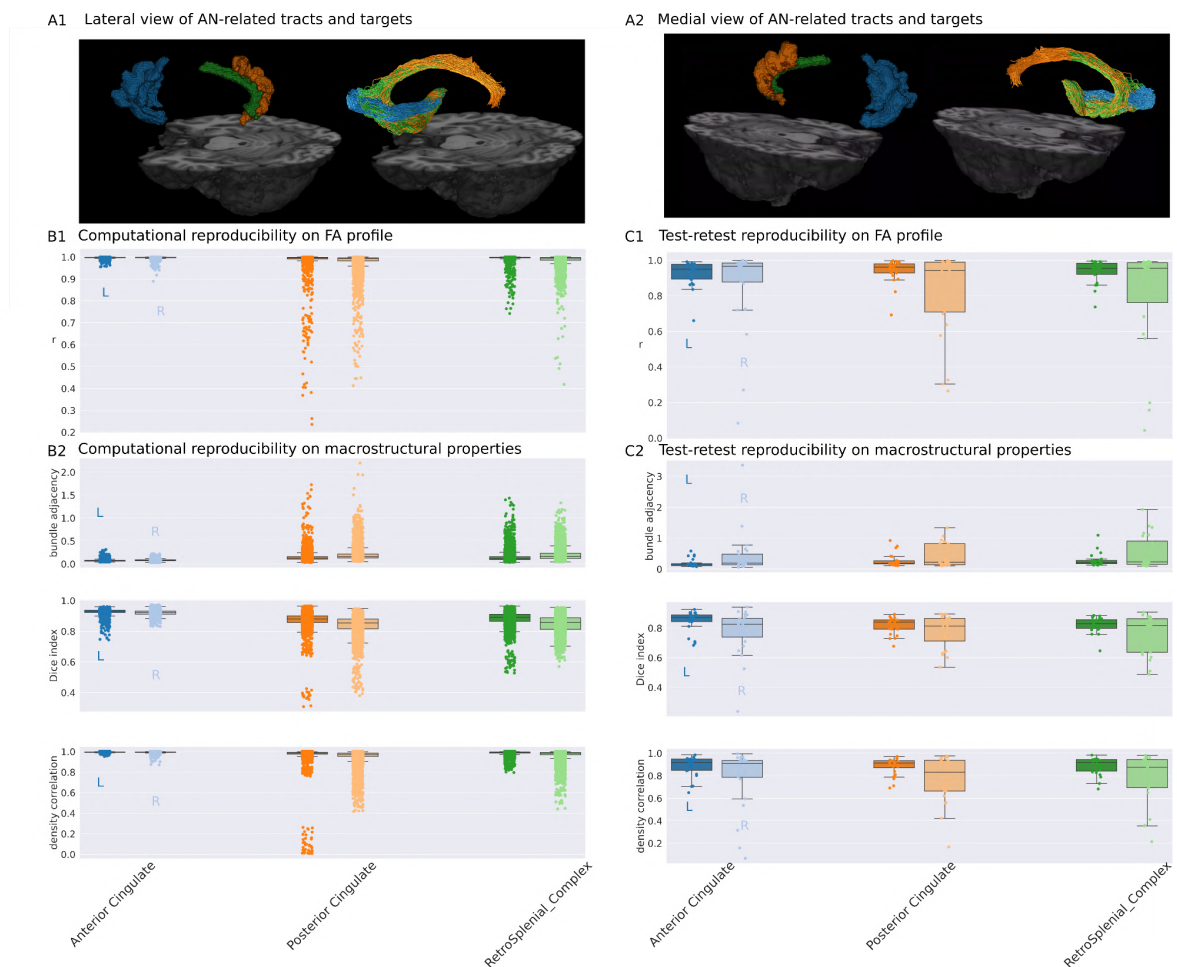


**Figure 7.1.** The computational and test-retest reproducibility of tracts connecting AN with cingulate and retrosplenial cortex. **A)** The lateral (A1) and medial (A2) views of the reconstructed tracts in a representative subject. Color scheme is the same as used in B and C. **B)** Computational reproducibility: B1) strip plots showing the distribution of correlation coefficients between all possible pairs computed for each tract and each subject (lighter color columns represent the left hemisphere; darker color columns represent the right hemisphere). Each dot represents the correlation coefficient for a specific computation pair for one participant; Box-and-whisker plots are overlaid on top to show the quartiles of the distribution. B2) Agreement indices distribution: bundle adjacency (top), Dice coefficient (middle), and density correlation (below) for all possible computation pairs for each tract and each subject (lighter color columns represent the left hemisphere, darker color columns represent the right hemisphere). **C)** Test-retest reproducibility with the same layout as panel B. The y axes of both panel B and C show the targets of those reconstructed tracts.

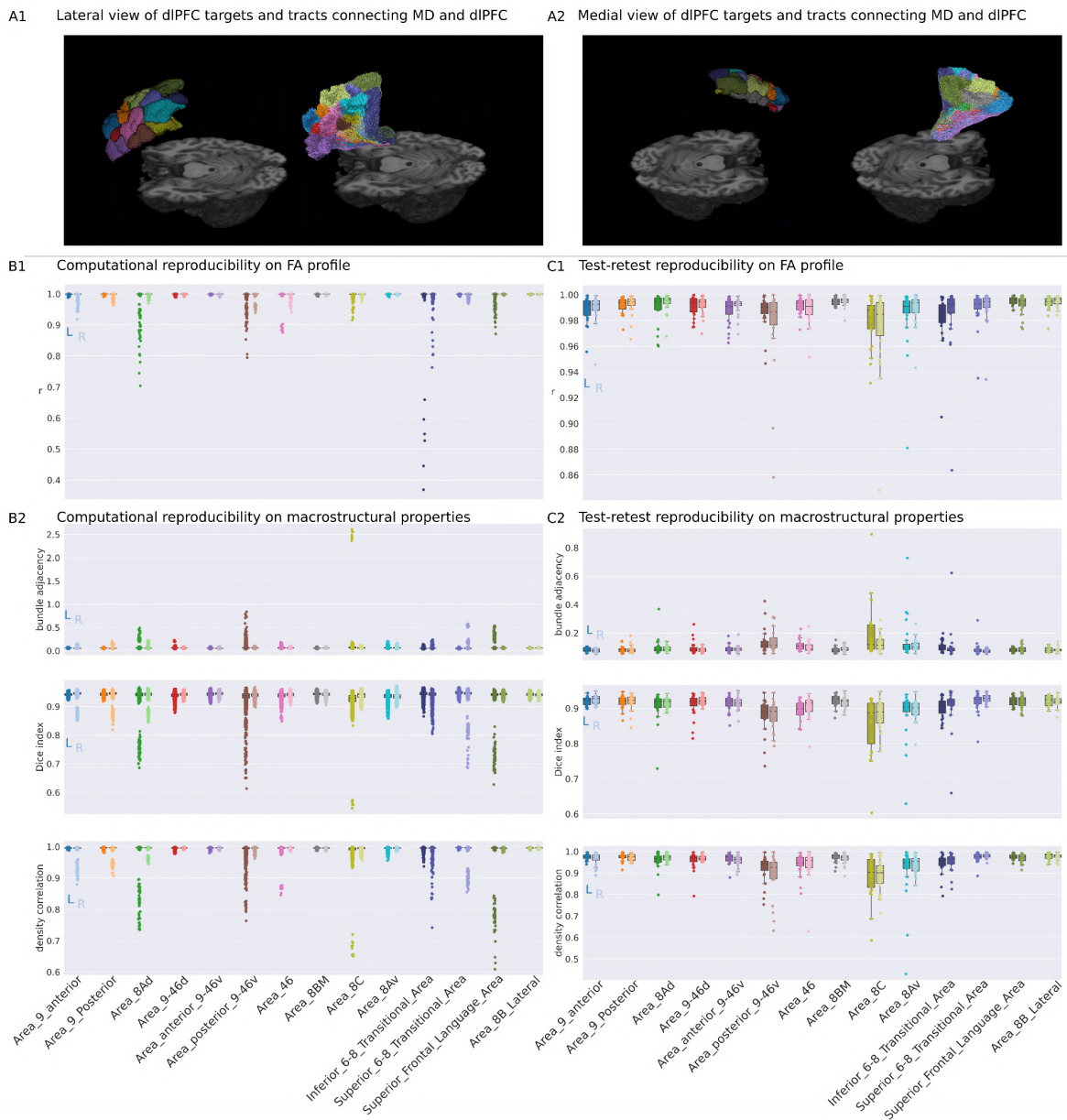
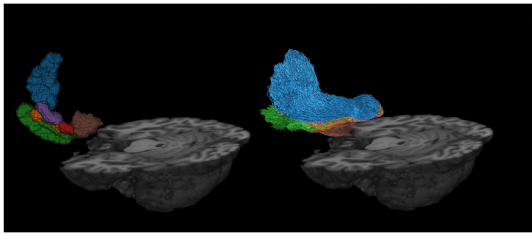
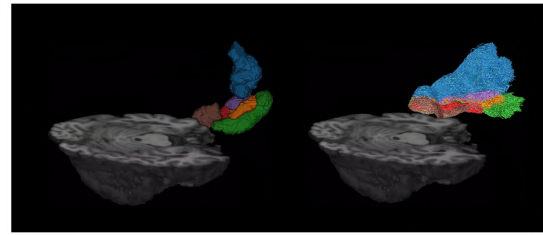


**Figure 7.2.** The computational and test-retest reproducibility of tracts connecting MD with dIPFC subregions. Details about each panel can be found in Figure 7.1 legend.

A1 Lateral view of mPFC targets and tracts connecting MD and mPFC



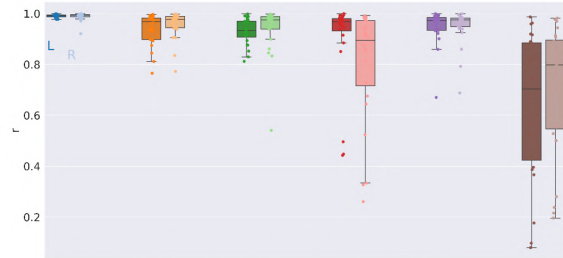
A2 Medial view of mPFC targets and tracts connecting MD and mPFC



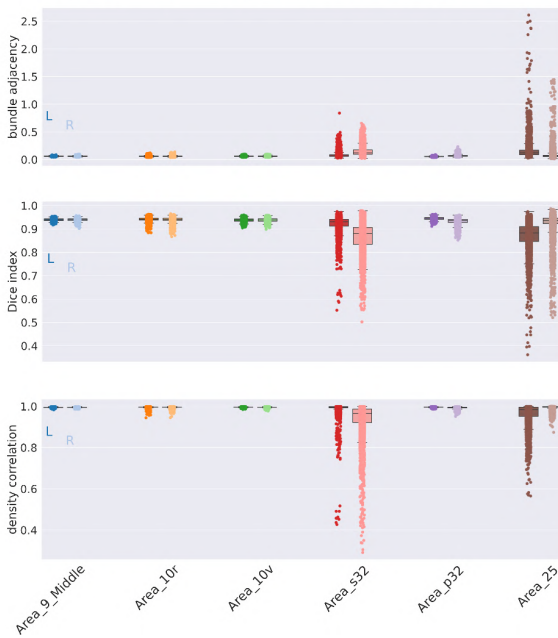
B1 Computational reproducibility on FA profile



C1 Test-retest reproducibility on FA profile



B2 Computational reproducibility on macrostructural properties



C2 Test-retest reproducibility on macrostructural properties

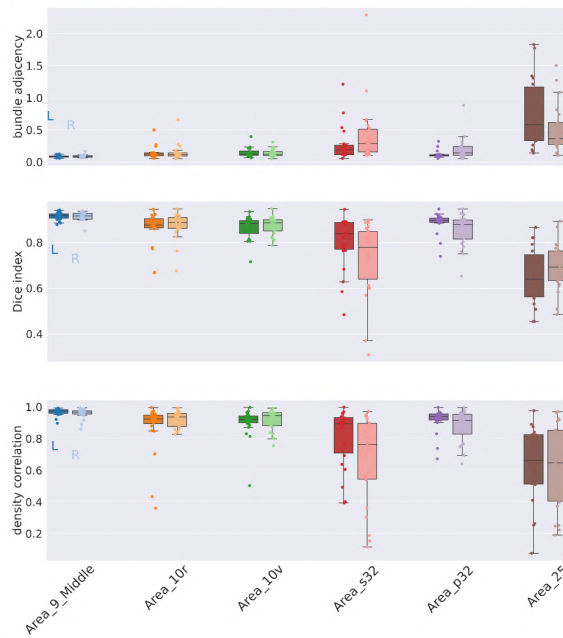


**Figure 7.3.** The computational and test-retest reproducibility of tracts connecting MD with mPFC subregions. Details about each panel can be found in Figure 7.1 legend.

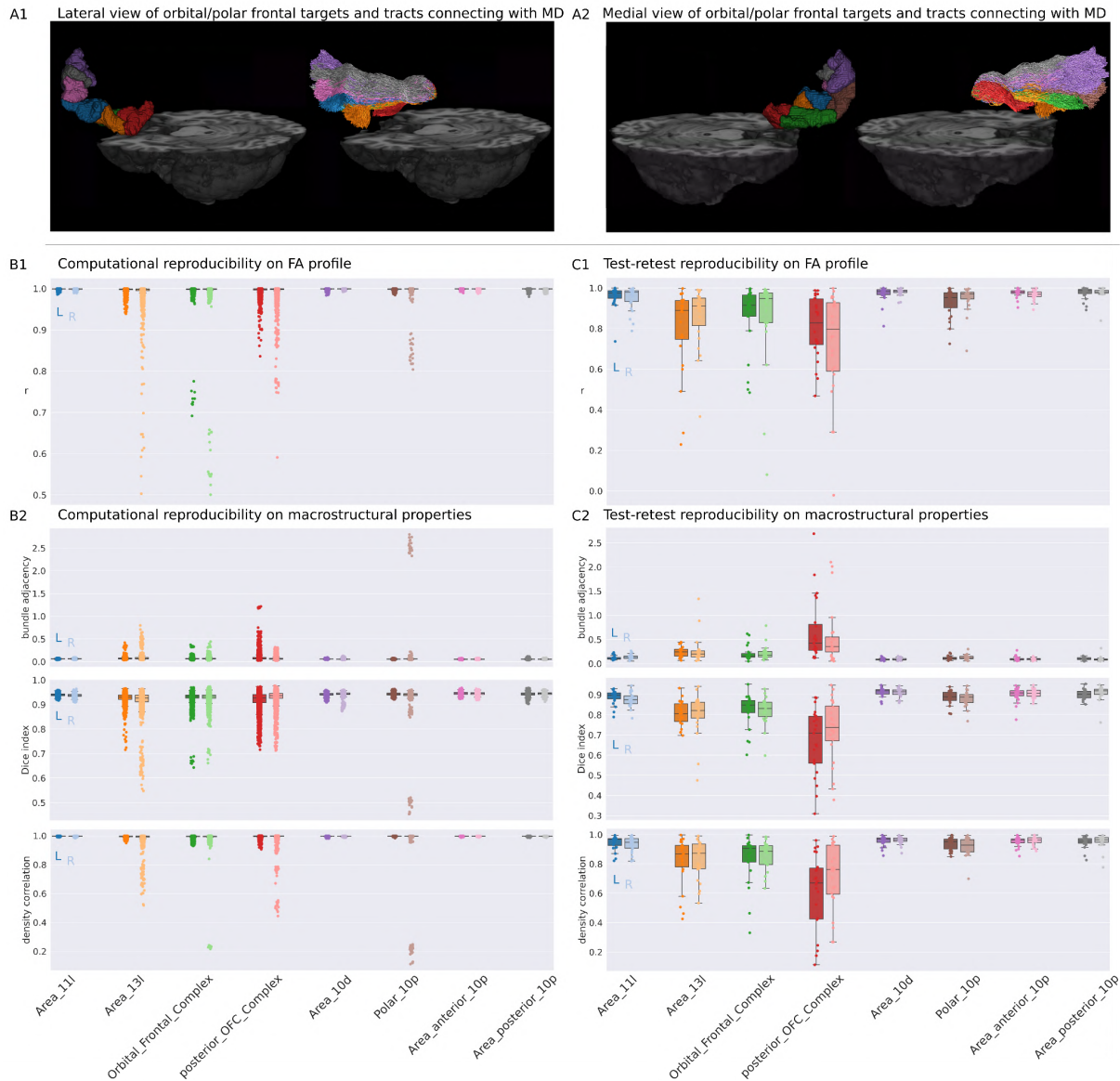


**Figure 7.4.** The computational and test-retest reproducibility of tracts connecting MD with subregions of orbital and polar frontal cortex. Details about each panel can be found in Figure 7.1 legend.

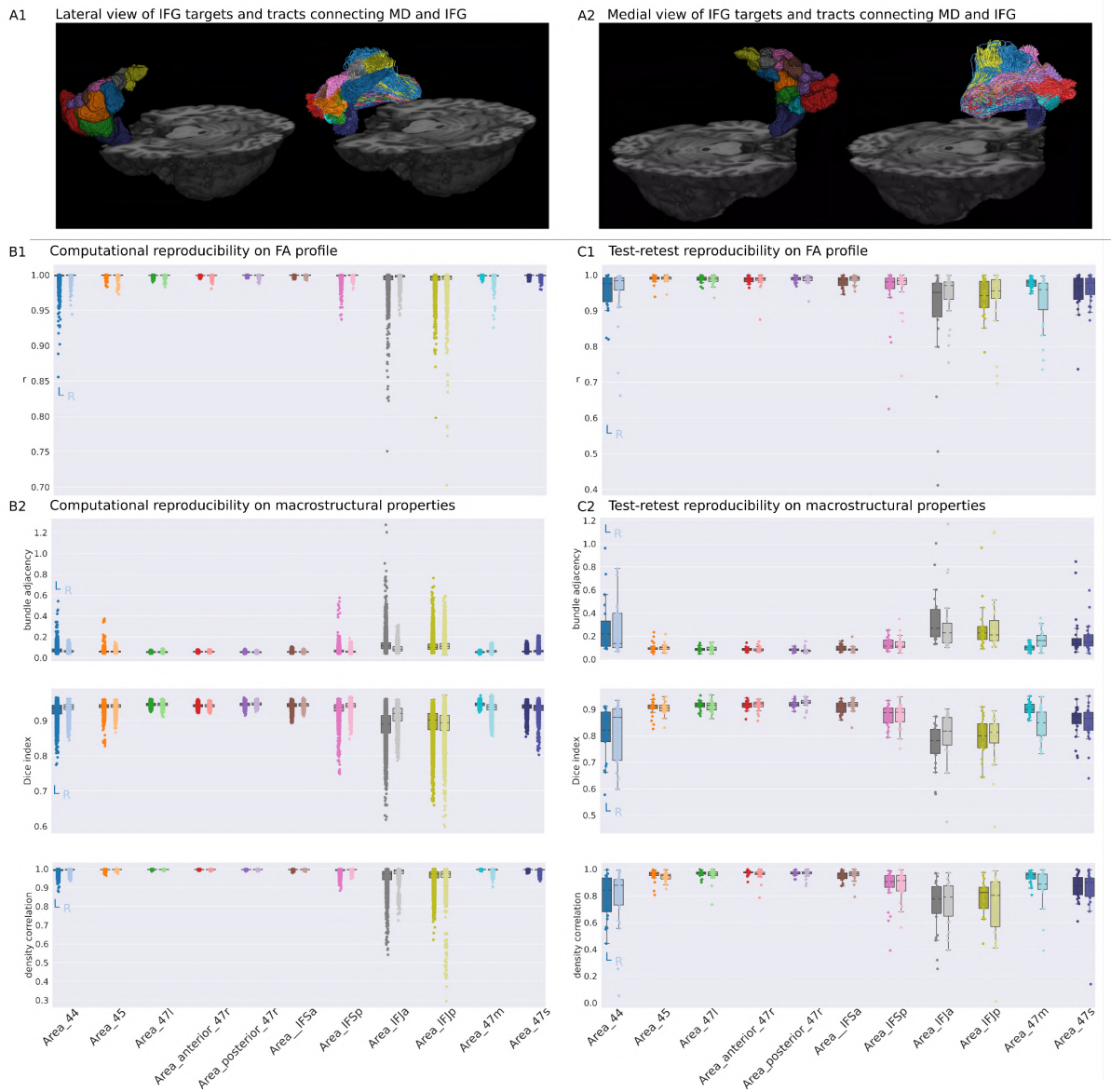


**Figure 7.5.** The computational and test-retest reproducibility of tracts connecting MD with IFG subregions. Details about each panel can be found in Figure 7.1 legend.

### 7.2.1 Computational reproducibility

For the 42 pairs of white-matter fibers with the established protocol, the repeated computations on the same diffusion data resulted in mostly identical tract profiles and high agreement of streamlines. The group mean correlations of FA profiles were above 0.97 for all the tracts examined. At the macrostructural level, the reproducibility is measured by calculating the adjacency, the streamline density correlation, and the Dice index of two repeated tracts. The results showed that the tracts have high reproducibility at macrostructural level in all three indices. The adjacency, which reflects the average distance between the two

tracts, ranges from 0.05 to 0.20 across all tracts. In all the tracts of interest, similar to it in FA profile correlation, the tracts connecting the right AN with the posterior cingulate and retrosplenial cortex have the highest adjacency, which are both 0.20. Similar high reproducibility is found in results of streamline density correlation and Dice index. The streamline density correlation ranges from 0.94 to 0.99. The Dice index showed that all tracts had high overlap between repeating computations, ranging from 0.84 to 0.95. Among all the tracts, the tracts connecting the right AN with the posterior cingulate and retrosplenial cortex showed good reproducibility but relatively low Dice index of 0.84 and 0.85 respectively.

### 7.2.2 Test-retest reproducibility

Twenty four participants were scanned for a second time with the exact same MRI protocol as the first scanning session. In this 24 participant test-retest subset, we measured how the protocol could reconstruct the tracts of interest reproducibly across test and retest. The same indices reflecting reproducibility at the microstructural and macrostructural levels were calculated. In general, the tracts of interest showed good test-retest reproducibility regarding the mean of FA profile correlations, although as expected the values were numerically lower than the ones observed in the computational reproducibility analyses. There are tracts showing relatively high variability, mostly the tracts connecting MD with orbital frontal cortex, such as the bilateral MD-Area25, with the group mean of 0.64 (left, the lowest correlation among all the tracts of interest) and 0.71 (right). Nevertheless, it is important to highlight that all the tracts have a high degree of reproducibility with a correlation average above 0.80, with only a few exceptions.

At the macrostructural level, the agreement indices showed similar patterns of reproducibility across tracts of interest. The group average of bundle adjacency, were all under 1 for all the tracts except the left MD-Area 25, which has an adjacency of 1.2,

indicating the streamlines identified in the test have very close distance to the streamlines identified in the retest. High reproducibility is also reflected by the Dice index, and streamline density correlation. Most tracts have the test-retest group average Dice index and density correlation above 0.7. Similar to the microstructural level of reproducibility, the tracts connecting MD with the orbital frontal cortex showed a relatively lower Dice index and density correlation.

### 7.2.3 Post-hoc analysis results

Post-hoc analysis was conducted separately for computational and test-retest reproducibility, to investigate the associations between the reproducibility and three factors of interest (diffusion data noise, tract streamline length and quantity). The results related to computational reproducibility showed that the diffusion noise has little correlation with the reproducibility indices except the FA profile correlation (Figure 7.6A), which has a moderate negative correlation (-0.38, higher noise in diffusion data with lower FA profile correlation). The streamline length and count both show high correlation with all the four reproducibility indices, only with the opposite direction. The length is negatively correlated with computational reproducibility: the longer the streamlines, the less reproducible across computations. Streamline count has the opposite pattern: the more streamlines one tract is composed of, the higher the reproducibility across computations.

The correlation results for the test-retest reproducibility have similar direction as in the computational reproducibility (Figure 7.6B). The noise has a negative correlation with test-retest reproducibility, ranging from -0.69 to -0.48. Opposite to the strong correlation between the tract streamline length and the computational reproducibility, the length has a null correlation with test-retest reproducibility. Regarding the correlation of the tract

streamline count, it has a similar strong correlation with test-retest reproducibility as it does with computational reproducibility.

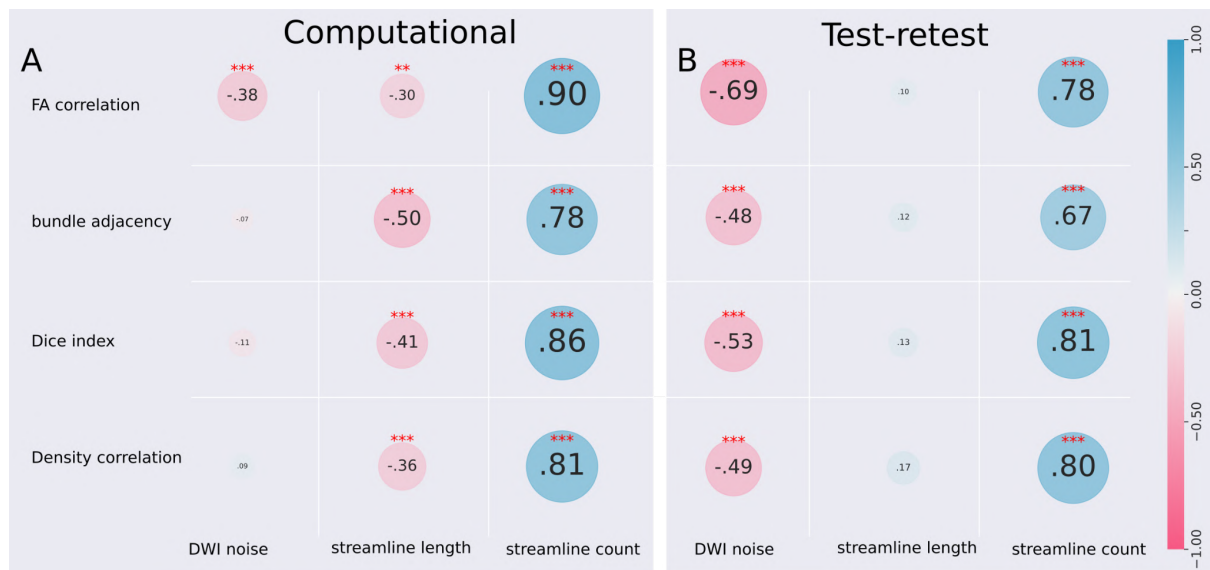


**Figure 7.6.** DWI noise, streamline length and streamline count were found to be correlated with reproducibility across tracts. **A)** The correlation between the three factors with four computational reproducibility indices. **B)** The correlation between the three factors with four test-retest reproducibility indices. \* $p < .05$ , \*\* $p < .01$ , \*\*\* $p < .001$ . The symbols of the correlation coefficients with bundle adjacency were reversed to simplify the illustration, as the value of bundle adjacency indicates the variance between tracts instead of similarity.

### 7.3 Discussion

The current study proposes a reproducible protocol to reconstruct the tractography of the AN and MD from the human thalamus. These nuclei play important roles in various cognitive processes, in particular during rapid integration of new learning, working memory, decision making and beyond. The reproducibility of the protocol for reliably obtaining these tracts of interest was measured by examining their microstructural tractometric properties and volume-based macrostructural similarity across repeating computations and test-retest sessions. Results revealed nearly perfect computational reproducibility across ten repetitions and high-to-excellent test-retest reproducibility of the AN and MD related thalamocortical tracts.

The structural connectivity profile of the higher-order thalamic nuclei, AN and MD, has been examined in numerous experiments on non-human primates (Bay & Çavdar, 2013;

Groenewegen, 1988; Lozsádi, 1995; Ray & Price, 1992; Vann et al., 2007) and postmortem studies on humans (Blennow et al., 2000; Cullen et al., 2003). However, the *in vivo* examinations of the white-matter connection of those nuclei with subcortical and cortical regions in humans are rare. Due to the lack of a well defined and validated thalamic segmentation, most tractography studies on humans used the whole thalamus (Fan et al., 2014; O’muirheartaigh et al., 2015; Pelzer et al., 2017) or segmentation in a common space (Klein et al., 2010) to estimate the structural connections of the thalamus. Unlike the first-order thalamic nuclei having relatively straightforward structural pathways with the sensorimotor cortical regions, the AN and especially MD, have more extensive and complex efferent and afferent pathways with cortical structures (Aggleton & Mishkin, 1984; Gower, 1989; Mai & Forutan, 2012; Shah et al., 2012). The current study adopted the first probabilistic atlas combining *ex vivo* MRI and histological data to define the thalamic seeds, which is implemented in Freesurfer (Iglesias et al., 2018). It provides a precise, reliable and automatic thalamic ROI definition, which is critical for the very basis of a reproducible and reliable protocol of thalamic tractography. Moreover, the major thalamic tracts of AN and MD were reconstructed from state-of-art DWI sequences according to the physiological descriptions from literature and guidance from an expert anatomist. The reproducibility of the reconstruction procedures is demonstrated in the current study. The reconstruction procedures are implemented in a containerized pipeline that allows other researchers to reconstruct the same tracts with their data. In the next section I will discuss the reproducibility of the protocol from two different approaches.

The computational reproducibility measures how reliable the protocol is to reconstruct the tracts of interest across multiple computations with the same data and same computation parameters. As expected, across ten separate and independent computations using the same raw data and protocol, the reproducibility is nearly perfect. Most tracts have high

reproducibility at both the microstructural (e.g. FA profile correlation) and the macrostructural (Dice index, density correlation and bundle adjacency) levels. Whereas there are some tracts showing relatively lower computational reproducibility, such as the tracts connecting the right AN with posterior cingulate and retrosplenial cortex. As discussed in chapter 6 section 6.2.1, the variance across computations is due to random seed selection from the probabilistic algorithm. As the AN-posterior cingulate and AN-retrosplenial cortex tracts are relatively long, the variance introduced by random seed selection is magnified exponentially as the tracking procedure continues along the streamlines. This result of relatively low reproducibility has significant value to the tractography community, as it alerts us that the assumption of no or slight changes could happen among computations may be flawed, especially for those studies using probabilistic algorithms to reconstruct specific white-matter tracts. In general, our protocol offers an efficient and reproducible guideline to reconstruct the AN and MD related tracts for neuroscientists and medical practitioners. By packing our solution in software containers that can be run using Singularity or Docker technologies, reproducibility can be maximally guaranteed regardless of the computational environment, such as different operating systems and associated libraries.

The test-retest reproducibility results showed the protocol could reliably reconstruct the AN and MD related tracts on the same samples across times. Although there are a few tracts that proved to be relatively less reproducible between test and retest than others, for example, the tracts connect MD with medial orbital frontal cortex (Area 25, posterior OFC). This reproducibility pattern is consistent among microstructural and macrostructural levels. For the rest of the tracts, the FA profile correlations are all above 0.8 and Dice indexes are above 0.7 at the group level, which indicates a high test-retest reliability. As discussed in chapter 6 section 6.3, most studies that calculated the Dice index on different white-matter bundles between test and retest reported an average Dice index of around 0.7 (Besseling et

al., 2012; Boukadi et al., 2019; Cousineau et al., 2017). It is worth noting that the tracts we reconstructed in the current study involve subcortico-cortical white-matter fibers, which are structurally complex and less thick than the main white-matter bundles in the human brain that are thoroughly investigated in previous studies.

The post-hoc analysis showed other interesting results that could be of interest to future researchers. The source of variance across repeating computations is due to random seed selection in the probabilistic algorithm (as discussed in chapter 6 section 6.2.1). For the test-retest computations, in addition to the random seed selection we know that the MRI environment and participant conditions between test and retest could introduce more variance. Ideally, both the random variance in computations and random-like variance in test-retest should not have systematic effects on the calculations. The post-hoc analysis reported in the current study suggested that while combining with other tracking factors, the random and random-like variance could yield systematic variance regarding the reproducibility. Three factors examined in the current study, the raw DWI data noise, the streamline length and count were all found to be associated with the reproducibility of computational and test-retest in different degrees. It seems that the raw DWI noise does not affect the computational reproducibility, at least at the macrostructural level, but it is strongly associated with the test-retest reproducibility. It is well established that susceptibility-induced field gradients could cause signal loss in the frontal orbital lobe (Glover & Law, 2001). The current study did observe relatively lower reproducibility of tracts terminating in medio-orbito frontal regions. The association between DWI noise and test-retest reproducibility and the lack of association with computational reproducibility could be explained by it: the computational reproducibility was measured from the same preprocessed DWI data, regardless of the signal-to-noise ratio of different regions, while the test-retest reproducibility was measured from different preprocessed DWI data. Therefore, those regions

that are more vulnerable to signal loss have more variance between test and retest as they are two different measurements in time, with their own noise pattern.

We reported a high negative correlation between computational reproducibility and streamline length as well. In probabilistic tractography, the fiber orientation distribution is calculated for each voxel (Behrens et al., 2007; Tournier et al., 2010), and a random sample is drawn in this distribution to determine the direction of the streamline propagation. The more voxels the streamline is transpassing (longer streamline), the more random samplings the algorithm has to make. Thus, more variance is introduced between computations when more random decisions are involved. The high association was not found between test-retest reproducibility and streamline length. This is probably because the variance between two different datasets (test and retest) is much more noticeable compared to the variance that comes from the nature of probabilistic tractography at the computational level.

Finally, the number of streamlines in one tract has a strong correlation with both the computational and test-retest reproducibility. All of those tracts were reconstructed by setting the desired number of fibers at 5000. Some tracts having fewer streamlines failed to generate enough streamlines even after iterating at specific times, mainly due to less robustness or thinner fiber bundles at anatomical level. Those tracts tend to have less reproducibility than those having more streamlines due to a relatively smaller sample size and more sensitivity to variance than those tracts that have more streamlines.

In sum, this study established a reliable protocol to obtain higher-order thalamic white-matter tracts from the AN and MD. Both the computational and test-retest reproducibility were measured and the results revealed a nearly perfect computational reproducibility and high-to-excellent test-retest reproducibility of the protocol at both microstructural and macrostructural levels, with some tracts showing relatively more

variance. DWI data noise, streamline length and quantity were examined and found to be associated with reproducibility. Future studies are needed to have systematic manipulations on the factors to examine the impact on reproducibility, especially the computational reproducibility that has been neglected for long in the tractography community.

## 8 Study 3: task-based fMRI study of thalamic involvement in human language systems

Classical views understand the thalamus as a simple transponder, relaying information to cortico-cortical and cortico-subcortical systems. Although these views have been extensively challenged over the last years, first-order relay thalamic nuclei seem to be mainly involved in receiving information from the periphery and relaying this information to the cerebral cortex. Over the last two decades, neuroimaging research has unveiled the contributions of cortical regions to human language. However, the role of the sensorimotor thalamic nuclei and their thalamocortical interactions in language processing remains widely unknown. The main human language systems rely on different types of sensorimotor information: reading relies on visual input, speech comprehension relies on auditory input and speech production relies on motor articulation. Thus, in the current study we examined the involvement of first-order relay thalamic nuclei in three human language systems: LGN in reading, MGN in speech comprehension and VLN in speech production. We hypothesize that the first-order relay thalamic nuclei have modality-specific involvement in the three language systems as a function of sensorimotor information being processed, and they have different activation patterns to linguistic and parallel non-linguistic tasks in each modality. In addition, we expect robust functional and structural connectivity between the first-order relay thalamic nuclei and their corresponding cortical structures that reflect the thalamocortical circuits.

### 8.1 Methods

#### 8.1.1 Participants

The study sample consisted of 40 participants (28 females, mean age  $24.0 \pm 4.6$  years, after 5 participants were excluded from further analyses due to excessive head motion during scanning). All participants were right-handed and had normal or corrected-to-normal vision. No participant had a history of major medical, neurological, or psychiatric disorders. The study protocol was approved by the Ethics Committee of the Basque Center on Cognition, Brain and Language (BCBL) and was carried out in accordance with the Code of Ethics of the World Medical Association (Declaration of

Helsinki) for experiments involving humans. Prior to their inclusion in the study, all subjects provided informed written consent. Participants received monetary compensation for their participation.

### 8.1.2 Materials and Experimental Procedure

The functional MRI study used a factorial within-subjects block design with the factors Task (linguistic and nonlinguistic) and Modality (visual, auditory and motor). The linguistic tasks consisted of word reading (visual modality), speech word comprehension (auditory modality), and speech word production (motor modality). The non-linguistic tasks consisted of seeing scrambled images (visual modality), listening to noise audios (auditory modality) and producing unintelligible sounds (motor modality).

Participants went through seven functional runs. Each run comprised six 12 s blocks of interest, one per each of the experimental conditions: linguistic visual, linguistic auditory, linguistic motor, non-linguistic visual, non-linguistic auditory, and non-linguistic motor. Activation blocks were separated by 13.5s rest blocks to allow the BOLD response to return to baseline before presenting the next activation block. The fMRI data was acquired with a sparse-sampling protocol (see MRI data acquisition for further details), thus within an activation block there were 12 silence breaks (each of them lasting 1.2s) before every functional MRI volume acquisition and the corresponding scanner noise.

In the linguistic visual or word reading blocks, 12 visual words were presented on the screen one after the other, and participants were instructed to read them silently. The non-linguistic visual condition presented 12 scrambled words on the screen, one by one, and participants only needed to fixate on them. In the linguistic auditory or speech word comprehension blocks, an instruction was shown on the screen to instruct the participants to close their eyes and listen to the auditorily presented words, which were twelve and were played to the participants one after another through the scanner sound system. In the non-linguistic auditory condition participants were also asked to close their eyes and listen to the noise audios, which were 12 and were presented auditorily through the scanner sound system. In the linguistic motor or speech production blocks, the participants were

presented with an instruction asking them to produce noun words with their eyes closed. Participants were instructed to produce one word during each silence of the sparse-sampling fMRI protocol. Similarly, in the non-linguistic motor condition participants were asked to produce 12 unintelligible sounds during each silence break while having their eyes closed. In every activation block during which the participants had their eyes closed (i.e., auditory linguistic, auditory non-linguistic, motor linguistic and motor non-linguistic conditions), there was a bell sound playing through the scanner sound system to signal participants the end of the activation block and that they have to open their eyes again.

A total of 168 Basque noun words (e.g. *poltsa*, *bag* in English) were selected for the visual and auditory tasks. Half of the words were presented visually in the reading task, and the remaining half were presented auditorily in speech comprehension tasks, in which the audio was recorded by a female Basque native speaker. Scrambled words in the visual non-linguistic task were designed by creating  $10 \times 10$  pixel tiles and mixing them randomly, using the same word images from the reading task. The noise audios in the auditory non-linguistic task were created by randomly shifting the auditory signal in time domain, using the same speech words used in the speech comprehension task. The stimuli in visual and auditory modalities were counterbalanced across participants such that the visual word images and corresponding perceptual stimuli used in half of the participants will be presented in auditory, and vice versa for auditory modality stimuli. In the linguistic motor or speech word production task, participants were instructed to produce object names existing in their familiar environment, such as a *table* or a *keyboard* in an office. In the non-linguistic motor, participants have to produce unintelligible sounds that the experimenter showed to the participant before undergoing MRI scanning. These unintelligible sounds (e.g., palatal click sound) had no semantic meaning. Before participants underwent MRI scanning, they practiced a behavioral version with the six main conditions of the fMRI experiment to familiarize them with the procedure and the instructions presented during the tasks.

### 8.1.3 MRI data acquisition

Whole-brain MRI data acquisition was conducted on a 3-T Siemens PRISMA Fit whole-body MRI scanner (Siemens Medical Solutions) using a 64-channel whole-head coil. Functional images were acquired with a sparse-sampling paradigm (effective repetition time (TR) = 2.9 s, real TR = 1.7 s) in a single gradient-echo echo-planar multiband pulse sequence with the following acquisition parameters: TE = 35 ms; MB acceleration factor = 5; 65 axial slices with a 2.4 mm<sup>3</sup> voxel resolution; no inter-slice gap; flip angle = 56°; FoV = 210 mm; 1169 volumes in 7 runs. High-resolution MPRAGE T1-weighted structural images were also collected for each participant with the following parameters: TR = 2530 ms; TE = 2.36 ms; flip angle = 7°; FoV = 256 mm; voxel resolution = 1 mm<sup>3</sup>; 176 slices. In total 100 diffusion weighted images were acquired with the anterior to posterior phase-encoding direction and 50 isotropically distributed diffusion-encoding gradient directions. The 100 diffusion weighted images included 50 images with b-values of 1000 s/mm<sup>2</sup> and 50 images with b-values of 2000 s/mm<sup>2</sup>. Twelve images with no diffusion weighted (b-values of 0 s/mm<sup>2</sup>) were obtained for motion correction and geometrical distortion correction, which comprised five images with the same phase-encoding direction as the DWI images and seven images with the reversed phase-encoding direction (posterior to anterior). Both DWIs and b0 images shared the following parameters: TR = 3600 ms, TE = 73 ms, FA = 78°, voxel size = 2 mm isotropic, 72 slices with no gap and a multiband acceleration factor of 3.

### 8.1.4 MRI data analysis

For *structural image analysis*, the T1w images were processed using RTP-anatROIs, which involves processing the subjects' anatomical T1w image with *recon-all* from freesurfer (<http://surfer.nmr.mgh.harvard.edu>) and extract ROIs. First, Freesurfer was used to perform cortical/subcortical segmentation and parcellation. Next, the thalamic nuclei were obtained by running the thalamic segmentation module implemented in Freesurfer on a probabilistic atlas built based on histological and high-resolution *ex vivo* MRI data (Iglesias et al., 2018). For this study, we only considered first-order relay nuclei as ROIs: the LGN, MGN and VLN. For functional and structural

connectivity analyses, we also extracted the cortical regions V1/V2, A1 and M1. To parcellate the visual cortex we ran the Neuropythy (Benson & Winawer, 2018; <https://github.com/noahbenson/neuropythy>) tool on the Freesurfer results. A combination of the resulting V1 and V2 ROIs was used for our visual cortex ROI. A1 and M1 were converted from the human connectome project (HCP) atlas (Glasser et al., 2016). To convert them to individual subject space, we performed a non-linear registration of a 1 mm<sup>3</sup> MNI template using Advanced Normalization Tools (ANTs, <http://stnava.github.io/ANTs/>).

For *functional images preprocessing*, we used SPM12 (Wellcome Center for Human Imaging, London) preprocessing routines and analysis methods. Images were corrected for differences in slice acquisition timing across every functional scan and then realigned for motion correction. Afterwards, each subject's functional volumes were smoothed using a 2 mm full-width half-maximum (FWHM) Gaussian kernel. Motion parameters were extracted from the realignment step to inform a volume repair procedure (ArtRepair; Stanford Psychiatric Neuroimaging Laboratory) that identified bad volumes on the basis of scan-to-scan movement (>0.5 mm) and signal fluctuations in global intensity (>1.3%) and corrected bad volumes *via* interpolation from the nearest non-repaired scans. Five participants with more than 15% to-be-corrected outlier functional volumes were excluded. After volume repair, functional volumes were separately coregistered in two different ways: 1) to MNI space in order to conduct whole-brain contrasts in normalized MNI space at the group level; 2) to high-resolution anatomical T1 images and resliced from the original 2.4 mm<sup>3</sup> functional voxel dimensions to 1 mm<sup>3</sup> voxels in anatomical T1 space for ROI analysis and functional connectivity. Finally, time series were temporally filtered to eliminate contamination from slow frequency drift (high-pass filter: 128s).

*Statistical analyses* were performed on each subject data from both the MNI space and individual space using the general linear model (GLM). A series of impulses convolved with a canonical hemodynamic response function (HRF) were used to model the fMRI time series data. The six main experimental conditions in our design (i.e., 2 Task X 3 Modaly) were modeled as epochs from the onset of the first trial within each block until the last trial within the block, resulting in 20.4s

(12 x 1.7) periods. These functions were used as covariates in the GLM. The motion parameters for translation (i.e., x, y, z) and rotation (i.e., yaw, pitch, roll) were used as covariates of non-interest in the GLM. SPM12 FAST was used for temporal autocorrelation modeling in this GLM due to its optimal performance in terms of removing residual autocorrelated noise in first-level analyses (Olszowy et al., 2019). The least-squares parameter estimates of the height of the best-fitting canonical HRF for each condition were used in pairwise contrasts. At the group level, whole-brain contrasts between conditions were computed in MNI space by performing paired t-tests on these images from different conditions, treating participants as a random effect. Three whole-brain contrasts were conducted: Visual tasks - (Auditory + Motor tasks), Auditory tasks - (Visual + Motor tasks) and Motor tasks - (Visual + Auditory tasks). These three contrasts were selected to examine the modality-specific regions at the whole-brain level. Our standard statistical threshold for whole-brain maps was a Family Wise Error (FWE) set to  $p < .05$  at the voxel level.

**Individual ROI analysis** was performed on GLM results from the individual space with the MARSBAR toolbox for use with SPM12. Given that this study focused on the involvement of first-order thalamic nuclei in language processing, the LGN, MGN and VLN were selected from both hemispheres as ROIs. Then, in line with our main experimental design, we extracted parameter estimates (i.e., scaled % signal change values) for each single region and subject individually and used them as dependent variables in 2 (Task: linguistic and non-linguistic) by 3 (Modality: visual, auditory and motor) repeated measures ANOVAs. As we were interested in whether there is a dissociation of thalamic involvement between linguistic and non-linguistic tasks, we tested the left and right thalamic ROIs separately and compared their involvement between linguistic and non-linguistic tasks in their corresponding modality based on our hypotheses.

**Functional connectivity** was examined between each first-order thalamic nuclei of interest (LGN, MGN and VLN) and the site of cortical termination of the corresponding sensorimotor pathways (V1/V2, A1 and M1). The functional connectivity analyses were conducted using the beta-series correlation method (Rissman et al., 2004), implemented in SPM12 with custom Matlab scripts. The canonical HRF in SPM was fit to each trial from each experimental condition and the

resulting parameter estimates (i.e., beta values) were sorted according to the study conditions to produce a condition-specific beta series for each voxel. Pairwise functional connectivity analysis between thalamic nuclei and cortical regions were conducted at the individual-subject level for each task in the corresponding sensorimotor modality (LGN-V1V2 in visual, MGN-A1 in auditory and VLN-M1 in motor). The beta-series correlation values (r values) were transformed to Fisher's z values by applying an arc hyperbolic tangent transform (Fisher, 1921) at the subject level for each pair of ROIs and each experimental condition. Since the correlation coefficient is inherently restricted to range from  $-1$  to  $+1$ , this transformation ensured the null hypothesis sampling distribution approached that of the normal distribution. To assess the significance of the correlation findings at the group level, the z-transformed correlation of the individual subjects were compared against zero at group level.

***Structural connectivity analysis*** was conducted by using the tractography protocol proposed in Study 1 to reconstruct the first-order relay thalamic tracts on the DWI data collected in this study. Three pairs of first order thalamic tracts were reconstructed: bilateral OR, AR and MR. The FA profile of each tract from each subject was obtained using RTP-pipeline. More details can be found in chapter 6, section 6.1.4. The mean of the FA profile was calculated as the index by averaging the 100 FA values in the FA profile for each tract and each subject. For each first-order thalamocortical pathway of interest, to examine the associations between the structural connectivity and functional connectivity, correlation analyses were conducted between the FA values from structural connectivity and z values from functional connectivity of the corresponding modality task.

## 8.2 Results

### 8.2.1 Whole-brain contrasts

To identify brain regions associated with processing specific modalities across all participants and linguistic-non linguistic tasks, we computed three whole-brain contrasts: visual > (auditory + motor); auditory > (visual + motor) and motor > (visual + auditory). These contrasts revealed the involvement of the first-order thalamic relay nuclei and the primary corresponding sensorimotor cortical regions in modality specific tasks. The visual > (auditory + motor) contrast showed increased

activation in bilateral LGN and primary and secondary visual cortex in visual tasks compared to tasks in other two modalities (Figure 8.1A). Similarly, the auditory > (visual + motor) contrast revealed the auditory thalamic nuclei bilateral MGN and A1 (Figure 8.1B). The motor > (visual + auditory) contrast showed higher involvement of the motor thalamic nuclei (bilateral VLN) and M1. Vermis III in the cerebellum also showed specific involvement in the motor contrast (Figure 8.1C). Using a mask of the entire thalamus with these same contrasts revealed the specificity of each of them showing functional activation of the expected thalamic nuclei: LGN for visual > (auditory + motor) contrast; MGN for auditory > (visual + motor) contrast; and, VLN extended to mediodorsal nucleus for the motor > (visual + auditory) contrast (Figure 8.1D)

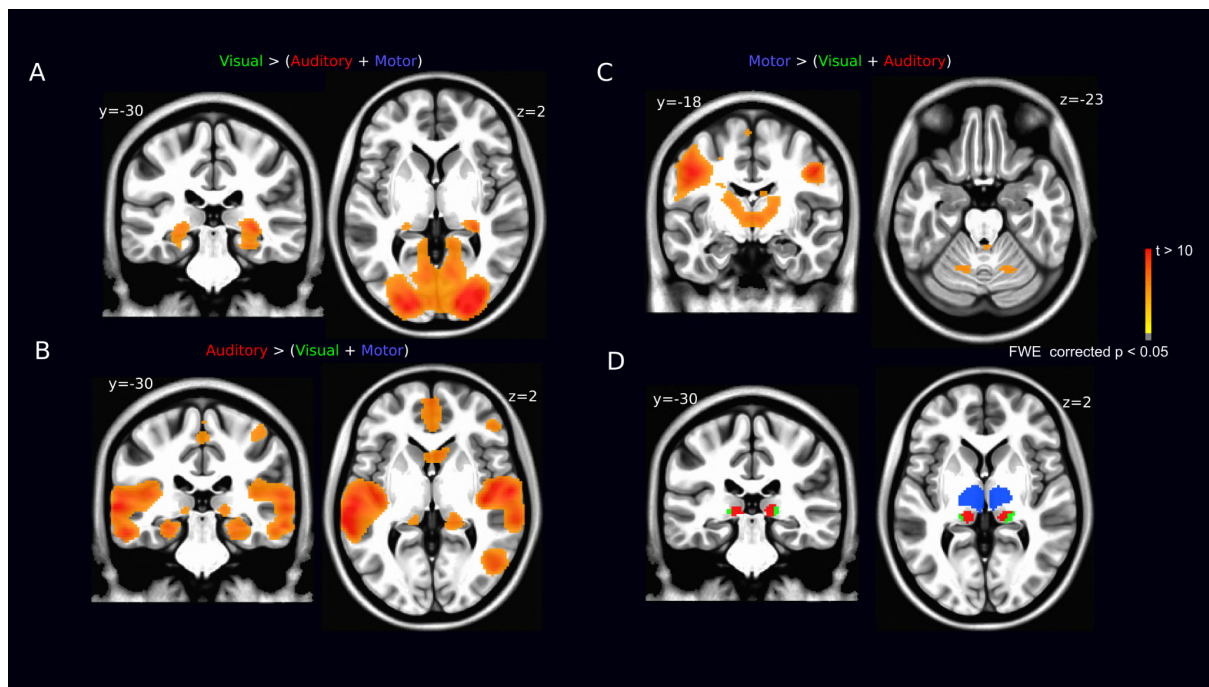


**Figure 8.1.** **A)** Brain sections showing activations for the visual > auditory + motor whole-brain contrast across all subjects. **B)** Brain sections showing activations for the auditory > visual + motor whole-brain contrast across all subjects. **C)** Brain sections showing activations for the motor > visual + auditory whole-brain contrast across all subjects. **D)** Brain sections showing the same three contrasts using a mask of the entire thalamus (green = visual > auditory + motor, red = auditory > visual + motor, blue = motor > visual + auditory). All brain sections presented here are in MNI space. The statistical threshold was  $p < 0.05$  FWE- corrected at the voxel level.

### 8.2.2 ROI results

ROI analyses were conducted to characterize the activation profile of the three thalamic ROIs (LGN, MGN and VLN) bilaterally for the main experimental tasks in three perceptual modalities. We

extracted fMRI parameter estimates from these six ROIs and conducted hypothesis-driven analyses based on planned comparisons between conditions.

*LGN.* Results from bilateral LGN are presented in Figure 8.2A. A repeated measures analysis of variance (ANOVA) was conducted for the LGN parameters estimates from both hemisphere separately showed a main effect of Modality, for left LGN [  $F(2,228) = 26.39; p < 0.001, \eta_p^2 = 0.19$ ] and right LGN [  $F(2,228) = 23.30; p < 0.001, \eta_p^2 = 0.17$ ], with stronger activation for the visual tasks relative to the auditory and motor tasks. Planned comparisons revealed that LGN showed higher activation in both linguistic and non-linguistic tasks in visual modality compared to their counterparts in auditory and motor modalities, with the exception of the right LGN activation to non-linguistic tasks having no difference between visual and motor modalities. More importantly, since we are interested in possibly different involvement of the first-order thalamic ROIs between linguistic and non-linguistic tasks in the corresponding modality, simple-effects comparisons between linguistic and non-linguistic tasks in visual modality were conducted for both left and right LGN. The results revealed that the left LGN showed higher involvement for visual linguistic task compared to visual non-linguistic task ( $p < 0.05$ ), while this difference was not observed for right LGN ( $p = 0.17$ ).

*MGN.* The repeated measures ANOVA conducted for bilateral MGN showed the main effect of Modality, for left MGN, [  $F(2,228) = 3.77; p < 0.05, \eta_p^2 = 0.03$ ]; for right MGN, [  $F(2,228) = 5.27; p < 0.01, \eta_p^2 = 0.04$ ], revealing stronger activation for auditory tasks relative to the motor tasks (Figure 8.2B). Simple effects comparisons revealed that left MGN showed higher activation for linguistic tasks in the auditory modality compared to both visual and motor modalities. Similar patterns were also found in right MGN, along with higher activation in non-linguistic tasks in the auditory modality than in the visual modality. Finally, the left MGN showed stronger engagement in the auditory modality for the linguistic task than for the non-linguistic task ( $p < 0.01$ ), and this effect was not observed for the right MGN ( $p = 0.79$ ).

*VLN.* As expected, same ANOVA conducted for bilateral VLN showed the main effect of Modality for left VLN, [  $F(2,228) = 48.8; p < 0.001, \eta_p^2 = 0.30$ ] and right VLN, [  $F(2,228) = 49.3; p <$

0.001,  $\eta_p^2 = 0.30$ ], with stronger activation for motor tasks relative to the visual and auditory tasks (Figure 8.2C). Simple-effects comparisons conducted separately for linguistic and non-linguistic revealed higher activation in both left and right VLN in the motor modality compared to both visual and auditory modalities. Different from the results of left and right LGN and MGN, comparison in the VLN between activation of linguistic and non-linguistic tasks in motor modality did not reveal statistically significant differences ( $ps > 0.12$ ).

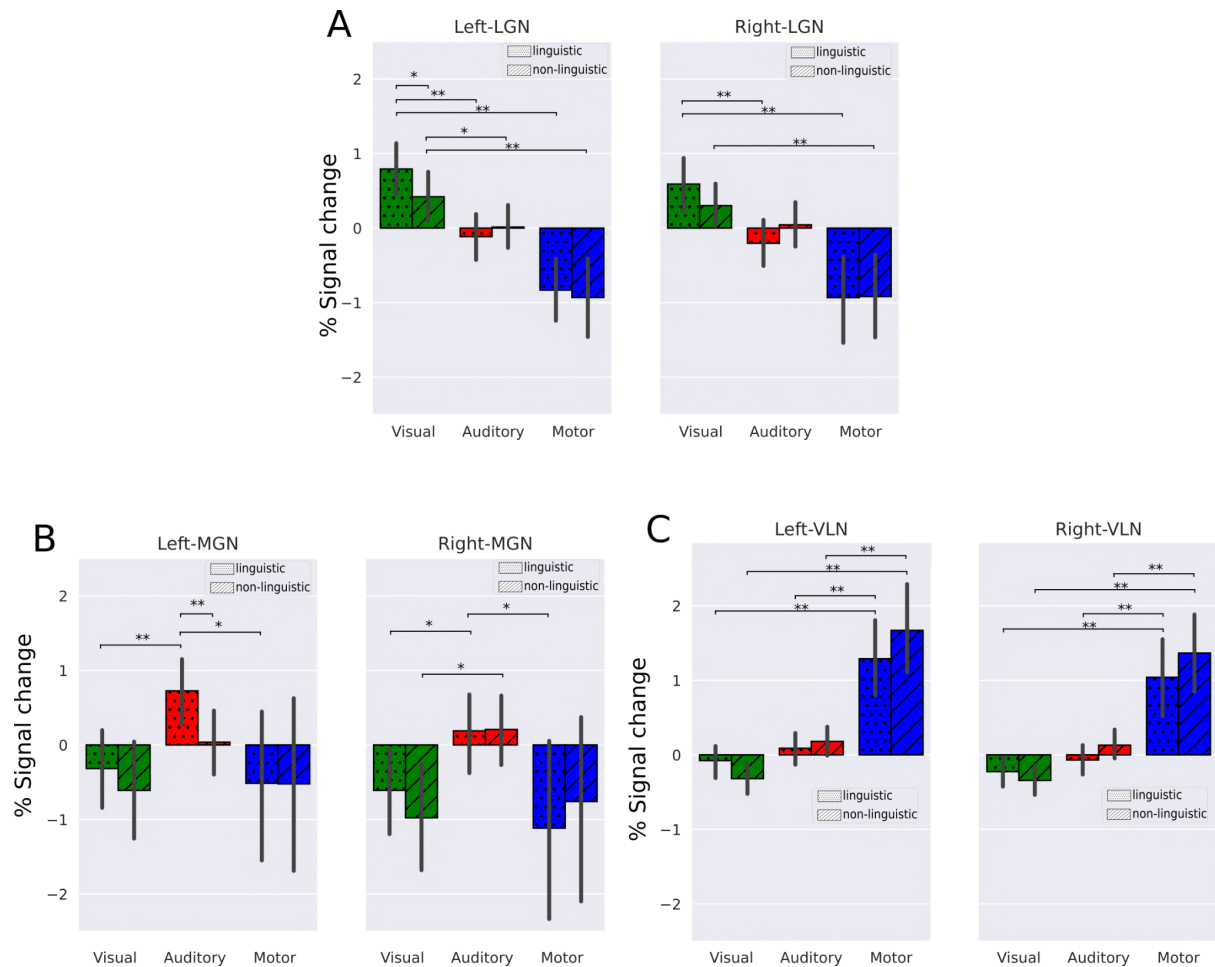


**Figure 8.2.** ROI analyses for three first-order relay thalamic nuclei: **A)** bilateral LGN; **B)** bilateral MGN and **C)** bilateral VLN. Bar graphs show averaged parameter estimates (% signal change) of each thalamic nuclei for linguistic and non-linguistic tasks in the three modalities: visual, auditory and motor. \* $p < 0.05$ , \*\* $p < 0.01$ .

### 8.2.3 Functional connectivity results

Pairwise functional connectivity analyses of three first-order relay thalamic pathways for the linguistic and non-linguistic tasks of the corresponding modalities were examined: LGN-V1/V2 visual pathway for linguistic and non-linguistic tasks in the visual modality; MGN-A1 auditory pathway for

linguistic and non-linguistic tasks in the auditory modality; and, VLN-M1 motor pathway for linguistic and non-linguistic tasks in the motor modality. To examine the significance of the correlation findings at the group level, the z-transformed correlation values of the individual subjects were compared against zero. The results revealed that predicted functional connections between regions based on known neuroanatomy were statistically significant for both linguistic (Figure 8.3A) and non-linguistic tasks (Figure 8.3B). For the visual pathway, functional coupling of LGN with V1/V2 for linguistic tasks ( $z=0.56, p < 0.001$  for left and  $z=0.58, p < 0.001$  for right) and non-linguistic task ( $z=0.52, p < 0.001$  for left;  $z=0.51, p < 0.001$  for right). Similarly significant functional coactivation was found between MGN and A1 for auditory linguistic and non-linguistic tasks, as well as between the VLN and M1 for motor linguistic and non-linguistic tasks. Simple-effect analyses were conducted to examine if there was any statistically significant difference between the functional connectivity in linguistic and non-linguistic tasks for each of these first-order thalamic pathways, with none of these comparisons revealing statistically significant differences ( $ps \geq 0.54$ ).

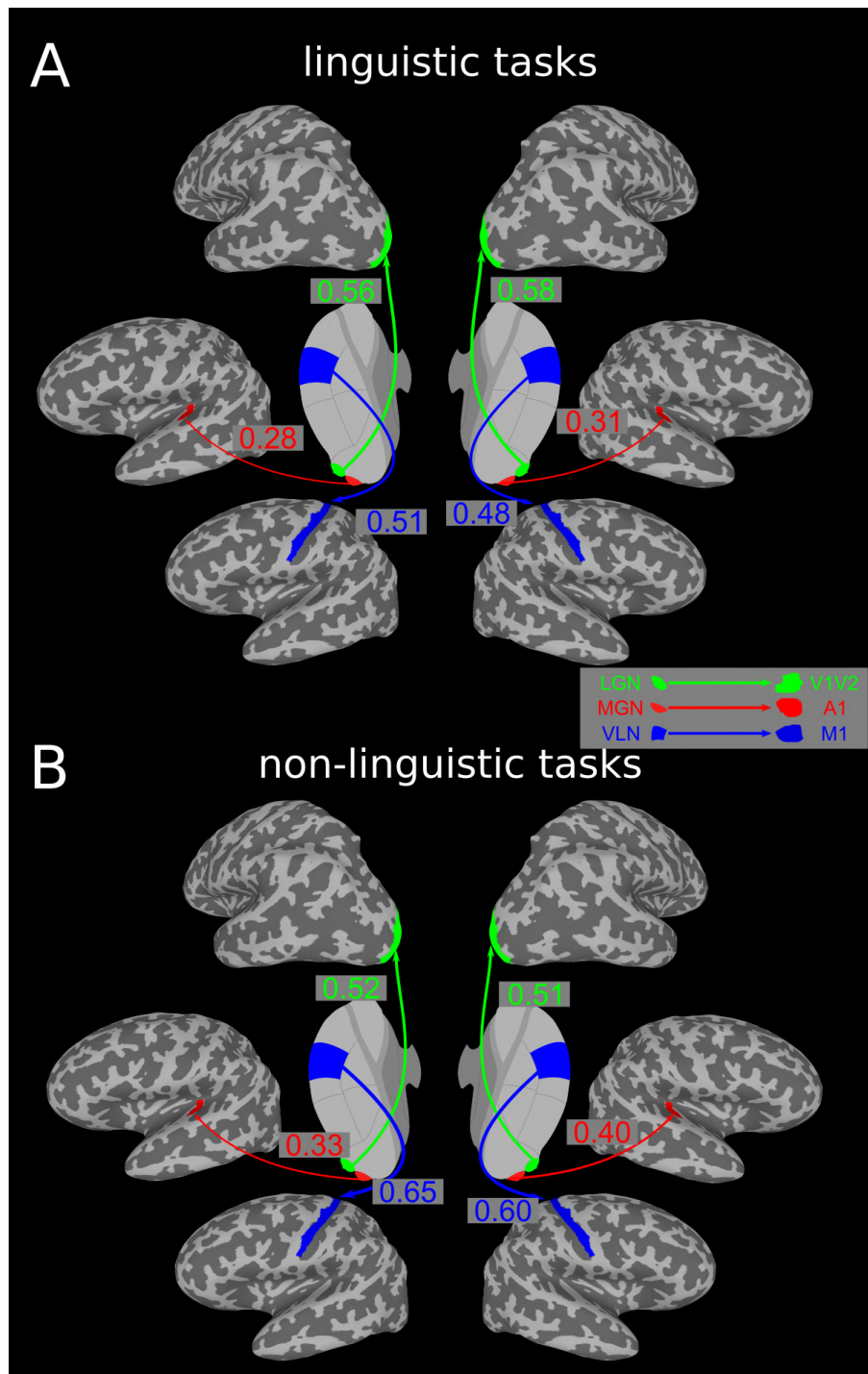


**Figure 8.3.** Functional connectivity analyses of three first-order relay thalamic pathways in **A)** linguistic and **B)** non-linguistic tasks for each of the corresponding modalities. Lines with an arrow represent the connection of the first-order thalamic relay nuclei with the cortical primary sensorimotor regions. Thalamic nuclei, cortical regions and the lines are colored as a function of sensorimotor modality: green indicates visual modality, red indicates auditory modality and blue indicates motor modality. The values along the arrow lines are the Fisher-transformed z values. All the reported z values are significant against zero with  $p < 0.001$  after Bonferroni FWE correction for multiple comparisons.

## 8.2.4 Structural connectivity

Taking the advantage of the containerized protocol proposed in Study 1, we successfully reconstructed the three pairs of homologous (i.e., left and right) first-order thalamic tracts: OR, AR and MR (Figure 8.4A) from each subject's DWI data. The FA profiles for each tract were generated and the group average profiles were shown in Figure 8.4B for the left hemisphere. The associations between the structural connectivity and functional connectivity were examined by conducting correlation analyses on the FA mean and Fisher's z values from every subject for each first-order thalamic pathway and each task, as exploratory analyses. However, the results did not reveal any statistically significant associations between these structural and functional measures for the different pathways and tasks conditions.

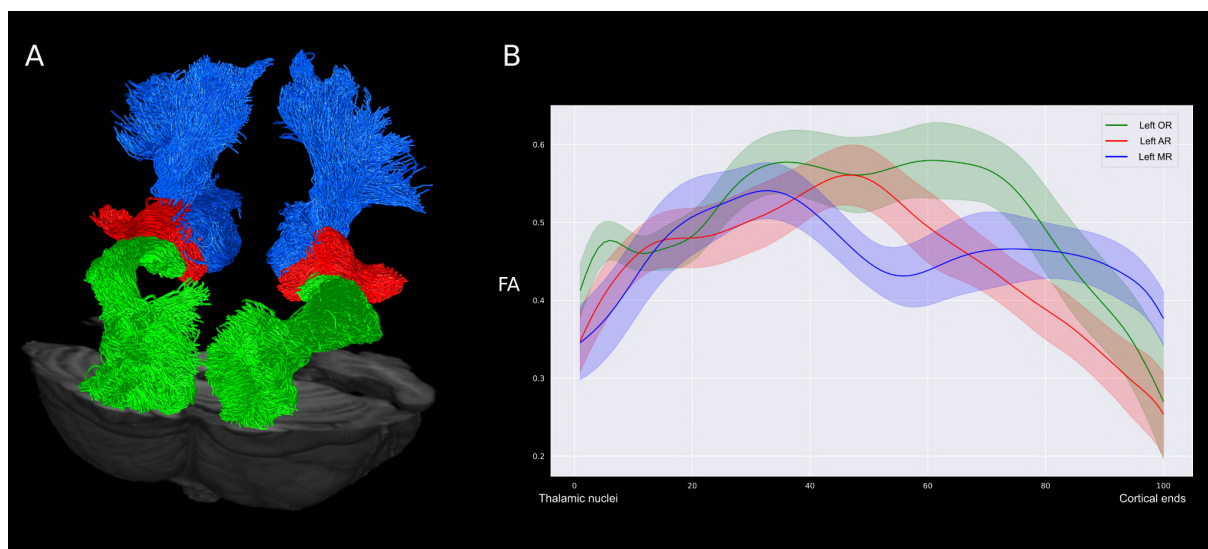


**Figure 8.4.** **A)** Three pairs of homologous first-order relay thalamic tracts: OR (green), AR (red) and MR (blue). **B)** The group average fractional anisotropy (FA) profiles of the three tracts in the left hemisphere. The mean profile (thin line) and  $\pm 1$  SD (shaded band) are shown.

## 8.3 Discussion

In the current study, using task-based fMRI we showed that the three first-order relay thalamic nuclei, LGN, MGN and VLN are involved in language processing in their corresponding sensorimotor modalities, i.e., reading, speech comprehension and speech production correspondingly. Results revealed that, even with the characteristic of these being first-order relay thalamic nuclei, the functional engagement of the LGN and MGN can be modulated as a function of the task demands. We

also characterized the functional connectivity and structural connectivity of the first-order relay thalamic pathways that transfer sensorimotor information from the thalamus to the corresponding cortical regions. In general, the present results imply that to fully understand the mechanisms of the main human language systems, it is necessary to take into account the role of the thalamus along with the thalamocortical and corticothalamic circuits (Sherman & Guillery, 2009).

The involvement of LGN, MGN and VLN in the sensorimotor tasks has been demonstrated with fMRI since two decades ago (e.g., LGN activation to checkerboard stimuli in [Chen et al., 1998](#); MGN activation to pure tones in [Husain et al., 2004](#); VLN activation in finger tapping task in [Lutz et al., 2000](#)). Since the three nuclei are critical to relay perceptual information and cerebellar inputs to the primary sensorimotor cortex (see [Sherman, 2017](#), for a review), it was expected that our task will elicit activation of the three thalamic nuclei in the corresponding sensorimotor tasks. To the best of our knowledge, the present study is the first study examining modality-specific involvement of the three first-order relay thalamic nuclei in three main language systems in one single task-based fMRI study. In line with previous evidence, the whole-brain contrasts across tasks in three modalities showed that the LGN was more strongly engaged for visual than for auditory and motor tasks; the MGN showed higher activation for auditory than for visual and motor tasks; and the VLN was more activated during motor than during visual and auditory tasks. The ROI analysis results confirmed this finding as well as that this effect was present for linguistic and for non-linguistic stimuli. These results indicate that language function in each specific modality only recruits the first-order thalamic nuclei that are responsible for relaying the corresponding sensorimotor information to cortical regions, i.e. reading- LGN, speech comprehension- MGN, and speech production- VLN.

Evidence in the field of neurobiology of language has ascribed language functions to multiple cortical structures ([Binder et al., 2009](#); [Friederici, 2011](#); [Hagoort & Indefrey, 2014](#); [Hickok & Poeppel, 2007](#)), while the subcortical structures such as the thalamus have long been ignored. Human language systems rely on perceptual information processing, such as reading requires visual processing circuits, speech comprehension and production requires auditory and motor circuits respectively. Neuroimaging studies on language often report thalamic involvement in tables, with very

scarce research discussing the functional role of the thalamus in human language (see Llano, 2013, for a review). One of the possible reasons for this is that most of the researchers in neurobiology of language do not include hypotheses about subcortical structures.

A second possible reason is that thalamic nuclei are in general small relative to the common voxel size used in fMRI (e.g., 3 mm isotropic), which makes it vulnerable to large-kernel signal smooth and person-to-person variability when warping different brains to a common space. The current study adopted a thalamic segmentation derived from a probabilistic atlas (Iglesias et al., 2018) that allows to segment the thalamus in individual space with high precision and to obtain all the thalamic nuclei of interest. Based on that, the ROI analysis in the current study was conducted in individual space with data smoothed with only a 2mm kernel.

A third potential reason for thalamus being often ignored in neuroimaging studies on language is also that this subcortical structure has long been perceived as a simple relay, especially for the first-order thalamic nuclei. While this is true, with the main role of the first-order thalamic nuclei is to relay periphery information to primary sensorimotor cortex, tracer studies demonstrated that layer 6 cells in primary sensorimotor cortex provide the feedback modulatory input to the first-order thalamic nuclei (Sherman & Guillery, 2009). In fact, recent evidence has shown task modulation on sensory thalamic nuclei, such as attention modulation in LGN (O'Connor et al., 2002) or speech modulation in MGN (Mihai et al., 2021). In line with these findings, the comparisons between linguistic and non-linguistic tasks in our ROI analysis results also provide evidence that the engagement of the first-order thalamic nuclei is modulated depending on the task. Both the LGN and MGN showed higher activation in response to linguistic stimuli relative to non-linguistic stimuli. We speculate that this modulation might be a result of the feedback from the primary sensory cortex and it is likely that this modulation is language specific, and not due to other related processes such attention. One finding supporting this speculation is that the modulation of LGN and MGN for linguistic versus non-linguistic stimuli was left-lateralized or only present in the left, but not in the right, hemisphere.. As well established, language is a left lateralized system (Binder et al., 1995; Frost et al., 1999). For example, Binder et al.'s (1995) study revealed that processing non-speech stimuli for

pitch and simple sequence information activates bilateral auditory cortex, while semantic processing task resulted in lateralized activity in distributed regions of the left hemisphere. The left-lateralized anatomy of language systems could lead to additional feedback from the left cerebral cortex to the ipsilateral first-order thalamic nuclei while conducting linguistic tasks. In contrast, equal feedback from the left and right cerebral cortex can occur while doing non-linguistic tasks.

Different from the LGN and MGN, the VLN did not show a modulatory engagement for speech production relative to producing unintelligible sounds. One of the first structures that has been related to vocalization was the face area of the motor cortex, which is located in the lateral part of the precentral cortex in primates. The main input structure of the motor cortex is the VLN, and one of the main input structures of the VLN is the cerebellum. In non-human primate studies, it was found that there is a large number of cells in the VLN becoming active already before vocalization onset (Farley, 1997). Thus, it is possible that the initial phase of vocal preparation is happening in the motor circuits before reaching the VLN, so this motor nuclei is simply relaying cerebellar information to the motor cortex. This may explain why we did not observe differences between speech production and producing unintelligible sounds in VLN in the present study. Another possible reason for the absence of differences between linguistic and non-linguistic conditions in the VLN during speech production could be the task manipulation adopted in the current study. In the speech production task participants were asked to freely say names of objects in their daily lives, such as *table, computer,....* In contrast, when they needed to produce unintelligible sounds, participants were asked to produce unintelligible sounds that we showed to them before entering the scanner. Both of these speech production tasks involved memory retrieval, but the memory load might be different just recalling object names that are very common in their daily life (i.e., linguistic speech production task) compared to recalling some new unintelligible sounds that they have just recently learned (i.e., non-linguistic speech production task) only. This could potentially make the speech production task less sensitive to capture differences in the activation of the VLN for linguistic versus non-linguistic stimuli.

In addition to the ROI results, we also observed strong functional coupling between the first-order relay thalamic nuclei and their corresponding primary sensorimotor cortex regions during

linguistic as well as non-linguistic tasks. These functional connectivity results are consistent with the well established roles of LGN, MGN and VLN as first-order relays (Saalman & Kastner, 2011; Sherman, 2016). However, we did not observe differences in functional coupling strength between linguistic and non-linguistic tasks. Previous evidence has shown functional connectivity between the first-order thalamic nuclei and their cortical counterparts in resting-state studies (e.g. visual pathway in Zou et al., 2009; auditory pathway in Eckert et al., 2008 and motor pathway in Steiner et al., 2020). As the functional coupling is strong even during resting-state, and as shown in the current study in both linguistic and non-linguistic tasks, it is possible that our tasks were not demanding enough to capture differences in connectivity as a function of the linguistic nature of the stimuli. Further studies are needed to examine this in more detail.

Reconstruction of the first-order thalamic tracts on this dataset using the protocol proposed in Study 1 has proved successful. The OR, AR and MR could be reliably reconstructed by the protocol in all participants (N = 40). To further explore whether or not there were associations between the structural connectivity indexes and task-based functional connectivity, we quantified the connection strength of each white-matter bundle by averaging the FA values in the tract FA profiles. There is no consensus on what proxy should be used to indicate the strength of structural connectivity in tractography. Previous research has been using streamline count (e.g. Müller-Axt et al., 2017), streamline density (e.g. Theisen et al., 2017) or the most commonly used one, FA values (e.g. (D'Arceuil & de Crespigny, 2007; Lebel et al., 2010; Takagi et al., 2009)). The current study did not find any associations between the structural connectivity and functional connectivity using FA values as the proxy for structural connectivity. Previous studies have examined the thalamocortical white-matter fibers and linked them to some language-related features, such as reading abilities in children (Fan et al., 2014), developmental dyslexia (Müller-Axt et al., 2017), suggesting linkages between the thalamus and reading ability. Future research should further investigate associations between first-order thalamic tracts and language abilities in the corresponding modality or with functional connectivity during specific language tasks. The containerized protocol proposed in Study 1 could further facilitate the reconstruction of these first-order thalamic tracts.

In sum, the present study examined the involvement of three sensorimotor thalamic nuclei in three human language systems (i.e., reading, speech comprehension and speech production) in one single experiment. We found that the first-order relay thalamic nuclei are modality-specific during language processing in line with the sensorimotor information transmitted (visual, auditory and motor). More importantly, LGN and MGN are modulated by the nature of the information being transmitted (linguistic, non-linguistic), which is not the case of VLN that responded similarly regardless of the nature of information. This study paves the way for understanding the role of first-order relay thalamic nuclei and their connections on the different language systems.

## 9 General Discussion

The current dissertation is focused on the human thalamus structure and function. In the first two empirical studies, I examined the white-matter fiber connections between the thalamus and cortical structures and subcortical structures, more specifically the first-order thalamic tracts of LGN, MGN and VLN in Study 1, and the higher-order thalamic tracts of AN and MD in Study 2. The protocols of the reconstruction of those tracts from DWI data have proved to have high reproducibility, and are made public for the scientific community to reproducibly reconstruct the same tracts in their own data. Moreover, as pioneering work, in study 3 we examined the function of human thalamus in language functions, more specifically, the involvement of the first-order thalamic nuclei in some of the main human language systems. We showed that the LGN and MGN activation is modulated as a function of the stimuli type. These results suggest that the thalamus is involved in human language processing and underscore the need for more systematic studies of the involvement of the thalamus in language processing.

In Study 1 of this doctoral dissertation, we focused on the first-order thalamic white-matter tracts, namely, the OR, AR, MR and DT. These thalamic tracts of interest are critical structures in relaying information from periphery or cerebellum to cortical structures. They are contrasted to higher-order thalamic white-matter tracts, such as those reported in Study 2, which are believed to serve as links in cortico-thalamo-cortical pathways that continue the information flow between cortical structures (Ramcharan et al., 2005). The tractography technology allows to visualize white matter fibers *in vivo* and offers the opportunity of extracting microstructural information to perform quantitative analyses. On the other hand, it is also well known that probabilistic tractography can come with false positive or negative results due to data noise, partial volume effects, and complex anatomical properties such as crossing fibers (Pierpaoli et al., 2001; Wiegell et al., 2000). In fact, the reproducibility of tractography has been under discussion for a long time, but there are no general answers to how to improve reproducibility of tractography, as it depends on the MRI sequences, tracking parameters and the specific tracts under investigation. Previous studies have used *in vivo*

tractography on DWI data to reconstruct these first-order thalamic tracts, but only a few of them have reported reproducibility measures about the reconstruction of the specific white-matter tracts.

Different from previous work, this study tested the first-order thalamic tracts in the same study using similar methods and reconstruction procedures across all them. Each tract has gone through multiple parameter iterations to obtain the most optimal trajectory that aligns with the extant neuroanatomical knowledge. More importantly, we specifically investigated in a large dataset the reliability of the reconstruction protocol in terms of both computational and test-retest reproducibility. The reproducibility was measured at both microstructural and macrostructural levels for each tract. Results from Study 1 revealed that the proposed protocol could reliably reconstruct these first-order thalamic tracts, and obtain reproducible microstructural and macrostructural measurements that can reflect the characteristics of these white-matter bundles. This protocol has been implemented in a docker container and made publicly available, so it can be easily used by other researchers in the community. This unique tool allows research to test hypotheses as to whether any of these specific first-order thalamic tracts are related with cognitive functions or diseases of interest, with the accuracy and reproducibility of the tract reconstruction guaranteed.

The Study 2 extends the rationale of Study 1 to higher-order thalamic white-matter bundles. Conventionally, the thalamic relays can be classified into first- and second (or higher)-order. First-order thalamic tracts connect these first-order thalamic relays with their corresponding sensorimotor cortical areas. In contrast, higher-order thalamic tracts relay information between cortical areas, such as the white-matter tracts connecting the MD and PFC, representing a cortico-thalamo-cortical circuit (Mitchell, 2015; Sherman, 2017). The higher-order thalamic tracts often have more structural and functional complexity and are far from being fully understood in humans. For example, the MD has extensive connections with practically the whole PFC, which is involved in numerous cognitive functions, such as working memory, attention, and decision making (Clark et al., 2010). Each subregion of the PFC has typically specific roles in cognition. These PFC subregions receive afferent fibers from the MD in the thalamus via the anterior thalamic radiation. In Study 2, the afferent fiber tracts from AN and MD were reconstructed from DWI data and the

corresponding computational and test-retest reproducibility was examined. Our protocol included 42 pairs of left and right hemispheric tracts, with 3 tracts being examined for the AN and 39 tracts being investigated for the MD). The reproducibility results showed that in general these tracts can be reliably reconstructed from DWI data with the proposed protocol. There were specific tracts showing relatively lower reproducibility, for example the AN related tracts and tracts connecting MD with orbital frontal cortex. To explore the associations between the reproducibility and the possible influential factors on reproducibility, a post-hoc analysis was conducted. The results unveiled three factors strongly associated with reproducibility of specific tracts. For example, noise in the diffusion data has strong negative correlation with the test-retest reproducibility. Also, the computational reproducibility is linked with the streamline length and count. If one tract has longer or less amount of streamlines, it might lead to relatively lower computational reproducibility. To the best of our knowledge, no study has investigated so far the computational reproducibility of tractography methods, as researchers assume that the same data and same methods mostly lead to the same results. These insights are valuable as it should promote the systematic investigation on computational reproducibility of tractography.

In the third and final empirical study, we investigated the involvement of the three first-order thalamic nuclei (LGN, MGN and VLN) in three main human language systems: reading, speech comprehension and production. The results revealed stronger engagement of the LGN, MGN and VLN for both linguistic and non-linguistic tasks in their corresponding modalities. More importantly, we found stronger activation for linguistic versus non-linguistic stimuli in reading and speech comprehension for LGN and MGN, respectively. For example, the LGN showed higher activation for reading words than for seeing scrambled pixels that are perceptually equal to visual words. Very few studies have investigated the subcortical contributions on high-level cognitive functions such as language (Parvizi, 2009), with most of the studies to date examining the neurobiology of language being focused on the cortical areas (Friederici, 2002; Hickok & Poeppel, 2007; Price, 2000). To the best of our knowledge, this study is the first to investigate the three modalities in relation to the involvement of first-order thalamic relays in their respective human language systems, and proved the

associations between linguistic and non-linguistic tasks in the LGN and MGN. Our findings showed that the responses in LGN and MGN during the processing of visual and auditory stimuli are task dependent, which implies the existence of a feedback mechanism that supports the recognition of visual and auditory information at the level of sensory thalamic nuclei. Given that this association has been found in the left thalamic nuclei but not on the right, we postulate that this feedback mechanism can be, very possibly, language-specific.

The studies in the current dissertation have some limitations. The first two studies have tested the reproducibility of the proposed protocol using a state-of-art DWI sequence, which includes, for example, multiband and multi-shell techniques. Although we cannot guarantee that the exact same computational and test-retest reproducibility will be obtained with different DWI acquisition protocols, we do not expect that the reproducibility profiles described here for these thalamocortical projections may change dramatically when using other DWI protocols widely used in the past, such as monoband or single-shell data. Despite the fact that in this study we decided to go with state-of-the-art DWI sequences, the current protocols can be easily adapted to different sequences. Furthermore, the reproducibility of the proposed protocol was measured on DWI acquired from a healthy population. It would be also relevant in the future to examine the reproducibility to reconstruct the thalamic tracts from DWI data in clinical populations. In Study 2, the reproducibility has been linked to some factors of the DWI data or the neuroanatomical characteristics of specific tracts. Three factors were under investigation in this work, and in future studies other possible factors that could be associated with reproducibility, such as pathological features or infant populations, should be examined. In the task-based fMRI Study 3, the experimental design examined the activation profile of the first-order thalamic nuclei for linguistic and for non-linguistic tasks attending to three modalities (visual, auditory, motor). This study paves the road for follow-up analyses and experiments. First, an open question from this study is the task-dependency on first-order thalamic nuclei in their language-specific modality. We hypothesized that this is very likely language-specific as we observed differences as a function of the linguistic nature of the stimuli in LGN and MGN only in the left hemisphere, which is the dominant hemisphere for language function. We plan to further explore these

differences and try to answer this question. Second, the role that task modulation on first-order thalamic nuclei plays in high-level cognitive functions, such as language, is still not clear. Future studies including more systematic manipulations might shed light on the mechanisms underlying task modulation on first-order thalamic nuclei.

In sum, the current dissertation successfully reconstructed first-order and higher-order thalamic white-matter tracts from DWI data, and has proved high reproducibility of the reconstruction protocol. This protocol could benefit the tractography community to better understand the structural connectivity of the thalamus with cortical and subcortical structures and facilitate the research on thalamocortical pathways in humans. We also found evidence for differences in the processing of linguistic and nonlinguistic stimuli in first-order thalamic nuclei through a task-based fMRI study. These results suggest that the first-order thalamic nuclei play roles in human language that are beyond relaying sensory information from periphery to cerebral cortex. These findings are important to push forward our understanding on the role of subcortical structures, such as the thalamus, in human language functions, and to urge a revisitation of existing language models taking the thalamus into consideration.

## 10 Bibliography

- Abivardi, A., & Bach, D. R. (2017). Deconstructing white matter connectivity of human amygdala nuclei with thalamus and cortex subdivisions in vivo. *Human Brain Mapping, 38*(8), 3927–3940. <https://doi.org/10.1002/hbm.23639>
- Aggleton, J. P., & Brown, M. W. (1999). Episodic memory, amnesia, and the hippocampal–anterior thalamic axis. *Behavioral and Brain Sciences, 22*(3), 425–444. <https://doi.org/10.1017/S0140525X99002034>
- Aggleton, J. P., & Mishkin, M. (1984). Projections of the amygdala to the thalamus in the cynomolgus monkey. *Journal of Comparative Neurology, 222*(1), 56–68.
- Alvarez, I., Schwarzkopf, D. S., & Clark, C. A. (2015). Extrastriate projections in human optic radiation revealed by fMRI-informed tractography. *Brain Structure and Function, 220*(5), 2519–2532. <https://doi.org/10.1007/s00429-014-0799-4>
- Anastasiades, P. G., Collins, D. P., & Carter, A. G. (2021). Mediodorsal and Ventromedial Thalamus Engage Distinct L1 Circuits in the Prefrontal Cortex. *Neuron, 109*(2), 314–330.e4. <https://doi.org/10.1016/j.neuron.2020.10.031>
- Andolina, I. M., Jones, H. E., Wang, W., & Sillito, A. M. (2007). Corticothalamic feedback enhances stimulus response precision in the visual system. *Proceedings of the National Academy of Sciences of the United States of America, 104*(5), 1685–1690. <https://doi.org/10.1073/pnas.0609318104>
- Arrigo, A., Calamuneri, A., Mormina, E., Gaeta, M., Quartarone, A., Marino, S., Anastasi, G. P., & Aragona, P. (2016). New insights in the optic radiations connectivity in the human brain. *Investigative Ophthalmology and Visual Science, 57*(1), 1–5. <https://doi.org/10.1167/iovs.15-18082>
- Aydogan, D. B., Jacobs, R., Dulawa, S., Thompson, S. L., Francois, M. C., Toga, A. W., Dong, H., Knowles, J. A., & Shi, Y. (2018). When tractography meets tracer injections: A systematic study of trends and variation sources of diffusion-based connectivity. *Brain Structure and Function, 223*(6), 2841–2858.

<https://doi.org/10.1007/s00429-018-1663-8>

- Bammer, R. (2003). Basic principles of diffusion-weighted imaging. *European Journal of Radiology*, 45(3), 169–184. [https://doi.org/10.1016/S0720-048X\(02\)00303-0](https://doi.org/10.1016/S0720-048X(02)00303-0)
- Bassi, L., Ricci, D., Volzone, A., Allsop, J. M., Srinivasan, L., Pai, A., Ribes, C., Ramenghi, L. A., Mercuri, E., Mosca, F., & others. (2008). Probabilistic diffusion tractography of the optic radiations and visual function in preterm infants at term equivalent age. *Brain*, 131(2), 573–582.
- Bay, H. H., & Çavdar, S. (2013). Regional connections of the mediodorsal thalamic nucleus in the rat. *Journal of Integrative Neuroscience*, 12(02), 201–219. <https://doi.org/10.1142/S021963521350012X>
- Behrens, T. E. J., Berg, H. J., Jbabdi, S., Rushworth, M. F. S., & Woolrich, M. W. (2007). Probabilistic diffusion tractography with multiple fibre orientations: What can we gain? *NeuroImage*, 34(1), 144–155. <https://doi.org/10.1016/j.neuroimage.2006.09.018>
- Behrens, T. E. J., Johansen-Berg, H., Woolrich, M. W., Smith, S. M., Wheeler-Kingshott, C. A. M., Boulby, P. A., Barker, G. J., Sillery, E. L., Sheehan, K., Ciccarelli, O., Thompson, A. J., Brady, J. M., & Matthews, P. M. (2003). Non-invasive mapping of connections between human thalamus and cortex using diffusion imaging. *Nature Neuroscience*, 6(7), 750–757. <https://doi.org/10.1038/nn1075>
- Benjamin, C. F. A., Singh, J. M., Prabhu, S. P., & Warfield, S. K. (2014). Optimization of tractography of the optic radiations. *Human Brain Mapping*, 35(2), 683–697. <https://doi.org/10.1002/hbm.22204>
- Benson, N. C., & Winawer, J. (2018). Bayesian analysis of retinotopic maps. *ELife*, 7, 1–29. <https://doi.org/10.7554/eLife.40224>
- Berker, E. A., Berker, A. H., & Smith, A. (1986). Translation of Broca's 1865 Report: Localization of Speech in the Third Left Frontal Convolution. *Archives of Neurology*, 43(10), 1065–1072. <https://doi.org/10.1001/archneur.1986.00520100069017>
- Berman, J. I., Lanza, M. R., Blaskey, L., Edgar, J. C., & Roberts, T. P. L. (2013). High angular resolution diffusion imaging probabilistic tractography of the auditory radiation.

*American Journal of Neuroradiology*, 34(8), 1573–1578.

<https://doi.org/10.3174/ajnr.A3471>

- Besseling, R. M. H., Jansen, J. F. A., Overvliet, G. M., Vaessen, M. J., Braakman, H. M. H., Hofman, P. A. M., Aldenkamp, A. P., & Backes, W. H. (2012). Tract specific reproducibility of tractography based morphology and diffusion metrics. *PLoS ONE*, 7(4). <https://doi.org/10.1371/journal.pone.0034125>
- Binder, J. R. (2015). The Wernicke area: Modern evidence and a reinterpretation. *Neurology*, 85(24), 2170–2175. <https://doi.org/10.1212/WNL.0000000000002219>
- Binder, J. R., Desai, R. H., Graves, W. W., & Conant, L. L. (2009). Where is the semantic system? A critical review and meta-analysis of 120 functional neuroimaging studies. *Cereb Cortex*, 19(12), 2767–2796. <https://doi.org/10.1093/cercor/bhp055>
- Binder, J. R., Rao, S. M., Hammeke, T. A., Frost, J. A., Bandettini, P. A., Jesmanowicz, A., & Hyde, J. S. (1995). Lateralized Human Brain Language Systems Demonstrated by Task Subtraction Functional Magnetic Resonance Imaging. *Archives of Neurology*, 52(6), 593–601. <https://doi.org/10.1001/archneur.1995.00540300067015>
- Blennow, K., Bogdanovic, N., Heilig, M., Grenfeldt, B., Karlsson, I., & Davidsson, P. (2000). Reduction of the synaptic protein rab3a in the thalamus and connecting brain regions in post-mortem schizophrenic brains. *Journal of Neural Transmission*, 107(8), 1085–1097.
- Bonilha, L., Gleichgerrcht, E., Fridriksson, J., Breedlove, J. L., Rorden, C., Nesland, T., Paulus, W., Helms, G., & Focke, N. K. (2015). Reproducibility of the structural brain connectome derived from diffusion tensor imaging. *PLoS ONE*, 10(9), 1–17. <https://doi.org/10.1371/journal.pone.0135247>
- Boukadi, M., Marcotte, K., Bedetti, C., Houde, J. C., Desautels, A., Deslauriers-Gauthier, S., Chapeau, M., Boré, A., Descoteaux, M., & Brambati, S. M. (2019). Test-retest reliability of diffusion measures extracted along white matter language fiber bundles using HARDI-based tractography. *Frontiers in Neuroscience*, 13(JAN). <https://doi.org/10.3389/fnins.2018.01055>

- Bridge, H., Leopold, D. A., & Bourne, J. A. (2016). Adaptive Pulvinar Circuitry Supports Visual Cognition. *Trends in Cognitive Sciences*, 20(2), 146–157.  
<https://doi.org/10.1016/j.tics.2015.10.003>
- Brugge, J. F. (2013). Anatomy and physiology of auditory pathways and cortex. *Handbook of Clinical Neurophysiology*, 10, 25–59.
- Buchanan, C. R., Pernet, C. R., Gorgolewski, K. J., Storkey, A. J., & Bastin, M. E. (2014). Test-retest reliability of structural brain networks from diffusion MRI. *NeuroImage*, 86, 231–243. <https://doi.org/10.1016/j.neuroimage.2013.09.054>
- Büchel, C., Turner, R., & Friston, K. (1997). Lateral geniculate activations can be detected using intersubject averaging and fMRI. *Magnetic Resonance in Medicine*, 38(5), 691–694.
- Bullier, J., & Kennedy, H. (1983). Projection of the lateral geniculate nucleus onto cortical area V2 in the macaque monkey. *Experimental Brain Research*, 53(1), 168–172.
- Chen, W., Kato, T., Zhu, X.-H., Ogawa, S., Tank, D. W., & Ugurbil, K. (1998). Human primary visual cortex and lateral geniculate nucleus activation during visual imagery. *Neuroreport*, 9(16), 3669–3674.
- Chen, W., Kato, T., Zhu, X.-H., Strupp, J., Ogawa, S., & Ugurbil, K. (1998). Mapping of lateral geniculate nucleus activation during visual stimulation in human brain using fMRI. *Magnetic Resonance in Medicine*, 39(1), 89–96.
- Cherches, I. M. (2016). Clinical neuroanatomy. In *Neurology Secrets: Sixth Edition*.  
<https://doi.org/10.1016/B978-0-323-35948-1.00002-4>
- Clark, D. L., Boutros, N. N., & Mendez, M. F. (2010). *The brain and behavior: An introduction to behavioral neuroanatomy*. Cambridge university press.
- Coenen, V. A., Allert, N., & Mädler, B. (2011). A role of diffusion tensor imaging fiber tracking in deep brain stimulation surgery: DBS of the dentato-rubro-thalamic tract (drt) for the treatment of therapy-refractory tremor. *Acta Neurochirurgica*, 153(8), 1579–1585.  
<https://doi.org/10.1007/s00701-011-1036-z>
- Coenen, V. A., Allert, N., Paus, S., Kronenburrger, M., Urbach, H., Mädler, B.,

- Kronenbürger, M., Urbach, H., & Mädler, B. (2014). Modulation of the Cerebello-Thalamo-Cortical network in thalamic deep brain stimulation for tremor: A diffusion tensor imaging study. *Neurosurgery*, *75*(6), 657–669.  
<https://doi.org/10.1227/NEU.0000000000000540>
- Concha, L., Gross, D. W., & Beaulieu, C. (2005). Diffusion tensor tractography of the limbic system. *American Journal of Neuroradiology*, *26*(9), 2267–2274.
- Cousineau, M., Jodoin, P. M., Morency, F. C., Rozanski, V., Grand'Maison, M., Bedell, B. J., & Descoteaux, M. (2017). A test-retest study on Parkinson's PPMI dataset yields statistically significant white matter fascicles. *NeuroImage: Clinical*, *16*(March), 222–233. <https://doi.org/10.1016/j.nicl.2017.07.020>
- Cudeiro, J., & Sillito, A. M. (2006). Looking back: Corticothalamic feedback and early visual processing. *Trends in Neurosciences*, *29*(6), 298–306.  
<https://doi.org/10.1016/j.tins.2006.05.002>
- Cullen, T. J., Walker, M. A., Parkinson, N., Craven, R., Crow, T. J., Esiri, M. M., & Harrison, P. J. (2003). A postmortem study of the mediodorsal nucleus of the thalamus in schizophrenia. *Schizophrenia Research*, *60*(2–3), 157–166.
- Dallapiazza, R. F., Lee, D. J., De Vloo, P., Fomenko, A., Hamani, C., Hodaie, M., Kalia, S. K., Fasano, A., & Lozano, A. M. (2019). Outcomes from stereotactic surgery for essential tremor. *Journal of Neurology, Neurosurgery and Psychiatry*, *90*(4), 474–482.  
<https://doi.org/10.1136/jnnp-2018-318240>
- D'Arceuil, H., & de Crespigny, A. (2007). The effects of brain tissue decomposition on diffusion tensor imaging and tractography. *NeuroImage*, *36*(1), 64–68.  
<https://doi.org/10.1016/j.neuroimage.2007.02.039>
- De Benedictis, A., Duffau, H., Paradiso, B., Grandi, E., Balbi, S., Granieri, E., Colarusso, E., Chioffi, F., Marras, C. E., & Sarubbo, S. (2014). Anatomic-functional study of the temporo-parieto-occipital region: Dissection, tractographic and brain mapping evidence from a neurosurgical perspective. *Journal of Anatomy*, *225*(2), 132–151.  
<https://doi.org/10.1111/joa.12204>

- Diaz, B., Hintz, F., Kiebel, S. J., & von Kriegstein, K. (2012). Dysfunction of the auditory thalamus in developmental dyslexia. *Proceedings of the National Academy of Sciences*, *109*(34), 13841–13846. <https://doi.org/10.1073/pnas.1119828109>
- Diedrichsen, J., Maderwald, S., Küper, M., Thürling, M., Rabe, K., Gizewski, E. R., Ladd, M. E., & Timmann, D. (2011). Imaging the deep cerebellar nuclei: A probabilistic atlas and normalization procedure. *NeuroImage*, *54*(3), 1786–1794. <https://doi.org/10.1016/j.neuroimage.2010.10.035>
- Duan, Y., Li, X., & Xi, Y. (2007). Thalamus segmentation from diffusion tensor magnetic resonance imaging. *International Journal of Biomedical Imaging*, *2007*, 3628–3631. <https://doi.org/10.1155/2007/90216>
- Eckert, M. A., Kamdar, N. V., Chang, C. E., Beckmann, C. F., Greicius, M. D., & Menon, V. (2008). A cross-modal system linking primary auditory and visual cortices: Evidence from intrinsic fMRI connectivity analysis. *Human Brain Mapping*, *29*(7), 848–857. <https://doi.org/10.1002/hbm.20560>
- Eckert, U., Metzger, C. D., Buchmann, J. E., Kaufmann, J., Osoba, A., Li, M., Safron, A., Liao, W., Steiner, J., Bogerts, B., & Walter, M. (2012). Preferential networks of the mediodorsal nucleus and centromedian-parafascicular complex of the thalamus-A DTI tractography study. *Human Brain Mapping*, *33*(11), 2627–2637. <https://doi.org/10.1002/hbm.21389>
- Fan, Q., Davis, N., Anderson, A. W., & Cutting, L. E. (2014). Thalamo-cortical connectivity: What can diffusion tractography tell us about reading difficulties in children? *Brain Connectivity*, *4*(6), 428–439. <https://doi.org/10.1089/brain.2013.0203>
- Farley, G. R. (1997). Neural firing in ventrolateral thalamic nucleus during conditioned vocal behavior in cats. *Experimental Brain Research*, *115*(3), 493–506. <https://doi.org/10.1007/PL00005719>
- Fiebelkorn, I. C., & Kastner, S. (2019). The Puzzling Pulvinar. *Neuron*, *101*(2), 201–203. <https://doi.org/10.1016/j.neuron.2018.12.032>
- Fischer, J., & Whitney, D. (2012). Attention gates visual coding in the human pulvinar. *Nature*

- Communications*, 3. <https://doi.org/10.1038/ncomms2054>
- Friederici, A. D. (2002). Towards a neural basis of auditory sentence processing. *Trends in Cognitive Sciences*, 6(2), 78–84. [https://doi.org/10.1016/S1364-6613\(00\)01839-8](https://doi.org/10.1016/S1364-6613(00)01839-8)
- Friederici, A. D. (2011). The brain basis of language processing: From structure to function. *Physiological Reviews*, 91(4), 1357–1392.  
<https://doi.org/10.1152/physrev.00006.2011>
- Friederici, A. D. (2012). The cortical language circuit: From auditory perception to sentence comprehension. *Trends Cogn Sci*, 16(5), 262–268.  
<https://doi.org/10.1016/j.tics.2012.04.001>
- Fromkin, V., Rodman, R., & Hyams, N. (2003). *An Introduction to Language SEVENTH EDITION*. <http://www.wadsworth.com>
- Frost, J. A., Binder, J. R., Springer, J. A., Hammeke, T. A., Bellgowan, P. S. F., Rao, S. M., & Cox, R. W. (1999). Language processing is strongly left lateralized in both sexes. Evidence from functional MRI. *Brain*, 122(2), 199–208.  
<https://doi.org/10.1093/brain/122.2.199>
- Galaburda, A. M., Menard, M. T., & Rosen, G. D. (1994). Evidence for aberrant auditory anatomy in developmental dyslexia. *Proceedings of the National Academy of Sciences*, 91(17), 8010–8013. <https://doi.org/10.1073/pnas.91.17.8010>
- Garey, L. J., & Powell, T. P. (1971). An experimental study of the termination of the lateral geniculo-cortical pathway in the cat and monkey. *Proceedings of the Royal Society of London. Series B, Biological Sciences*, 179(1054), 41–63.  
<https://doi.org/10.1098/rspb.1971.0080>
- Geschwind, N. (1970). The Organization of Language and the Brain. In *New Series* (Vol. 170, Issue 3961, pp. 940–944).
- Geschwind, N. (1972). *LANGUAGE AND THE BRAIN*. 226(4), 76–83.  
<https://doi.org/10.2307/24927318>
- Geschwind, N. (1974). Carl Wernicke, The Breslau School and The History of Aphasia. In N. Geschwind (Ed.), *Selected Papers on Language and the Brain* (pp. 42–61). Springer

- Netherlands. [https://doi.org/10.1007/978-94-010-2093-0\\_4](https://doi.org/10.1007/978-94-010-2093-0_4)
- Giraldo-Chica, M., Rogers, B. P., Damon, S. M., Landman, B. A., & Woodward, N. D. (2018). Prefrontal-Thalamic Anatomical Connectivity and Executive Cognitive Function in Schizophrenia. *Biological Psychiatry*, *83*(6), 509–517. <https://doi.org/10.1016/j.biopsych.2017.09.022>
- G. Jones, E. (1985). The Thalamus. In *Neuroscience in Medicine: Third Edition*. [https://doi.org/10.1007/978-1-60327-455-5\\_26](https://doi.org/10.1007/978-1-60327-455-5_26)
- Glasser, M. F., Coalson, T. S., Robinson, E. C., Hacker, C. D., Harwell, J., Yacoub, E., Ugurbil, K., Andersson, J., Beckmann, C. F., Jenkinson, M., Smith, S. M., & Van Essen, D. C. (2016). A multi-modal parcellation of human cerebral cortex. *Nature*, *536*(7615), 171–178. <https://doi.org/10.1038/nature18933>
- Glover, G. H., & Law, C. S. (2001). Spiral-in/out BOLD fMRI for increased SNR and reduced susceptibility artifacts. *Magnetic Resonance in Medicine*, *46*(3), 515–522. <https://doi.org/10.1002/mrm.1222>
- Gower, E. C. (1989). Efferent projections from limbic cortex of the temporal pole to the magnocellular medial dorsal nucleus in the rhesus monkey. *Journal of Comparative Neurology*, *280*(3), 343–358. <https://doi.org/10.1002/cne.902800303>
- Granziera, C., Hadjikhani, N., Arzy, S., Seeck, M., Meuli, R., & Krueger, G. (2011). In-vivo magnetic resonance imaging of the structural core of the Papez circuit in humans. *NeuroReport*, *22*(5), 227–231. <https://doi.org/10.1097/WNR.0b013e328344f75f>
- Grisot, G., Haber, S. N., & Yendiki, A. (2021). Diffusion MRI and anatomic tracing in the same brain reveal common failure modes of tractography. *NeuroImage*, *239*(January), 118300. <https://doi.org/10.1016/j.neuroimage.2021.118300>
- Groenewegen, H. J. (1988). Organization of the afferent connections of the mediodorsal thalamic nucleus in the rat, related to the mediodorsal-prefrontal topography. *Neuroscience*, *24*(2), 379–431.
- Guillery, R. W. (1995). Anatomical evidence concerning the role of the thalamus in corticocortical communication: A brief review. *Journal of Anatomy*, *187* ( Pt 3,

583–592.

- Guillery, R. W., & Sherman, S. M. (2002). Thalamic relay functions and their role in corticocortical communication: Generalizations from the visual system. *Neuron*, 33(2), 163–175. [https://doi.org/10.1016/S0896-6273\(01\)00582-7](https://doi.org/10.1016/S0896-6273(01)00582-7)
- Hagoort, P. (2005). On Broca, brain, and binding: A new framework. *Trends Cogn Sci*, 9(9), 416–423. <https://doi.org/10.1016/j.tics.2005.07.004>
- Hagoort, P. (2013). MUC (memory, unification, control) and beyond. *Frontiers in Psychology*, 4(JUL), 1–13. <https://doi.org/10.3389/fpsyg.2013.00416>
- Hagoort, P., & Indefrey, P. (2014). The Neurobiology of Language Beyond Single Words. *Annual Review of Neuroscience*, 37(1), 347–362. <https://doi.org/10.1146/annurev-neuro-071013-013847>
- Hale, J. R., Mayhew, S. D., Mullinger, K. J., Wilson, R. S., Arvanitis, T. N., Francis, S. T., & Bagshaw, A. P. (2015). Comparison of functional thalamic segmentation from seed-based analysis and ICA. *NeuroImage*, 114, 448–465. <https://doi.org/10.1016/j.neuroimage.2015.04.027>
- Hamani, C., Dostrovsky, J. O., & Lozano, A. M. (2006). The motor thalamus in neurosurgery. *Neurosurgery*, 58(1), 146–157. <https://doi.org/10.1227/01.NEU.0000192166.62017.C1>
- Hickok, G., & Poeppel, D. (2000). Towards a functional neuroanatomy of speech perception. *Trends in Cognitive Sciences*, 4(4), 131–138. [https://doi.org/10.1016/S1364-6613\(00\)01463-7](https://doi.org/10.1016/S1364-6613(00)01463-7)
- Hickok, G., & Poeppel, D. (2007). The cortical organization of speech processing. *Nat Rev Neurosci*, 8(5), 393–402. <https://doi.org/10.1038/nrn2113>
- Husain, F. T., Tagamets, M. A., Fromm, S. J., Braun, A. R., & Horwitz, B. (2004). Relating neuronal dynamics for auditory object processing to neuroimaging activity: A computational modeling and an fMRI study. *NeuroImage*, 21(4), 1701–1720. <https://doi.org/10.1016/j.neuroimage.2003.11.012>
- Hyam, J. A., Owen, S. L. F., Kringelbach, M. L., Jenkinson, N., Stein, J. F., Green, A. L., &

- Aziz, T. Z. (2012). Contrasting connectivity of the ventralis intermedius and ventralis oralis posterior nuclei of the motor thalamus demonstrated by probabilistic tractography. *Neurosurgery*, *70*(1), 162–169.  
<https://doi.org/10.1227/NEU.0b013e3182262c9a>
- Iglesias, J. E., Insausti, R., Lerma-Usabiaga, G., Bocchetta, M., Van Leemput, K., Greve, D. N., van der Kouwe, A., Fischl, B., Caballero-Gaudes, C., & Paz-Alonso, P. M. (2018). A probabilistic atlas of the human thalamic nuclei combining ex vivo MRI and histology. *NeuroImage*, *183*(July), 314–326.  
<https://doi.org/10.1016/j.neuroimage.2018.08.012>
- Ilinsky, I. A., & Kultas-Ilinsky, K. (2002). Motor thalamic circuits in primates with emphasis on the area targeted in treatment of movement disorders. *Movement Disorders*, *17*(SUPPL. 3). <https://doi.org/10.1002/mds.10137>
- Indefrey, P. (2011). The spatial and temporal signatures of word production components: A critical update. *Frontiers in Psychology*, *2*(OCT), 1–16.  
<https://doi.org/10.3389/fpsyg.2011.00255>
- Indefrey, P., & Levelt, W. J. M. (2004). The spatial and temporal signatures of word production components. *Cognition*, *92*(1–2), 101–144.  
<https://doi.org/10.1016/j.cognition.2002.06.001>
- Jakab, A., Blanc, R., & Berényi, E. L. (2012). Mapping changes of in vivo connectivity patterns in the human mediodorsal thalamus: Correlations with higher cognitive and executive functions. *Brain Imaging and Behavior*, *6*(3), 472–483.  
<https://doi.org/10.1007/s11682-012-9172-5>
- Javad, F., Warren, J. D., Micallef, C., Thornton, J. S., Golay, X., Yousry, T., & Mancini, L. (2014). Auditory tracts identified with combined fMRI and diffusion tractography. *NeuroImage*, *84*, 562–574. <https://doi.org/10.1016/j.neuroimage.2013.09.007>
- Jenkinson, M., Beckmann, C. F., Behrens, T. E. J., Woolrich, M. W., & Smith, S. M. (2012). FSL. *NeuroImage*, *62*(2), 782–790. <https://doi.org/10.1016/j.neuroimage.2011.09.015>
- Jeurissen, B., Tournier, J. D., Dhollander, T., Connelly, A., & Sijbers, J. (2014). Multi-tissue

- constrained spherical deconvolution for improved analysis of multi-shell diffusion MRI data. *NeuroImage*, *103*, 411–426. <https://doi.org/10.1016/j.neuroimage.2014.07.061>
- Ji, B., Li, Z., Li, K., Li, L., Langley, J., Shen, H., Nie, S., Zhang, R., & Hu, X. (2016). Dynamic thalamus parcellation from resting-state fMRI data. *Human Brain Mapping*, *37*(3), 954–967. <https://doi.org/10.1002/hbm.23079>
- Ji, Q., Edwards, A., Glass, J. O., Brinkman, T. M., Patay, Z., & Reddick, W. E. (2019). Measurement of Projections Between Dentate Nucleus and Contralateral Frontal Cortex in Human Brain Via Diffusion Tensor Tractography. *Cerebellum*, *18*(4), 761–769. <https://doi.org/10.1007/s12311-019-01035-3>
- Johansen-Berg, H., Behrens, T. E. J., Sillery, E., Ciccarelli, O., Thompson, A. J., Smith, S. M., & Matthews, P. M. (2005). Functional-anatomical validation and individual variation of diffusion tractography-based segmentation of the human thalamus. *Cerebral Cortex*, *15*(1), 31–39. <https://doi.org/10.1093/cercor/bhh105>
- Jones, E. G. (2012). *The thalamus*. Springer Science & Business Media.
- Kasenburg, N., Darkner, S., Hahn, U., Liptrot, M., & Feragen, A. (2016). Structural parcellation of the thalamus using shortest-path tractography. *Proceedings - International Symposium on Biomedical Imaging, 2016-June*, 559–563. <https://doi.org/10.1109/ISBI.2016.7493330>
- Kastner, S., O'Connor, D. H., Fukui, M. M., Fehd, H. M., Herwig, U., & Pinsk, M. A. (2004). Functional imaging of the human lateral geniculate nucleus and pulvinar. *Journal of Neurophysiology*, *91*(1), 438–448.
- Kellner, E., Dhital, B., Kiselev, V. G., & Reiser, M. (2016). Gibbs-ringing artifact removal based on local subvoxel-shifts. *Magnetic Resonance in Medicine*, *76*(5), 1574–1581. <https://doi.org/10.1002/mrm.26054>
- Kennedy, H., & Bullier, J. (1985). A double-labeling investigation of the afferent connectivity to cortical areas V1 and V2 of the macaque monkey. *Journal of Neuroscience*, *5*(10), 2815–2830.
- Khalsa, S., Mayhew, S. D., Chechlac, M., Bagary, M., & Bagshaw, A. P. (2014). The

structural and functional connectivity of the posterior cingulate cortex: Comparison between deterministic and probabilistic tractography for the investigation of structure-function relationships. *NeuroImage*, 102(P1), 118–127.

<https://doi.org/10.1016/j.neuroimage.2013.12.022>

Klein, J. C., Rushworth, M. F. S., Behrens, T. E. J., Mackay, C. E., de Crespigny, A. J., D'Arceuil, H., & Johansen-Berg, H. (2010). Topography of connections between human prefrontal cortex and mediodorsal thalamus studied with diffusion tractography. *NeuroImage*, 51(2), 555–564.

<https://doi.org/10.1016/j.neuroimage.2010.02.062>

Krauth, A., Blanc, R., Poveda, A., Jeanmonod, D., Morel, A., & Székely, G. (2010). A mean three-dimensional atlas of the human thalamus: Generation from multiple histological data. *NeuroImage*, 49(3), 2053–2062.

<https://doi.org/10.1016/j.neuroimage.2009.10.042>

Kruper, J., Yeatman, J. D., Richie-Halford, A., Bloom, D., Grotheer, M., Caffarra, S., Kiar, G., Karipidis, I. I., Roy, E., Chandio, B. Q., Garyfallidis, E., & Rokem, A. (2021).

Evaluating the Reliability of Human Brain White Matter Tractometry. *Aperture Neuro*, 1(1). <https://doi.org/10.52294/e6198273-b8e3-4b63-babb-6e6b0da10669>

Kwon, H. G., Hong, J. H., Hong, C. P., Lee, D. H., Ahn, S. H., & Jang, S. H. (2011).

Dentatorubrothalamic tract in human brain: Diffusion tensor tractography study. *Neuroradiology*, 53(10), 787–791. <https://doi.org/10.1007/s00234-011-0878-7>

Lambert, C., Simon, H., Colman, J., & Barrick, T. R. (2017). Defining thalamic nuclei and topographic connectivity gradients in vivo. *NeuroImage*, 158(September 2016), 466–479. <https://doi.org/10.1016/j.neuroimage.2016.08.028>

Lau, E. F., Phillips, C., & Poeppel, D. (2008). A cortical network for semantics:

(De)constructing the N400. *Nature Reviews Neuroscience*, 9(12), 920–933.

<https://doi.org/Doi 10.1038/Nrn2532>

Le Reste, P. J., Haegelen, C., Gibaud, B., Moreau, T., & Morandi, X. (2016). Connections of the dorsolateral prefrontal cortex with the thalamus: A probabilistic tractography

- study. *Surgical and Radiologic Anatomy*, 38(6), 705–710.  
<https://doi.org/10.1007/s00276-015-1603-8>
- Lebel, C., Caverhill-Godkewitsch, S., & Beaulieu, C. (2010). Age-related regional variations of the corpus callosum identified by diffusion tensor tractography. *NeuroImage*, 52(1), 20–31. <https://doi.org/10.1016/j.neuroimage.2010.03.072>
- Leh, S. E., Chakravarty, M. M., & Ptito, A. (2008). The connectivity of the human pulvinar: A diffusion tensor imaging tractography study. *International Journal of Biomedical Imaging*, 2008(1). <https://doi.org/10.1155/2008/789539>
- Lehéricy, S., Benali, H., Van De Moortele, P. F., Péligrini-Issac, M., Waechter, T., Ugurbil, K., & Doyon, J. (2005). Distinct basal ganglia territories are engaged in early and advanced motor sequence learning. *Proceedings of the National Academy of Sciences of the United States of America*, 102(35), 12566–12571.  
<https://doi.org/10.1073/pnas.0502762102>
- Lerma-Usabiaga, G., Liu, M., Paz-Alonso, P. M., & Wandell, B. A. (2022). Reproducible Tract Profiles (RTP2): From diffusion MRI acquisition to clinical practice and research. *BioRxiv*. <https://doi.org/10.1101/2022.03.17.484761>
- Lerma-Usabiaga, G., Mukherjee, P., Perry, M. L., & Wandell, B. A. (2020). Data-science ready, multisite, human diffusion MRI white-matter-tract statistics. *Scientific Data*, 7(1), 1–9. <https://doi.org/10.1038/s41597-020-00760-3>
- Lerma-Usabiaga, G., Mukherjee, P., Ren, Z., Perry, M. L., & Wandell, B. A. (2019). Replication and generalization in applied neuroimaging. *NeuroImage*, 202(December 2018), 116048. <https://doi.org/10.1016/j.neuroimage.2019.116048>
- Li, K., Fan, L., Cui, Y., Wei, X., He, Y., Yang, J., Lu, Y., Li, W., Shi, W., Cao, L., Cheng, L., Li, A., You, B., & Jiang, T. (2022). The human mediodorsal thalamus: Organization, connectivity, and function. *NeuroImage*, 249, 118876.  
<https://doi.org/10.1016/j.neuroimage.2022.118876>
- Lichtheim, L. (1885). On aphasia. *Brain*, 7, 433–484.
- Llano, D. A. (2013). Functional imaging of the thalamus in language. *Brain and Language*,

126(1), 62–72. <https://doi.org/10.1016/j.bandl.2012.06.004>

Lozsádi, D. A. (1995). Organization of connections between the thalamic reticular and the anterior thalamic nuclei in the rat. *Journal of Comparative Neurology*, *358*(2), 233–246.

Lutz, K., Specht, K., Shah, N. J., & Jenkinson, E. (2000). Tapping movements according to regular and irregular visual timing signals investigated with fMRI. *Neuroreport*, *11*(6), 1301–1306.

Maciewicz, R. J. (1975). Thalamic afferents to areas 17, 18 and 19 of cat cortex traced with horseradish peroxidase. *Brain Research*, *84*(2), 308–312.  
[https://doi.org/10.1016/0006-8993\(75\)90985-3](https://doi.org/10.1016/0006-8993(75)90985-3)

Maffei, C., Jovicich, J., De Benedictis, A., Corsini, F., Barbareschi, M., Chioffi, F., & Sarubbo, S. (2018). Topography of the human acoustic radiation as revealed by ex vivo fibers micro-dissection and in vivo diffusion-based tractography. *Brain Structure and Function*, *223*(1), 449–459. <https://doi.org/10.1007/s00429-017-1471-6>

Maffei, C., Sarubbo, S., & Jovicich, J. (2019). Diffusion-based tractography atlas of the human acoustic radiation. *Scientific Reports*, *9*(1), 1–13.  
<https://doi.org/10.1038/s41598-019-40666-8>

Mai, J. K., & Forutan, F. (2012). Thalamus. In *The Human Nervous System*.  
<https://doi.org/10.1016/B978-0-12-374236-0.10019-7>

Mai, J. K., & Majtanik, M. (2019). Toward a common terminology for the Thalamus. *Frontiers in Neuroanatomy*, *12*(January), 1–23. <https://doi.org/10.3389/fnana.2018.00114>

Maleki, N., Becerra, L., Upadhyay, J., Burstein, R., & Borsook, D. (2012). Direct optic nerve pulvinar connections defined by diffusion MR tractography in humans: Implications for photophobia. *Human Brain Mapping*, *33*(1), 75–88.  
<https://doi.org/10.1002/hbm.21194>

Mallol, R., Barrós-Loscertales, A., López, M., Belloch, V., Parcet, M. A., & Ávila, C. (2007). Compensatory cortical mechanisms in Parkinson's disease evidenced with fMRI during the performance of pre-learned sequential movements. *Brain Research*,

- 1147(1), 265–271. <https://doi.org/10.1016/j.brainres.2007.02.046>
- Mang, S. C., Busza, A., Reiterer, S., Grodd, W., & Klose, A. U. (2012). Thalamus segmentation based on the local diffusion direction: A group study. *Magnetic Resonance in Medicine*, 67(1), 118–126. <https://doi.org/10.1002/mrm.22996>
- Manger, P. R., & Rosa, M. G. P. (2005). Visual thalamocortical projections in the flying fox: Parallel pathways to striate and extrastriate areas. *Neuroscience*, 130(2), 497–511. <https://doi.org/10.1016/j.neuroscience.2004.09.047>
- McFadyen, J., Mattingley, J. B., & Garrido, M. I. (2019). An afferent white matter pathway from the pulvinar to the amygdala facilitates fear recognition. *eLife*, 8, 1–51. <https://doi.org/10.7554/eLife.40766>
- Meola, A., Comert, A., Yeh, F. C., Sivakanthan, S., & Fernandez-Miranda, J. C. (2016). The nondecussating pathway of the dentatorubrothalamic tract in humans: Human connectome-based tractographic study and microdissection validation. *Journal of Neurosurgery*, 124(5), 1406–1412. <https://doi.org/10.3171/2015.4.JNS142741>
- Mihai, P. G., Tschentscher, N., & von Kriegstein, K. (2021). Modulation of the Primary Auditory Thalamus When Recognizing Speech with Background Noise. *The Journal of Neuroscience*, 41(33), 7136–7147. <https://doi.org/10.1523/jneurosci.2902-20.2021>
- Mitchell, A. S. (2015). The mediodorsal thalamus as a higher order thalamic relay nucleus important for learning and decision-making. *Neuroscience and Biobehavioral Reviews*, 54, 76–88. <https://doi.org/10.1016/j.neubiorev.2015.03.001>
- Mori, S., & Van Zijl, P. C. M. (2002). Fiber tracking: Principles and strategies—A technical review. *NMR in Biomedicine*, 15(7–8), 468–480. <https://doi.org/10.1002/nbm.781>
- Mukherjee, P., Berman, J. I., Chung, S. W., Hess, C. P., & Henry, R. G. (2008). Diffusion tensor MR imaging and fiber tractography: Theoretic underpinnings. *American Journal of Neuroradiology*, 29(4), 632–641.
- Müller-Axt, C., Anwender, A., & von Kriegstein, K. (2017). Altered Structural Connectivity of the Left Visual Thalamus in Developmental Dyslexia. *Current Biology*, 27(23), 3692–3698.e4. <https://doi.org/10.1016/j.cub.2017.10.034>

- Nowacki, A., Schlaier, J., Debove, I., & Pollo, C. (2019). Validation of diffusion tensor imaging tractography to visualize the dentatorubrothalamic tract for surgical planning. *Journal of Neurosurgery*, *130*(1), 99–108. <https://doi.org/10.3171/2017.9.JNS171321>
- O'Connor, D. H., Fukui, M. M., Pinsk, M. A., & Kastner, S. (2002). Attention modulates responses in the human lateral geniculate nucleus. *Nature Neuroscience*, *5*(11), 1203–1209. <https://doi.org/10.1038/nn957>
- Ojemann, G. A. (1975). Language and the thalamus: Object naming and recall during and after thalamic stimulation. *Brain and Language*, *2*(C), 101–120. [https://doi.org/10.1016/S0093-934X\(75\)80057-5](https://doi.org/10.1016/S0093-934X(75)80057-5)
- Ojemann, G. A. (1991). *Cortical Organization of Language and Verbal Memory Based on Intraoperative Investigations*. August, 193–230. [https://doi.org/10.1007/978-3-642-75964-2\\_4](https://doi.org/10.1007/978-3-642-75964-2_4)
- Olszowy, W., Aston, J., Rua, C., & Williams, G. B. (2019). Accurate autocorrelation modeling substantially improves fMRI reliability. *Nature Communications*, *10*(1), 1220. <https://doi.org/10.1038/s41467-019-09230-w>
- O'muircheartaigh, J., Keller, S. S., Barker, G. J., & Richardson, M. P. (2015). White matter connectivity of the thalamus delineates the functional architecture of competing thalamocortical systems. *Cerebral Cortex*, *25*(11), 4477–4489. <https://doi.org/10.1093/cercor/bhv063>
- Ouhaz, Z., Fleming, H., & Mitchell, A. S. (2018). Cognitive functions and neurodevelopmental disorders involving the prefrontal cortex and mediodorsal thalamus. *Frontiers in Neuroscience*, *12*(FEB), 1–18. <https://doi.org/10.3389/fnins.2018.00033>
- Parent, M., Lévesque, M., & Parent, A. (1999). The pallidofugal projection system in primates: Evidence for neurons branching ipsilaterally and contralaterally to the thalamus and brainstem. *Journal of Chemical Neuroanatomy*, *16*(3), 153–165.
- Parmeggiani, P. L., Azzaroni, A., & Lenzi, P. (1971). On the functional significance of the circuit of Papez. *Brain Research*, *30*(2), 357–374.

[https://doi.org/10.1016/0006-8993\(71\)90086-2](https://doi.org/10.1016/0006-8993(71)90086-2)

- Párraga, R. G., Ribas, G. C., Welling, L. C., Alves, R. V., & De Oliveira, E. (2012). Microsurgical anatomy of the optic radiation and related fibers in 3-dimensional images. *Neurosurgery*, *71*(SUPPL.1), 160–172.  
<https://doi.org/10.1227/NEU.0b013e3182556fde>
- Parvizi, J. (2009). Corticocentric myopia: Old bias in new cognitive sciences. *Trends in Cognitive Sciences*, *13*(8), 354–359. <https://doi.org/10.1016/j.tics.2009.04.008>
- Pelzer, E. A., Melzer, C., Timmermann, L., von Cramon, D. Y., & Tittgemeyer, M. (2017). Basal ganglia and cerebellar interconnectivity within the human thalamus. *Brain Structure and Function*, *222*(1), 381–392. <https://doi.org/10.1007/s00429-016-1223-z>
- Pergola, G., Danet, L., Pitel, A. L., Carlesimo, G. A., Segobin, S., Pariente, J., Suchan, B., Mitchell, A. S., & Barbeau, E. J. (2018). The Regulatory Role of the Human Mediodorsal Thalamus. *Trends in Cognitive Sciences*, *22*(11), 1011–1025.  
<https://doi.org/10.1016/j.tics.2018.08.006>
- Pergola, G., Ranft, A., Mathias, K., & Suchan, B. (2013). The role of the thalamic nuclei in recognition memory accompanied by recall during encoding and retrieval: An fMRI study. *NeuroImage*, *74*, 195–208. <https://doi.org/10.1016/j.neuroimage.2013.02.017>
- Petrovici, J.-N. (1980). Speech disturbances following stereotaxic surgery in ventrolateral thalamus. *Neurosurgical Review*, *3*(3), 189–195.
- Pierpaoli, C., Barnett, A., Pajevic, S., Chen, R., Penix, L., Virta, A., & Basser, P. (2001). Water Diffusion Changes in Wallerian Degeneration and Their Dependence on White Matter Architecture. *NeuroImage*, *13*(6), 1174–1185.  
<https://doi.org/10.1006/nimg.2001.0765>
- Price, C. J. (2000). The anatomy of language: Contributions from functional neuroimaging. *Journal of Anatomy*, *197*(3), 335–359. <https://doi.org/10.1017/S0021878299006901>
- Prochnow, D., Kossack, H., Brunheim, S., Müller, K., Wittsack, H.-J., Markowitsch, H.-J., & Seitz, R. J. (2013). Processing of subliminal facial expressions of emotion: A behavioral and fMRI study. *Social Neuroscience*, *8*(5), 448–461.

- Profant, O., Škoch, A., Balogová, Z., Tintěra, J., Hlinka, J., & Syka, J. (2014). Diffusion tensor imaging and MR morphometry of the central auditory pathway and auditory cortex in aging. *Neuroscience*, *260*, 87–97.  
<https://doi.org/10.1016/j.neuroscience.2013.12.010>
- Pugh, K. R., Mencl, W. E., Jenner, A. R., Katz, L., Frost, S. J., Lee, J. R., Shaywitz, S. E., & Shaywitz, B. A. (2000). Functional neuroimaging studies of reading and reading disability (developmental dyslexia). *Mental Retardation and Developmental Disabilities Research Reviews*, *6*(3), 207–213.  
[https://doi.org/10.1002/1098-2779\(2000\)6:3<207::AID-MRDD8>3.0.CO;2-P](https://doi.org/10.1002/1098-2779(2000)6:3<207::AID-MRDD8>3.0.CO;2-P)
- Pugh, K. R., Mencl, W. E., Jenner, A. R., Katz, L., Frost, S. J., Lee, J. R., Shaywitz, S. E., & Shaywitz, B. A. (2001). Neurobiological studies of reading and reading disability. *Journal of Communication Disorders*, *34*(6), 479–492.  
[https://doi.org/10.1016/S0021-9924\(01\)00060-0](https://doi.org/10.1016/S0021-9924(01)00060-0)
- Ramcharan, E. J., Gnadt, J. W., & Sherman, S. M. (2005). Higher-order thalamic relays burst more than first-order relays. *Proceedings of the National Academy of Sciences of the United States of America*, *102*(34), 12236–12241.  
<https://doi.org/10.1073/pnas.0502843102>
- Ray, J. P., & Price, J. L. (1992). The organization of the thalamocortical connections of the mediodorsal thalamic nucleus in the rat, related to the ventral forebrain—Prefrontal cortex topography. *Journal of Comparative Neurology*, *323*(2), 167–197.
- Rissman, J., Gazzaley, A., & D'Esposito, M. (2004). Measuring functional connectivity during distinct stages of a cognitive task. *NeuroImage*, *23*(2), 752–763.  
<https://doi.org/10.1016/j.neuroimage.2004.06.035>
- Rokem, A., Takemura, H., Bock, A. S., Scherf, K. S., Behrmann, M., Wandell, B. A., Fine, I., Bridge, H., & Pestilli, F. (2017). The visual white matter: The application of diffusion MRI and fiber tractography to vision science. *Journal of Vision*, *17*(2), 4.  
<https://doi.org/10.1167/17.2.4>
- Saalman, Y. B., & Kastner, S. (2011). Cognitive and Perceptual Functions of the Visual

- Thalamus. *Neuron*, 71(2), 209–223. <https://doi.org/10.1016/j.neuron.2011.06.027>
- Schilling, K. G., Rheault, F., Petit, L., Hansen, C. B., Nath, V., Yeh, F. C., Girard, G., Barakovic, M., Rafael-Patino, J., Yu, T., Fisci-Gomez, E., Pizzolato, M., Ocampo-Pineda, M., Schiavi, S., Canales-Rodríguez, E. J., Daducci, A., Granziera, C., Innocenti, G., Thiran, J. P., ... Descoteaux, M. (2021). Tractography dissection variability: What happens when 42 groups dissect 14 white matter bundles on the same dataset? *NeuroImage*, 243(November 2020), 118502. <https://doi.org/10.1016/j.neuroimage.2021.118502>
- Shah, A., Jhawar, S. S., & Goel, A. (2012). Analysis of the anatomy of the Papez circuit and adjoining limbic system by fiber dissection techniques. *Journal of Clinical Neuroscience*, 19(2), 289–298. <https://doi.org/10.1016/j.jocn.2011.04.039>
- Sherbondy, A. J., Dougherty, R. F., Napel, S., & Wandell, B. A. (2008). Identifying the human optic radiation using diffusion imaging and fiber tractography. *Journal of Vision*, 8(10), 1–11. <https://doi.org/10.1167/8.10.12>
- Sherman, S. M. (2005). Thalamic relays and cortical functioning. *Progress in Brain Research*, 149, 107–126. [https://doi.org/10.1016/S0079-6123\(05\)49009-3](https://doi.org/10.1016/S0079-6123(05)49009-3)
- Sherman, S. M. (2007). The thalamus is more than just a relay. *Current Opinion in Neurobiology*, 17(4), 417–422. <https://doi.org/10.1016/j.conb.2007.07.003>
- Sherman, S. M. (2012). Thalamocortical interactions. *Current Opinion in Neurobiology*, 22(4), 575–579. <https://doi.org/10.1016/j.conb.2012.03.005>
- Sherman, S. M. (2016). Thalamus plays a central role in ongoing cortical functioning. *Nature Neuroscience*, 19(4), 533–541. <https://doi.org/10.1038/nn.4269>
- Sherman, S. M. (2017). Functioning of circuits connecting thalamus and cortex. *Comprehensive Physiology*, 7(2), 713–739. <https://doi.org/10.1002/cphy.c160032>
- Sherman, S. M., & Guillery, R. W. (2009). Exploring the Thalamus and Its Role in Cortical Function. In *Tohoku Mathematical Journal* (Vol. 35, Issue 1). The MIT Press. <https://doi.org/10.7551/mitpress/2940.001.0001>
- Small, S. L., & Hickok, G. (2016). Chapter 1—The Neurobiology of Language. In G. Hickok &

- S. L. Small (Eds.), *Neurobiology of Language* (pp. 3–9). Academic Press.  
<https://doi.org/10.1016/B978-0-12-407794-2.00001-8>
- Smith, S. M., Jenkinson, M., Woolrich, M. W., Beckmann, C. F., Behrens, T. E. J., Johansen-Berg, H., Bannister, P. R., De Luca, M., Drobnjak, I., Flitney, D. E., Niazy, R. K., Saunders, J., Vickers, J., Zhang, Y., De Stefano, N., Brady, J. M., & Matthews, P. M. (2004). Advances in functional and structural MR image analysis and implementation as FSL. *NeuroImage*, 23(SUPPL. 1), 208–219.  
<https://doi.org/10.1016/j.neuroimage.2004.07.051>
- Steiner, L., Federspiel, A., Slavova, N., Wiest, R., Grunt, S., Steinlin, M., & Everts, R. (2020). Functional topography of the thalamo-cortical system during development and its relation to cognition. *NeuroImage*, 223(September), 117361.  
<https://doi.org/10.1016/j.neuroimage.2020.117361>
- Takagi, T., Nakamura, M., Yamada, M., Hikishima, K., Momoshima, S., Fujiyoshi, K., Shibata, S., Okano, H. J., Toyama, Y., & Okano, H. (2009). Visualization of peripheral nerve degeneration and regeneration: Monitoring with diffusion tensor tractography. *NeuroImage*, 44(3), 884–892. <https://doi.org/10.1016/j.neuroimage.2008.09.022>
- Theaud, G., Houde, J. C., Boré, A., Rheault, F., Morency, F., & Descoteaux, M. (2020). TractoFlow: A robust, efficient and reproducible diffusion MRI pipeline leveraging Nextflow & Singularity. *NeuroImage*, 218(September 2019).  
<https://doi.org/10.1016/j.neuroimage.2020.116889>
- Theisen, F., Leda, R., Pozorski, V., Oh, J. M., Adluru, N., Wong, R., Okonkwo, O., Dean, D. C., Bendlin, B. B., Johnson, S. C., Alexander, A. L., & Gallagher, C. L. (2017). Evaluation of striatonigral connectivity using probabilistic tractography in Parkinson's disease. *NeuroImage: Clinical*, 16(July), 557–563.  
<https://doi.org/10.1016/j.nicl.2017.09.009>
- Tournier, J. D., Calamante, F., Connelly, A., & others. (2010). Improved probabilistic streamlines tractography by 2nd order integration over fibre orientation distributions. *Proceedings of the International Society for Magnetic Resonance in Medicine*, 1670.

- Tournier, J. D., Smith, R., Raffelt, D., Tabbara, R., Dhollander, T., Pietsch, M., Christiaens, D., Jeurissen, B., Yeh, C. H., & Connelly, A. (2019). MRtrix3: A fast, flexible and open software framework for medical image processing and visualisation. *NeuroImage*, 202(August), 116137. <https://doi.org/10.1016/j.neuroimage.2019.116137>
- Tourville, J. A., & Guenther, F. H. (2011). The DIVA model: A neural theory of speech acquisition and production. *Language and Cognitive Processes*, 26(7), 952–981. <https://doi.org/10.1080/01690960903498424>
- Traynor, C., Heckemann, R. A., Hammers, A., O’Muircheartaigh, J., Crum, W. R., Barker, G. J., & Richardson, M. P. (2010). Reproducibility of thalamic segmentation based on probabilistic tractography. *NeuroImage*, 52(1), 69–85. <https://doi.org/10.1016/j.neuroimage.2010.04.024>
- Tremblay, P., & Dick, A. S. (2016). Broca and Wernicke are dead, or moving past the classic model of language neurobiology. *Brain and Language*, 162, 60–71. <https://doi.org/10.1016/j.bandl.2016.08.004>
- Tsai, S. Y. (2018). Reproducibility of structural brain connectivity and network metrics using probabilistic diffusion tractography. *Scientific Reports*, 8(1), 1–12. <https://doi.org/10.1038/s41598-018-29943-0>
- Tschentscher, N., Ruisinger, A., Blank, H., Díaz, B., & von Kriegstein, K. (2019). Reduced structural connectivity between left auditory thalamus and the motion-sensitive planum temporale in developmental dyslexia. *Journal of Neuroscience*, 39(9), 1720–1732. <https://doi.org/10.1523/JNEUROSCI.1435-18.2018>
- Vann, S. D., Saunders, R. C., & Aggleton, J. P. (2007). Distinct, parallel pathways link the medial mammillary bodies to the anterior thalamus in macaque monkeys. *European Journal of Neuroscience*, 26(6), 1575–1586.
- Veraart, J., Novikov, D. S., Christiaens, D., Ades-aron, B., Sijbers, J., & Fieremans, E. (2016). Denoising of diffusion MRI using random matrix theory. *NeuroImage*, 142, 394–406. <https://doi.org/10.1016/j.neuroimage.2016.08.016>
- Villeneuve, M. Y., Kupers, R., Gjedde, A., Ptito, M., & Casanova, C. (2005). Pattern-motion

- selectivity in the human pulvinar. *NeuroImage*, 28(2), 474–480.  
<https://doi.org/10.1016/j.neuroimage.2005.06.015>
- Vo, A., Sako, W., Niethammer, M., Carbon, M., Bressman, S. B., Ulug, A. M., & Eidelberg, D. (2015). Thalamocortical connectivity correlates with phenotypic variability in dystonia. *Cerebral Cortex*, 25(9), 3086–3094. <https://doi.org/10.1093/cercor/bhu104>
- von Kriegstein, K., Patterson, R. D., & Griffiths, T. D. (2008). Task-Dependent Modulation of Medial Geniculate Body Is Behaviorally Relevant for Speech Recognition. *Current Biology*, 18(23), 1855–1859. <https://doi.org/10.1016/j.cub.2008.10.052>
- Ward, R., Calder, A. J., Parker, M., & Arend, I. (2007). Emotion recognition following human pulvinar damage. *Neuropsychologia*, 45(8), 1973–1978.  
<https://doi.org/10.1016/j.neuropsychologia.2006.09.017>
- Wei, P. H., Mao, Z. Q., Cong, F., Yeh, F. C., Wang, B., Ling, Z. P., Liang, S. L., Chen, L., & Yu, X. G. (2017). In vivo visualization of connections among revised Papez circuit hubs using full q-space diffusion spectrum imaging tractography. *Neuroscience*, 357, 400–410. <https://doi.org/10.1016/j.neuroscience.2017.04.003>
- Wiegell, M. R., Larsson, H. B., & Wedeen, V. J. (2000). Fiber crossing in human brain depicted with diffusion tensor MR imaging. *Radiology*, 217(3), 897–903.  
<https://doi.org/10.1148/radiology.217.3.r00nv43897>
- Wiegell, M. R., Tuch, D. S., Larsson, H. B. W., & Wedeen, V. J. (2003). Automatic segmentation of thalamic nuclei from diffusion tensor magnetic resonance imaging. *NeuroImage*, 19(2), 391–401. [https://doi.org/10.1016/S1053-8119\(03\)00044-2](https://doi.org/10.1016/S1053-8119(03)00044-2)
- Winer, J. A., Miller, L. M., Lee, C. C., & Schreiner, C. E. (2005). Auditory thalamocortical transformation: Structure and function. *Trends in Neurosciences*, 28(5), 255–263.  
<https://doi.org/10.1016/j.tins.2005.03.009>
- Zafar, R., Malik, A. S., Kamel, N., Dass, S. C., Abdullah, J. M., Reza, F., & Abdul Karim, A. H. (2015). Decoding of visual information from human brain activity: A review of fMRI and EEG studies. *Journal of Integrative Neuroscience*, 14(02), 155–168.
- Zhang, F., Wu, Y., Norton, I., Rathi, Y., Golby, A. J., & O'Donnell, L. J. (2019). Test–retest

reproducibility of white matter parcellation using diffusion MRI tractography fiber clustering. *Human Brain Mapping*, 40(10), 3041–3057.

<https://doi.org/10.1002/hbm.24579>

Zou, Q., Long, X., Zuo, X., Yan, C., Zhu, C., Yang, Y., Liu, D., He, Y., & Zang, Y. (2009).

Functional connectivity between the thalamus and visual cortex under eyes closed and eyes open conditions: A resting-state fMRI study. *Human Brain Mapping*, 30(9), 3066–3078. <https://doi.org/10.1002/hbm.20728>